ENGINEERING ARTICULAR CARTILAGE WITH BONE MORPHOGENETIC PROTEINS

A Dissertation

by

YU-LIEH LIN

Submitted to the Graduate and Professional School of
Texas A&M University
in partial fulfillment of the requirements for the degree of

DOCTOR OF PHILOSOPHY

Chair of Committee,	Ken Muneoka
Committee Members,	Larry J. Suva
	William B. Saunders
	Carl A. Gregory
	Ivan V. Ivanov
Head of Department,	Larry J. Suva

May 2022

Major Subject: Biomedical Sciences

ABSTRACT

Osteoarthritis, the progressive degeneration of articular cartilage, affects more than 200 million people worldwide and represents a major health problem. Current therapeutic strategies to restore the joint function are based on engineering functional articular cartilage for transplantation into chondral lesions. We previously found that BMP9 is a remarkable inducer for joint regeneration in a mouse digit amputation model, suggesting that chondrocyte progenitor cells are present in the amputation wound. In Chapter 2, the in vivo findings of BMP9 induced chondrogenesis was replicated in vitro, demonstrating that amputation wound fibroblasts are BMP9 responsive, and a mouse digit fibroblast cell line (P3) displayed a parallel chondrogenic response. For chondrogenic differentiation, a self-aggregation protocol with BMP9 treatment was developed to differentiate P3 fibroblasts into transplantable hyaline cartilage. In Chapter 3, clones of P3 fibroblasts were established and screened for BMP9 induced chondrogenesis. This screen identified clonal lines that differentiated distinct cartilage phenotypes and identified a chondroprogenitor line for articular cartilage (P3_D8 clone) and one for hypertrophic cartilage (P3_E3 clone). These clones were used to enhance the self-aggregation protocol by improving self-aggregation with growth factor treatment. Using this modified protocol, the P3_D8 clonal cells differentiate stable articular cartilage based on in vivo transplantation into an acute joint defect. Detailed studies with the P3_D8 clonal line found that articular cartilage differentiates with an encapsulating fibrous connective tissue layer that contains sequestered progenitor cells that can be

rederived following multiple rounds of differentiation. P3_D8 clonal cells as well as rederived cells display a cell surface marker profile similar to skeletal stem cells and can differentiate into osteoblasts indicating that they are multipotent progenitor cells. P3_E3 clonal cells display similar multipotent characteristics. Since osteoarthritis progression is associated with the transition of articular chondrocytes to hypertrophic chondrocytes, we used RNAseq to establish transcriptional signatures that distinguish the P3_D8 and P3_E3 clonal cells during cartilage differentiation. This dissertation bridges in vivo regeneration with in vitro tissue engineering strategies, identifies articular and hypertrophic chondrocyte progenitor cell lines, established a novel cartilage differentiation protocol, and identifies a transcriptional signature that distinguishes articular and hypertrophic chondrocyte differentiation.

ACKNOWLEDGEMENTS

I would like to thank my committee chair and mentor, Dr. Ken Muneoka, for bringing me to the field of digit and joint regeneration and providing me with a very collaborative and supportive environment to complete my PhD studies. I really enjoy the time I stopped by his office every Friday afternoon with my new data and new ideas. He is always open mind and willing to spend time on these confusing results and pointed out what we can learn from these data. He showed me how to be a rigorous and creative scientist and I truly learn a lot from him.

I would also like to thank my committee members, Dr. Larry J. Suva, Dr. William B. Saunders, Dr. Carl A. Gregory and Dr. Ivan V. Ivanov for their guidance and support throughout the course of this research. Their expertise, encouragement and advice were essential to this dissertation. Special thanks to Dr. Beiyan Zhou for giving me the opportunity to pursue my PhD at Texas A&M University.

Thanks also go to my friends and colleagues, Ling Yu, Mingquan Yan, Regina Brunauer, Lindsay A. Dawson, Connor P. Dolan, Katie Zimmel, Osama Qureshi and Felisha Imholt for making my time at Texas A&M University a great experience. Their friendship and support are meaningful to me and encouraged me to be a good scientist in my future endeavors.

Finally, thanks to my parents and my brother for their encouragement and to my wife for her patience and love. Their love and support allow me to face all the difficulties and never give up.

CONTRIBUTORS AND FUNDING SOURCES

Contributors

This work was supervised by a dissertation committee consisting of Dr. Ken Muneoka and Dr. Larry J. Suva, Dr. William B. Saunders and Dr. Ivan V. Ivanov of the Department of Veterinary Physiology and Pharmacology and Dr. Carl A. Gregory of the Department of Molecular & Cellular Medicine.

Chapter 2 was originally published in 2022 (Development), and was co-first authored by Ling Yu and Yu-Lieh Lin, and co-authored by Mingquan Yan, Tao Li, Emily Y. Wu, Katherine Zimmel, Osama Qureshi, Alyssa Falck, Kirby M. Sherman, Shannon S. Huggins, Daniel Osorio Hurtado, Larry Suva, Dana Gaddy, James Cai, Regina Brunauer, Lindsay A. Dawson and Ken Muneoka.

In Chapter 3 and Chapter 4, all hypotheses and study designs were developed jointly by Yu-Lieh Lin, Ling Yu and Ken Muneoka. Cellular and molecular experiments were developed by Yu-Lieh Lin, Ling Yu, Mingquan Yan, Emily Y. Wu and were performed by Yu-Lieh Lin and Katherine Zimmel. Animal studies were developed by Ling Yu, Mingquan Yan and Tao Li and performed by Yu-Lieh Lin and Ling Yu. Histological and immunohistochemical experiments were performed by Yu-Lieh Lin and were supported by Mingquan Yan, Katherine Zimmel, Regina Brunauer and Lindsay A. Dawson. Bulk RNAseq and scRNAseq studies were performed by Yu-Lieh Lin and were supported by Ken Muneoka, Ivan V. Ivanov and James Cai. All statistical analyses were performed by Yu-Lieh Lin.

Funding Sources

The research is funded by W911NF-06-1-0161 from DARPA, W911NF-09-1-0305 from the US Army Research Center, the John L. and Mary Wright Ebaugh Endowment Fund at Tulane University, and Texas A&M University.

TABLE OF CONTENTS

Page

LIST OF FIGURES

Page

LIST OF TABLES

Page

1 INTRODUCTION

1.1 Summary

Osteoarthritis (OA) is caused by damage or degeneration of articular cartilage (AC) between bones and affects more than 30 million people with approximately 128 billion dollars cost in annual healthcare in the United States. A significant problem of OA is the limitation of AC to self-repair in response to degeneration. With severe OA, the complete replacement of the joint with an implanted artificial mechanical joint is the standard therapy. Besides the joint replacement surgery that introduces additional foreign matter to the human body, many alternative cell-based treatments have been studied to restore a healthy AC phenotype. The ideal strategy of cell-based OA treatment is to differentiate stem/progenitor cells into articular chondrocytes in vitro, and then transplant the engineered cartilage to the injury site of AC. Unfortunately, the effective long-term outcome is still limited due to the tendency of engrafts to produce fibrocartilage or hypertrophic chondrocyte (HC). In addition, several studies have reported that pellet culture, the most popular differentiation protocol, results in cells in the center becoming necrotic. In our previous studies, we demonstrated that bone morphogenetic protein 9 (BMP9) stimulates joint regeneration after digit amputation in vivo. Furthermore, our in vitro study indicated that fibroblasts isolated from mouse digit tip (P3 fibroblasts) can be induced to differentiate hyaline cartilage by a novel self-aggregation protocol with BMP9 treatment (SA/BMP9 protocol). However, although these findings suggest that P3 fibroblast displays a good cell source for in vitro AC regeneration, the1 challenge of P3 fibroblasts lies in its heterogeneity. In this project we intend to identify the articular chondrocyte progenitor cells that exist in heterogeneous P3 fibroblasts.

1.2 Articular Cartilage and Osteoarthritis

Osteoarthritis (OA), the most prevalent form of arthritis, is caused by damage or degeneration of articular cartilage (AC) between bones. It affects more than 30 million people and costs approximately 128 billion dollars in annual healthcare in the United States (Barbour et al., 2017). In healthy synovial joints, AC covers bones with a frictionless weight bearing surface which can prevent skeletal wear and tear, and resistance to mechanical loading during movement. In preclinical stages of OA, the healthy joint begins to break down, and once joint loss is more than 10% of the AC, it is considered to be clinical OA (Cicuttini and Wluka, 2014). The progression of OA usually goes slowly and gets worse over time with the changes in AC that include increasing levels of proteolytic enzymes (such as MMP13), the appearance of hypertrophy markers (such as ColX), and enhanced cartilage matrix calcification (van der Kraan and van den Berg, 2012) (Dreier, 2010). These changes are normally observed in the hypertrophic layer of growth plate cartilage during long bone formation and thus results in the progressive degradation of AC coupled with osteophyte formation.

The evaluation of OA was first developed in 1961. The Outerbridge classification graded the severity of cartilage lesions from Grade 0 with normal cartilage to Grade IV when the subchondral bone is exposed (Outerbridge, 1961). Since then, several modified evaluation systems have been established. For example, the ICRS Cartilage Injury Evaluation Package generated from the International Cartilage Repair Society (ICRS) has been used to score both injury classification and repair assessment. This evaluation system is based on scores given for the degree of defect repair, integration to border zones based on macroscopic appearance with

Grade I defined as normal, Grade II as near normal, Grade III as abnormal, and Grade IV as severely abnormal (van den Borne et al., 2007). In addition to scoring systems based on the macroscopic appearance of the AC defect repair, measurements of functional mechanical load exams, such as wear and tear testing, elasticity testing, and coefficient of friction (COF) measurements, are also considered essential factors for evaluating AC repair outcome (Wang et al., 2018). These evaluation systems were developed based on an understanding of the etiology of OA and the nature of articular cartilage biology.

There are three different types of cartilage tissues in the body: hyaline, elastic, and fibrous cartilages. These cartilages are classified by their histology, biochemical composition, and biomechanical properties, which is strongly correlated to their different functions (Athanasiou et al., 2013). Hyaline cartilage is the most abundant type of cartilage and can be found in AC and epiphyseal growth plate. The AC is a highly specialized tissue consisting of hyaline chondrocytes embedded in matrix with type II collagen and proteoglycans, which allows it to provide protection from the wear and tear associated with skeletal movement. The hyaline chondrocytes in growth plate cartilage will undergo hypertrophic terminal differentiation and eventually differentiate into osteoblasts or be replaced by osteoblasts and thus serve as a template for bone elongation (Tsang et al., 2015). Elastic cartilage contains large amounts of elastin fibers in the matrix, which provides flexibility in tissues of the outer ear, the pharyngotympanic tube, the larynx, and the epiglottis (Hutmacher et al., 2003). Fibrocartilage has been characterized by the presence of type I collagen and, compared to hyaline cartilage, has reduced content of type II collagen and proteoglycans. Fibrous chondrocytes are surrounded by the connective tissue bundles, which help to protect tissues such as intervertebral disc, knee meniscus, and temporomandibular joint disc from mechanical loads (Athanasiou et al., 2013; Detamore and

Athanasiou, 2003; Makris et al., 2011). Due to the variation in structure and function of these cartilage tissues, they provide proper protections to other associated tissues. Therefore, the joint repair for OA treatment aims to specifically regenerate articular hyaline cartilage to restore the appropriate function of AC that lost by AC-related disease.

Although AC contains a single type of cell (hyaline chondrocyte), it can be divided into 4 zones: the superficial zone (SZ), the middle zone (MZ), the deep zone (DZ) and the calcified zone (Figure 1.1). Cells in different zones show distinct morphologies (i.e. cell size, cell density, extracellular matrix (ECM) composition, and collagen fibers orientation), thus display distinct functions (Di Bella et al., 2015). Hyaline chondrocytes in the SZ express the protein proteoglycan 4 (PRG4) and are usually small and flat. Studies have reported that this region of AC contains relatively low proteoglycan composition and articular chondrocyte progenitor cells (ACPCs) are present (Dowthwaite et al., 2004; Hattori et al., 2007; Roelofs et al., 2017). The MZ contains round hyaline chondrocytes that express Collagen ll, aggrecan and cartilage intermediate layer protein 1(CILP; (Bernardo et al., 2011; Lorenzo et al., 1998), and has the highest proteoglycan content in AC. Because hyaline chondrocytes in MZ produce and maintain all typical cartilage matrix collagens and proteins, they most likely contribute to the key biomechanical resilience of AC (Decker et al., 2015). The DZ with the slightly enlarged cells is the last region containing hyaline chondrocytes in the AC. This zone has lower levels of proteoglycan compared to in the MZ, and has the lowest cell density of the three hyaline cartilaginous zones (Athanasiou et al., 2013; Muir, 1978). The calcified zone is separated from the DZ by the tidemark. Cells in this zone are very large chondrocytes that express markers like Col10a1, Runx2, Mmp13 and alkaline phosphatase (ALP; (Chau et al., 2014) and are identified as hypertrophic chondrocytes. The subchondral bone is beneath the calcified zone and separates

AC layers from the bone marrow. In general, the OA process usually begins with the damage of SZ and progressively degenerate through the MZ and DZ to the subchondral bone in later stages (Tummala et al., 2011).

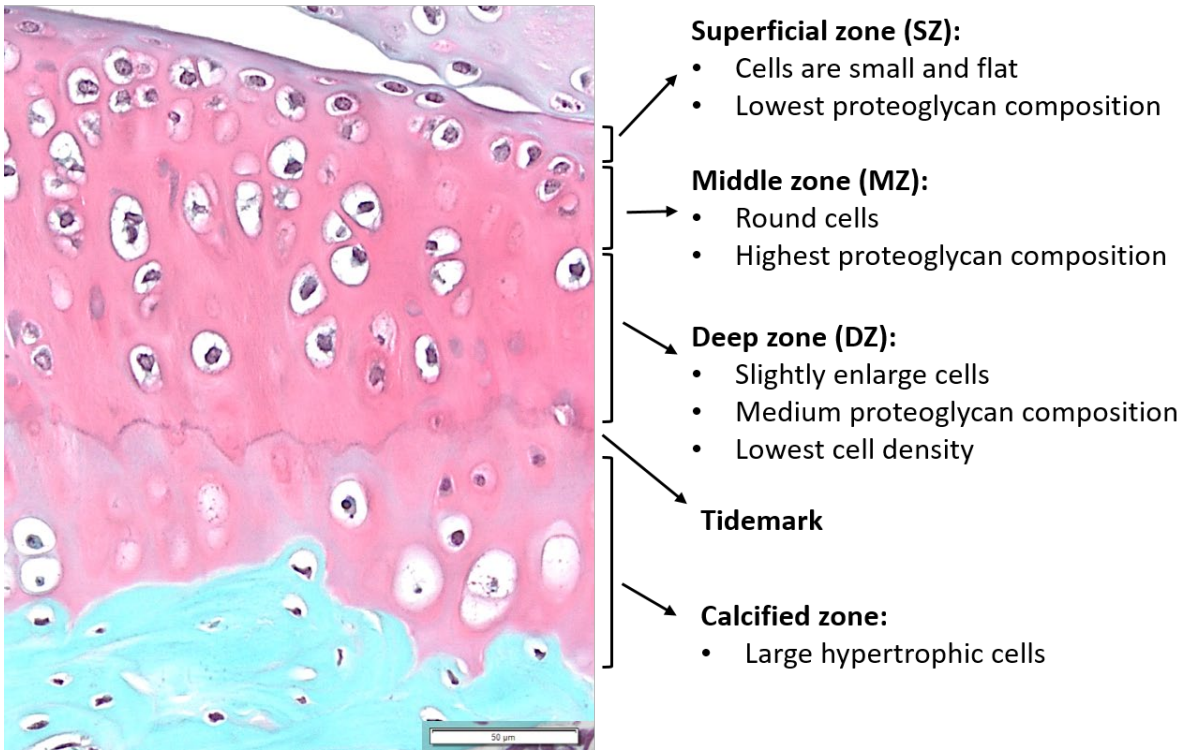

Figure 1.1 Mouse knee joint stained by Safranin O/fast green.
Safranin O identifies mucopolysaccharides prevalent in AC matrix to red/orange, and fast green stains other connective tissue with bluish green.

1.3 Current Therapies of OA

The significant problem of OA is the limitation of AC to self-repair in response to degeneration that is often attributed to an absence of blood vessels and nerves in cartilage tissue. Since there is no cure for OA, the typical therapeutic approaches for patients with OA mostly

focus on relieving pain and/or slowing down disease progression by symptomatic treatment. The treatments for early and middle stages of OA are usually combined with joint-friendly physical activity, weight loss, and anti-inflammatory medications. With severe OA, the complete replacement of the joint with an implanted artificial mechanical joint is the standard therapy. Joint replacement surgery is restricted to shoulder, hip and knee joints and is not typically performed on other damaged joints, such as joints of the hand or foot. Besides joint replacement surgery that introduces additional foreign matter to the human body, an alternative strategy of autologous or allografts of AC are considered a clinical option (Correa and Lietman, 2017). In addition, several cell-based therapies that aim to restore healthy AC phenotype by implanting stem cells or in vitro engineered cartilage into joint lesions are under development. These approaches include microfracture, autologous chondrocyte implantation (ACI), and in vitro AC bio-engineering (Correa and Lietman, 2017; Medvedeva et al., 2018). Overall, the choice of proper clinical options is dependent on the lesion size and inflammatory situation of surrounding tissues.

Microfracture is a simple, quick and low-cost surgery requiring 30-90 minutes and can be only applied to small lesions (Gobbi et al., 2014). The surgical process involves removing damaged AC and adjacent subchondral bone, then drilling a hole to connect into the underlying bone marrow, therefore allowing the recruitment of stem cells and other factors from bone marrow to the defect. This surgery results in bleeding and clot formation which initiates a healing response which is eventually replaced by fibrocartilage. Since fibrocartilage has less mechanically resistance compared to hyaline cartilage, microfracture only serves as a short-term treatment (Mithoefer et al., 2009). To improve it, studies have investigated combinations microfracture with additional treatments such as BMP4 (Zhang et al., 2008), BMP7 (Kuo et al.,

2006), and BMP2 plus VEGFR antagonist (Murphy et al., 2020). The outcomes are encouraging but, for clinical use, subsequent follow-up studies are needed (Athanasiou et al., 2013; Medvedeva et al., 2018).

The autologous transplant and allografts of AC provide a more desirable functional outcome compared to microfracture since the grafted tissue is comparable to the damaged tissue. The procedure of autologous transplant is to harvest full-thickness punches of non-weight-bearing AC from patients and then implant into the defect region (Jacobi et al., 2011). The limitations of autologous transplant include: 1) the limited amount of available donor cartilage tissues thus it can be only applied to small or intermediate-size defects (less than 2 cm^2), 2) the healthy donor sites require treatment to prevent inflammatory arthritis, and 3) the differences of mechanically suitability and shape between the donor and recipient sites (Lamplot et al., 2018). In allograft procedures, the injury sites can be much larger because the size of the donor tissue is not limited since they are derived from deceased donors. However, the challenges of this technique are: 1) the availability of donor tissue, 2) the appropriate storage of the grafts prior to transplantation, and 3) the potential for disease transmission. In addition, poor integration between host cartilage and the allograft coupled with the potential for an immune response by the recipient represents a significant concern (Athanasiou et al., 2013; Medvedeva et al., 2018).

To improve the tissue availability for the autologous transplant technique, in vitro cell-based approaches have been developed. In 1994, Brittberg et al first developed an in vitro cell-based cartilage regeneration approach – autologous chondrocyte implantation (ACI). The procedure of ACI is to isolate chondrocytes from healthy, non-bearing region of AC, followed by cell expansion in monolayer culture, and then inject cultured cells into the defects (Brittberg et al., 1994). The injected cells were covered by a membrane obtained from autologous periosteum

to restrict cells to the defects where they can undergo chondrogenesis. Subsequently, to avoid the invasiveness of periosteal and hypertrophic chondrocyte formation associated with periosteum, ACI was modified in various ways. For example, a porcine-derived collagenous membrane is used to replace the periosteal patch. Another example is seeding the autologous chondrocytes into a matrix-rich three-dimensional carrier before implantation (MACI; (Jacobi et al., 2011). Due to the in vitro expansion procedure, ACI can be applied to larger AC lesions. However, the limitations of ACI include high cost and the risk of injuring of healthy chondrocytes. More significantly, the tissues that formed from ACI can include fibrocartilage which results from the de-differentiation of autologous chondrocytes during cell expansion (Athanasiou et al., 2013; Demoor et al., 2014; Medvedeva et al., 2018).

Cell proliferation and re-differentiation capabilities of in vitro cultured ACI chondrocytes are negatively impacted by a limited number of expansion passages coupled with the age of donors (Li et al., 2013; Schulze-Tanzil et al., 2002). Thus, alternative cell types that can be expanded in culture which retain chondrogenic differentiation ability have been studied for cell-based OA treatments, such as mesenchymal stem cells (MSCs), induced pluripotent stem cells (iPSCs), and embryonic stem cells (ESCs). The strategy of using these stem cells as sources for OA therapy avoids the invasion of healthy AC thus reduces some critical problems of ACI. In addition, chondrocyte stem/progenitor cells (CSPCs) have also be studied to generate in vitro AC for OA treatments.

MSCs have been characterized as a cell type with great proliferation and multi-lineage differentiation capabilities, and can be found from several tissues, such as the bone marrow, bone, adipose tissue, synovial membrane, cord blood, periosteum, and muscle (Ogata et al., 2015; Pittenger et al., 1999). MSCs also display anti-inflammatory and immunomodulatory

properties, which improved transplanted tissue survival and avoided immune response by the host. The International Society for Cellular Therapies (ISCT) has determined the minimal criteria of human MSCs in 2006, including 1) plastic-adherent when maintained in standard culture conditions; 2) positive for CD105, CD73, and CD90 as well as negative to CD45, CD34, CD14 or CD11b, CD79a or CD19 and HLA-DR; and 3) must be able to differentiate to osteoblasts, adipocytes, and chondrocytes in vitro (Dominici et al., 2006). Followed by ISCT, studies have identified several surface markers for characterizing MSCs like CD29, CD44, CD106, CD166 and Sca-1 (murine MSCs only). However, unfortunately, none of these markers are specific to MSCs (Denu et al., 2016; Halfon et al., 2011; Ichim et al., 2018). For cell-based OA therapy, a study has reported that the chondrogenic potential of MSCs vary greatly according to the tissue sources. The MSCs isolated from bone marrow and synovium showed greater chondrogenic potential than adipose and muscle MSCs (Koga et al., 2008). In general, MSCs display a promising cell source for clinical cell-based OA therapy, especially for bone marrow and synovium MSCs. However, similar to ACI, the transplanted MSC-derived cartilage tends to differentiate into fibrous cartilage or hypertrophic cartilage, which is not suitable for AC function (Correa and Lietman, 2017; Demoor et al., 2014; Medvedeva et al., 2018). Therefore, improvements to the differentiation protocols for in vitro hyaline cartilage formation is required for successful MSCs-base OA treatment.

CSPCs existing in the superficial zone of AC have been reported with the characteristics of 1) adhesion to fibronectin, 2) expression of MSC markers, 3) proliferation in culture, and 4) ability to differentiate into chondrocytes (Dowthwaite et al., 2004; Hattori et al., 2007). One study compared equine bone marrow MSCs (BMSCs) and AC superficial zone CSPCs and revealed that both cell types can differentiate to osteoblasts, adipocytes, and chondrocytes.

However, the hypertrophic and angiogenic markers (ColX, matrilin-1 and Runx2) that are expressed in BMSC-derived cartilage are not expressed in CSPC-derived cartilage, suggesting that the CSPC-derived cartilage is restricted to hyaline chondrocytes (McCarthy et al., 2012). Another study that investigated zonal specific CSPCs reported that the CSPCs in deep zone display greater chondrogenic and osteogenic potential than superficial zone CSPCs (Yu et al., 2014b). This study identified one problem with in vitro chondrogenesis using CSPCs was the heterogeneity of the cell population, and suggested that a more homogenous stem/progenitor cells are needed to elucidate their differential roles in AC repair. The challenges of CSPCs-based OA therapy include the absence of well-defined markers to CSPCs, and protocols to maintain CSPCs potency and their differentiation into stable hyaline chondrocytes are still lacking.

CSCPs can also be isolated from other tissues, such as growth plate, periosteum, bone, and digits (Chan et al., 2015; Murphy et al., 2020; Yu et al., 2022), which provides alternative cell sources for AC regeneration without invading healthy AC. Chan et al have identified post-natal mouse skeletal stem cells (mSSCs) with the surface marker expression of CD45-/TER119-/TIE2-/CD51+/CD90-/6C3-/CD105- , that display a potential to differentiate to bone and cartilage, but not fat. These cells can be found in the growth plate, periosteum, and bone and can self-renew when expanded in monolayer culture or transplanted onto kidney capsule (Chan et al., 2015; Murphy et al., 2020). Yu et al first discovered that Bone Morphogenetic Protein (BMP) 9 stimulates joint regeneration in non-regenerative mouse P2 digit amputation model and this regenerative event is Prg4 dependent (Yu et al., 2019). Furthermore, to bridge findings from digit tip regeneration to in vitro cell-based therapy of OA, Yu et al(Yu et al., 2022) provided evidence that BMP9 responsive CSCPs exist in the neonatal P2 digit amputation wounds and adult fibroblasts isolated from P3 skeletal elements. After treatment with BMP9, these cells

differentiated to hyaline cartilage in vitro, and maintained stable hyaline chondrocyte phenotype when transplanted into acute joint defects (Yu et al., 2022). These remarkable studies provide evidence that the CSCPs are present in tissues outside of AC, however the long-term translational potential of these findings need further study.

Pluripotent stem cells (including ESCs and iPSCs) have unlimited proliferation and self-renewal potential and can differentiate into all kinds of somatic cell types. Several studies intended to regenerate AC using these cells and the most successful protocol involves differentiation-mimicking embryonic development. The procedural involves stem cells expansion, mesodermal lineage specification, chondrocyte progenitor cells generation, and hyaline chondrocytes differentiation, thus the whole procedural takes about 2 to 4 months (Craft et al., 2015). In addition, the results of this study indicate that the chondrocyte progenitor cells derived from pluripotent stem cells retain plasticity to differentiate into distinct types of chondrocytes according to the treatments they received (i.e. TGFβ3 for hyaline chondrocyte and BMP4 for hypertrophic chondrocyte). The long procedural of differentiating iPSCs to chondrocytes raised the question of whether it is necessary to reprogram somatic cells all the way back to pluripotency. One recent study has introduced two reprogramming factors (c-Myc and Klf4) coupled with one chondrogenic factor (Sox9) to induced adult dermal fibroblasts to chondrogenic potential cells. These cells can differentiate into stable hyaline chondrocytes in vivo and in vitro without the expression of type I collagen. However, some induced cell lines formed tumors when subcutaneously injected into nude mice (Hiramatsu et al., 2011). Although tumor formation remains a risk, and there are ethical concerns with using human embryonic stem cells, these approaches support the concept that by mimicking the morphogenetic environment

guiding embryonic cartilage formation, hyaline chondrocytes can be successfully differentiated in vitro.

1.4 Development of AC

AC development is a complex and dynamic process that requires various types of signals and growth factors involved. Therefore, the ideal treatment for in vitro AC differentiation should include appropriate treatments at different stages of AC formation (Correa and Lietman, 2017). The development of the appendicular skeletal system begins with limb bud formation and an initial anlagen of cartilage tissue formation that precedes synovial joint formation during fetal development, and the maturation of AC after birth. To better understand the pathology of AC degenerative diseases and investigate clinically effective cell-based therapy, it is important to understand the process of AC formation and the cellular events during AC development and maturation.

Prior to bone and cartilage differentiation, condensation of mesenchymal cells is the first identifiable sign that skeletogenesis has started. Several growth factors such as BMP2, MSX1, and TGFβ have been reported to play a key role in inducing condensation formation (Giffin et al., 2019). The condensing cells establish a boundary and keep growing by cell proliferation, while cells outside of condensation may recruit and migrate toward the condensation center thus also contributing to condensation growth (Giffin et al., 2019). Once the condensation reaches a critical size, cells within condensation differentiate into ColII-positive chondrocytes and form a continuous and uninterrupted cartilaginous anlage (Hyde et al., 2008). In the cartilaginous anlage, some chondrocytes de-differentiate (chondrocyte-to-mesenchymal transition), down-

regulate ColII expression, and undergo compaction to establish the interzone at the site of the future synovial joints (Bian et al., 2020; Decker et al., 2015; Giffin et al., 2019; Rux et al., 2019; Tong et al., 2019). The interzone consists of mesenchymal cells that separate neighboring skeletal elements in the cartilaginous anlage. Microsurgical removal of the prospective interzone site from the developing chick embryo results in the failure of joint formation (Holder, 1977). Sox9 is a master chondrogenic transcription factor and has been identified to be expressed before condensation begins. Condensation does not occur in Sox9 mutants indicating a requirement of Sox9 for condensation (Bi et al., 1999). In addition, lineage tracing of Gdf-5 expressing cells, one of the earliest markers of interzone cells, indicate that interzone cells contribute to all major joint elements including AC, ligament, meniscus and synovium (Bian et al., 2020; Shwartz et al., 2016; Wu et al., 2016). These studies indicate that interzone cells are required for synovial joint and synovial tissues formation.

Since condensations are fundamental cellular events for osteogenic and chondrogenic differentiations, in vitro chondrogenic differentiation protocols mimic cell condensation by either centrifugation to form a cell pellet, or by suspending cells at a high concentration so they can plate at high density (Estes et al., 2010; Greco et al., 2011). Although these high-density culture protocols differentiate cells that express chondrocyte-associated genes and are positive to cartilage-specific staining, some studies have reported that these methods also result in a portion of the cells becoming necrotic (Estes and Guilak, 2011; Markway et al., 2010; Yu et al., 2022). Therefore, establishing a chondrogenic differentiation protocol that allows cell condensation while maintaining cell viability is important to generate clinically available engrafts for OA treatment.

Just prior to joint cavitation during fetal development, the interzone is a tripartite structure containing an intermediate zone and two outer layers associated with the ends of the two opposing skeletal elements. A transcriptional study of these compartments has reported that the intermediate zone expresses more joint formation-related genes while the outer layers express genes associated with cartilage maturation and hypertrophy (Jenner et al., 2014). This study concluded that cells in the intermediate zone give rise to form articular cartilage and cells in the outer layers will develop to secondary ossification center shortly after birth.

Several hypotheses have been proposed that involved in the process of joint cavitation, including cell death and hyaluronic acid (HA) synthesis (Moskalewski et al., 2013). Cell necrosis was observed immediately after interzone formation in chicken and rat embryos, however it was not observed during cavitation in rat or rabbit developing knee joints (Ito and Kida, 2000; Kavanagh et al., 2002; Mitrovic, 1978; Mitrovic, 1977). Therefore, there is little evidence to support that cell death contributes to the cavitation process directly. On the other hand, HA and HA syntheses increased in the interzone before and at the time of cavitation (Dowthwaite et al., 1998; Pitsillides et al., 1995; Pitsillides and Ashhurst, 2008). HA has been reported to promotor either cell aggregation at low concentration or cell separation at high concentration in vitro between adjacent cells (Hay, 1981), thus joint cavitation could be facilitated by increased accumulation of HA in the future synovium cavity sites. In addition, during skeletal development, CD44, a cell surface receptor for HA, was expressed in the interzone (Edwards et al., 1994). These studies suggested that the HA accumulation in the interzone induces cavity formation of synovial joints.

At birth, the joint consists of a cavity connecting epiphyseal cartilage tissues capping the abutting skeletal elements. The epiphyseal cartilage is surrounded by a layer of flattened

fibroblastic-like cells at the periarticular regions respectively. This layer contains progenitor cells with multi-lineage potential when culturing in vitro and expresses ColI and ColII. One study using Col2/Tomato mice has revealed that at postnatal day 5-6, the progenitor cells of the lateral periarticular region contribute to the formation of a secondary ossification center by generating cartilage canals which allow endothelial progenitor cells to migrate into the central cartilage (Tong et al., 2019). Alternatively, the terminal progenitor cells of the periarticular region are responsible for AC development by differentiating into articular chondrocytes throughout all layers of AC in the early stage of postnatal AC growth (Decker et al., 2015; Decker et al., 2017; Kozhemyakina et al., 2015).

In the newborn mouse knee, the incipient AC is thin and consists of small Prg4 positive cells with little matrix accumulation (Li et al., 2017; Rhee et al., 2005; Rux et al., 2019). With time the AC becomes thicker, matrix rich, and acquires its zonal organization. There are two models used to describe the process of AC development and growth: appositional and interstitial growth models. In the appositional growth model, the progenitor cells subsequently differentiate into articular chondrocytes from SZ to MZ and DZ. In the interstitial growth model, AC zonal-specific progenitor cells in each zone contribute to the expansion of their own zones and thus contribute to the growth of the AC zones (Tiku and Sabaawy, 2015). Cell proliferation studies have identified proliferative cells in the SZ and suggested that these cells contribute to AC growth and thickness by the appositional growth model. At a later stage, a population of slow-cycling cells presents in SZ and a rapidly proliferating chondrocyte population were identified in deeper zones suggesting that cells in deeper zones promote AC growth by the interstitial growth model (Archer et al., 1994; Hayes et al., 2001; Mankin, 1962). These findings led to a hypothesis that SZ proliferative cells are responsible for lateral AC growth and the rapidly proliferating

chondrocytes in deeper zones contribute to the vertical expansion of AC, thus both growth models are needed for AC expansion.

Recently, lineage-tracing studies using Prg4CreERT2; R26-Confetti transgenic mice have reported that at birth, the Prg4 reporter positive cells can only be found in the SZ of AC representing an AC progenitor population that can give rise to daughter chondrocytes throughout all layers of AC with time (appositional growth model). Later on, in deeper zones, clones of these Prg4 expressing daughter chondrocytes form cell clusters that participate in zonal expansion by proliferation coupled with an increase in cell size (interstitial growth model). In addition, adult AC did not align or form clonal clusters suggesting the possibility of rearrangement or re-orientation of neighboring cells as the AC matures (Decker et al., 2015; Decker et al., 2017; Kozhemyakina et al., 2015). Taken together, these studies support the conclusion that postnatal AC growth begins with the progenitor cells in SZ contributing to all layers of the AC by appositional growth, and then zonal specific chondrocytes proliferate and increased in size to support zonal expansion by interstitial growth. There is a study that investigated zonal specific CSPCs and pointed out that the CSPCs in deep zone display greater chondrogenic and osteogenic potential than superficial zone CSPCs, which also supports the conclusion that the zonal-specific CSPCs are existed (Yu et al., 2014b). In summary, the evidence indicates that zonal-specific chondrocytes of the AC display distinct growth and differentiative characteristics that are important for proper AC function. These characteristics represent important considerations for engineering AC for clinical use.

1.5 Growth Factors in Chondrogenesis

Chondrogenesis is regulated by the interaction of several external growth factors, including TGFβ, WNT, SHH, NOTCH, IGF and FGF families (Correa and Lietman, 2017; Yu et al., 2012a). The TGFβ superfamily plays an extremely important role during cartilage development and has been tested as chondrogenic inducers, alone or in combination, in several studies. The TGFβ superfamily includes more than 35 factors but the most chondrogenic related members are TGFβ1 and 3, BMP2, 4, 6 and 7. Recently, BMP9 has been found to stimulate joint regeneration in vivo and to be a potent inducer of hyaline chondrocytes differentiation in vitro (Morgan et al., 2020; Yu et al., 2019; Yu et al., 2022). The traditional in vitro chondrogenic differentiation protocol largely relies on treating cells with an identical concentration of TGFβ1 or 3 throughout all culture periods, which might be insufficient when considering the complexity and dynamics of AC development. Therefore, to enhance the success of generating functional AC in bio-engineering study, the understanding of the timings and effects of these growth factors during AC development and in vitro AC regeneration is important (Correa and Lietman, 2017).

TGFβs is one of the most important growth factors that initiate mesenchymal condensation by stimulating fibronectin and N-cadherin synthesis which enhances cell-cell interactions (Giffin et al., 2019). Treatment of TGFβs in culture promotes cell proliferation and chondrogenic differentiation by decreasing ColI and increasing ColII expression. During mesenchymal condensation associated with cranial suture fusion, two TGFβs isoforms, TGFβ1 and TGFβ3, display different effects: TGFβ3 induces mesenchymal cell proliferation, while TGFβ1 stimulates mesenchymal cell condensation (James et al., 2009). TGFβs also can prevent, or delay chondrocyte hypertrophy and thus maintain cells in a stable pre-hypertrophic phenotype (Ballock

et al., 1993; Mueller et al., 2010; van Caam et al., 2015; Yang et al., 2001; Zhang et al., 2004). However, studies in which overexpression of active TGFβ1 in the mouse knee results in deleterious side effects, including synovial proliferation and fibrosis, inflammatory attraction to the synovial lining, and osteophyte formation (Fortier et al., 2011). Considering these reported side effects additional studies of TGFβ1 and its effects in the synovial membrane are necessary prior to clinical use. In combination with BMP2, TGFβs has been shown to increase the expression of cartilage-associated marker genes (Mehlhorn et al., 2007; Toh et al., 2005). Moreover, another study has reported that TGFβs promote BMPs induced signaling in the early stages of chondrogenesis, and in the later stages, BMPs alone are sufficient to induce cells to differentiate into chondrocytes (Karamboulas et al., 2010). A similar study using micro-pellet models of BM-MSCs has also revealed that a single day of TGFβ1 exposure followed by the basal medium condition for the remaining period of culture activates chondrogenic and hypertrophic differentiation (Futrega et al., 2021). Taken together, these studies suggest that TGFβs play an important role in mesenchymal condensation and early stages of chondrogenesis to potentiate chondrogenic differentiation, and at later stages by preventing chondrocyte hypertrophy.

BMP2, 4, 6 and 7 have been studied to induce regeneration in both chondrogenic and osteogenic tissues in vivo and in vitro (Dawson et al., 2017; Ide, 2012; Miljkovic et al., 2008; Yu et al., 2012b). BMP2 plays a major role in mesenchymal condensation (Giffin et al., 2019), and is known to have two distinct effects in skeletal tissues differentiation (Denker et al., 1999). At low concentrations (50 ng/ml), BMP2 exhibits positive effects on chondrocyte differentiation and maturation by stimulating cartilaginous ECM production and reducing ColI gene expression

(Gibson et al., 2017; Wei et al., 2006). At high doses (100 to 1000 ng/ml), BMP2 stimulates ColX expression leading to hypertrophic chondrocyte differentiation and bone mineralization (Demoor et al., 2014; Denker et al., 1999; Valcourt et al., 2002). Studies that compared growth factors in chondrogenesis reveal that BMP2 display better chondrogenic effects than BMP4, BMP6 and TGFβs in increasing proteoglycan and ColII production (Sekiya et al., 2005; Shintani and Hunziker, 2007; Valcourt et al., 1999). BMP4 and BMP6 have also been showed to upregulate expression of cartilage-specific markers, however the long-term treatment of BMP6 increases a hypertrophic chondrocyte phenotype (Diekman et al., 2010). In addition, another study found that BMP4 treatment of iPSCs-derived chondrocyte progenitor cells resulted in hypertrophic chondrocyte formation (Craft et al., 2015). BMP7, also called osteogenic protein-1, is released by chondrocytes and enhances aggrecan and ColII expression when treated alone or with a combination of TGFβ3, however long-term exposure of BMP7 also results in hypertrophic chondrocyte differentiation (Caron et al., 2013; Correa and Lietman, 2017; Shen et al., 2010; Shintani and Hunziker, 2007). Overall, it appears that these BMPs have both chondrogenic and osteogenic effects, and whether this bi-functional inductive ability is dose-dependent, i.e. low concentration vs. high concentration, is still unclear.

BMP9, as a member of the BMP family, is relatively uncharacterized and also plays a dual role in osteogenic and chondrogenic differentiation. BMP9 has been reported with highly osteogenic differentiation capacity, when compared with 13 other BMPs, in mouse embryonic fibroblast and muscle cells (Kang et al., 2004; Sharff et al., 2009). On the other hand, our lab has demonstrated that BMP9 is transiently expressed by interzone cells associated with synovial cavity during digit joint development and can stimulate joint regeneration in mouse digit amputation model (Yu et al., 2019). Our in vitro studies further revealed that BMP9 induces

fibroblasts isolated from the amputated wound (ampWCs) or digit fibroblasts (P3 fibroblasts) to differentiate into hyaline cartilage. Another group using chondro-progenitor cells to compare BMP9 with TGFβ1, 2, 3 and BMP2 in inducing hyaline chondrocyte differentiation revealed that BMP9 exhibits the best chondrogenic effect, thus is a potent chondrogenic inducer (Morgan et al., 2020). Together, these studies suggest that BMP9 acts in a context-dependent manner, and the cell types and the timing of BMP9 treatment may decide the outcome of BMP9 stimulation. In addition to skeletal tissues differentiation and regeneration, BMP9 also shows controversial results in angiogenesis. Some studies reported that BMP9 is an angiogenesis inhibitor in endothelial cells while other studies indicated that BMP9 acts as an angiogenesis inducer in endothelial cells and MSCs (David et al., 2008; Poirier et al., 2012; Richter et al., 2019; Xiao et al., 2020; Yu et al., 2014a). Considering that during limb development endochondral ossification requires blood vessel formation while the AC differentiation occurs without vascularization, it will be interesting to investigate the relationship between angiogenesis and chondrogenic/osteogenic differentiation in the context of BMP9 signaling (Bae et al., 2018; Lee et al., 2013).

Overall, TGFβs and BMPs have been demonstrated that play an important role in chondrogenesis in vivo and in vitro. However, they also have negative effects on AC regeneration due to their osteogenic induction capacity. It was expected that no articular cartilage-specific growth factor has been discovered to date because of the complexity and dynamics of skeletal development. Therefore, an ideal treatment regime for engineering AC will need to take into consideration timing and combinatorial growth factor treatments to promote the development of AC and to maximize the success of in vitro articular cartilage differentiation.

1.6 References

1. Archer, C.W., Morrison, H., Pitsillides, A.A., 1994. Cellular aspects of the development of diarthrodial joints and articular cartilage. Journal of anatomy 184 (Pt 3), 447-456.
2. Athanasiou, K., Darling, E., Duraine, G., Hu, J., Reddi, A., 2013. Articular Cartilage.
3. Bae, H.C., Park, H.J., Wang, S.Y., Yang, H.R., Lee, M.C., Han, H.S., 2018. Hypoxic condition enhances chondrogenesis in synovium-derived mesenchymal stem cells. Biomater Res 22, 28.
4. Ballock, R.T., Heydemann, A., Wakefield, L.M., Flanders, K.C., Roberts, A.B., Sporn, M.B., 1993. TGF-beta 1 prevents hypertrophy of epiphyseal chondrocytes: regulation of gene expression for cartilage matrix proteins and metalloproteases. Dev Biol 158, 414-429.
5. Barbour, K.E., Helmick, C.G., Boring, M., Brady, T.J., 2017. Vital Signs: Prevalence of Doctor-Diagnosed Arthritis and Arthritis-Attributable Activity Limitation - United States, 2013-2015. MMWR Morb Mortal Wkly Rep 66, 246-253.
6. Bernardo, B.C., Belluoccio, D., Rowley, L., Little, C.B., Hansen, U., Bateman, J.F., 2011. Cartilage intermediate layer protein 2 (CILP-2) is expressed in articular and meniscal cartilage and down-regulated in experimental osteoarthritis. J Biol Chem 286, 37758-37767.
7. Bi, W., Deng, J.M., Zhang, Z., Behringer, R.R., de Crombrugghe, B., 1999. Sox9 is required for cartilage formation. Nature genetics 22, 85-89.
8. Bian, Q., Cheng, Y.H., Wilson, J.P., Su, E.Y., Kim, D.W., Wang, H., Yoo, S., Blackshaw, S., Cahan, P., 2020. A single cell transcriptional atlas of early synovial joint development. Development 147.
9. Brittberg, M., Lindahl, A., Nilsson, A., Ohlsson, C., Isaksson, O., Peterson, L., 1994. Treatment of deep cartilage defects in the knee with autologous chondrocyte transplantation. N Engl J Med 331, 889-895.
10. Caron, M.M., Emans, P.J., Cremers, A., Surtel, D.A., Coolsen, M.M., van Rhijn, L.W., Welting, T.J., 2013. Hypertrophic differentiation during chondrogenic differentiation of progenitor cells is stimulated by BMP-2 but suppressed by BMP-7. Osteoarthritis Cartilage 21, 604-613.
11. Chan, C.K., Seo, E.Y., Chen, J.Y., Lo, D., McArdle, A., Sinha, R., Tevlin, R., Seita, J., Vincent-Tompkins, J., Wearda, T., Lu, W.J., Senarath-Yapa, K., Chung, M.T., Marecic, O., Tran, M., Yan, K.S., Upton, R., Walmsley, G.G., Lee, A.S., Sahoo, D., Kuo, C.J., Weissman, I.L., Longaker, M.T., 2015. Identification and specification of the mouse skeletal stem cell. Cell 160, 285-298.
12. Chau, M., Lui, J.C., Landman, E.B., Spath, S.S., Vortkamp, A., Baron, J., Nilsson, O., 2014. Gene expression profiling reveals similarities between the spatial architectures of postnatal articular and growth plate cartilage. PLoS One 9, e103061.

13. Cicuttini, F.M., Wluka, A.E., 2014. Osteoarthritis: Is OA a mechanical or systemic disease? Nat Rev Rheumatol 10, 515-516.

14. Correa, D., Lietman, S.A., 2017. Articular cartilage repair: Current needs, methods and research directions. Semin Cell Dev Biol 62, 67-77.

15. Craft, A.M., Rockel, J.S., Nartiss, Y., Kandel, R.A., Alman, B.A., Keller, G.M., 2015. Generation of articular chondrocytes from human pluripotent stem cells. Nat Biotechnol 33, 638-645.

16. David, L., Mallet, C., Keramidas, M., Lamande, N., Gasc, J.M., Dupuis-Girod, S., Plauchu, H., Feige, J.J., Bailly, S., 2008. Bone morphogenetic protein-9 is a circulating vascular quiescence factor. Circ Res 102, 914-922.

17. Dawson, L.A., Yu, L., Yan, M., Marrero, L., Schanes, P.P., Dolan, C., Pela, M., Petersen, B., Han, M., Muneoka, K., 2017. The periosteal requirement and temporal dynamics of BMP2-induced middle phalanx regeneration in the adult mouse. Regeneration (Oxf) 4, 140-150.

18. Decker, R.S., Koyama, E., Pacifici, M., 2015. Articular Cartilage: Structural and Developmental Intricacies and Questions. Curr Osteoporos Rep 13, 407-414.

19. Decker, R.S., Um, H.B., Dyment, N.A., Cottingham, N., Usami, Y., Enomoto-Iwamoto, M., Kronenberg, M.S., Maye, P., Rowe, D.W., Koyama, E., Pacifici, M., 2017. Cell origin, volume and arrangement are drivers of articular cartilage formation, morphogenesis and response to injury in mouse limbs. Dev Biol 426, 56-68.

20. Demoor, M., Ollitrault, D., Gomez-Leduc, T., Bouyoucef, M., Hervieu, M., Fabre, H., Lafont, J., Denoix, J.M., Audigie, F., Mallein-Gerin, F., Legendre, F., Galera, P., 2014. Cartilage tissue engineering: molecular control of chondrocyte differentiation for proper cartilage matrix reconstruction. Biochim Biophys Acta 1840, 2414-2440.

21. Denker, A.E., Haas, A.R., Nicoll, S.B., Tuan, R.S., 1999. Chondrogenic differentiation of murine C3H10T1/2 multipotential mesenchymal cells: I. Stimulation by bone morphogenetic protein-2 in high-density micromass cultures. Differentiation 64, 67-76.

22. Denu, R.A., Nemcek, S., Bloom, D.D., Goodrich, A.D., Kim, J., Mosher, D.F., Hematti, P., 2016. Fibroblasts and Mesenchymal Stromal/Stem Cells Are Phenotypically Indistinguishable. Acta Haematologica 136, 85-97.

23. Detamore, M.S., Athanasiou, K.A., 2003. Tensile properties of the porcine temporomandibular joint disc. J Biomech Eng 125, 558-565.

24. Di Bella, C., Fosang, A., Donati, D.M., Wallace, G.G., Choong, P.F., 2015. 3D Bioprinting of Cartilage for Orthopedic Surgeons: Reading between the Lines. Front Surg 2, 39.

25. Diekman, B.O., Estes, B.T., Guilak, F., 2010. The effects of BMP6 overexpression on adipose stem cell chondrogenesis: Interactions with dexamethasone and exogenous growth factors. J Biomed Mater Res A 93, 994-1003.

26. Dominici, M., Le Blanc, K., Mueller, I., Slaper-Cortenbach, I., Marini, F., Krause, D., Deans, R., Keating, A., Prockop, D., Horwitz, E., 2006. Minimal criteria for defining multipotent mesenchymal stromal cells. The International Society for Cellular Therapy position statement. Cytotherapy 8, 315-317.

27. Dowthwaite, G.P., Bishop, J.C., Redman, S.N., Khan, I.M., Rooney, P., Evans, D.J., Haughton, L., Bayram, Z., Boyer, S., Thomson, B., Wolfe, M.S., Archer, C.W., 2004. The surface of articular cartilage contains a progenitor cell population. J Cell Sci 117, 889-897.

28. Dowthwaite, G.P., Edwards, J.C.W., Pitsillides, A.A., 1998. An Essential Role for the Interaction Between Hyaluronan and Hyaluronan Binding Proteins During Joint Development. Journal of Histochemistry & Cytochemistry 46, 641-651.

29. Dreier, R., 2010. Hypertrophic differentiation of chondrocytes in osteoarthritis: the developmental aspect of degenerative joint disorders. Arthritis research & therapy 12, 216.

30. Edwards, J.C., Wilkinson, L.S., Jones, H.M., Soothill, P., Henderson, K.J., Worrall, J.G., Pitsillides, A.A., 1994. The formation of human synovial joint cavities: a possible role for hyaluronan and CD44 in altered interzone cohesion. Journal of anatomy 185 (Pt 2), 355-367.

31. Estes, B.T., Diekman, B.O., Gimble, J.M., Guilak, F., 2010. Isolation of adipose-derived stem cells and their induction to a chondrogenic phenotype. Nat Protoc 5, 1294-1311.

32. Estes, B.T., Guilak, F., 2011. Three-dimensional culture systems to induce chondrogenesis of adipose-derived stem cells. Methods Mol Biol 702, 201-217.

33. Fortier, L.A., Barker, J.U., Strauss, E.J., McCarrel, T.M., Cole, B.J., 2011. The role of growth factors in cartilage repair. Clin Orthop Relat Res 469, 2706-2715.

34. Futrega, K., Robey, P.G., Klein, T.J., Crawford, R.W., Doran, M.R., 2021. A single day of TGF-beta1 exposure activates chondrogenic and hypertrophic differentiation pathways in bone marrow-derived stromal cells. Commun Biol 4, 29.

35. Gibson, J.D., O'Sullivan, M.B., Alaee, F., Paglia, D.N., Yoshida, R., Guzzo, R.M., Drissi, H., 2017. Regeneration of Articular Cartilage by Human ESC-Derived Mesenchymal Progenitors Treated Sequentially with BMP-2 and Wnt5a. Stem Cells Transl Med 6, 40-50.

36. Giffin, J.L., Gaitor, D., Franz-Odendaal, T.A., 2019. The Forgotten Skeletogenic Condensations: A Comparison of Early Skeletal Development Amongst Vertebrates. J Dev Biol 7.

37. Gobbi, A., Karnatzikos, G., Kumar, A., 2014. Long-term results after microfracture treatment for full-thickness knee chondral lesions in athletes. Knee Surg Sports Traumatol Arthrosc 22, 1986-1996.

38. Greco, K.V., Iqbal, A.J., Rattazzi, L., Nalesso, G., Moradi-Bidhendi, N., Moore, A.R., Goldring, M.B., Dell'Accio, F., Perretti, M., 2011. High density micromass cultures of a human chondrocyte cell line: a reliable assay system to reveal the modulatory functions of pharmacological agents. Biochem Pharmacol 82, 1919-1929.

39. Halfon, S., Abramov, N., Grinblat, B., Ginis, I., 2011. Markers distinguishing mesenchymal stem cells from fibroblasts are downregulated with passaging. Stem Cells Dev 20, 53-66.

40. Hattori, S., Oxford, C., Reddi, A.H., 2007. Identification of superficial zone articular chondrocyte stem/progenitor cells. Biochem Biophys Res Commun 358, 99-103.

41. Hay, E.D., 1981. Extracellular matrix. J Cell Biol 91, 205s-223s.

42. Hayes, A.J., MacPherson, S., Morrison, H., Dowthwaite, G., Archer, C.W., 2001. The development of articular cartilage: evidence for an appositional growth mechanism. Anatomy and embryology 203, 469-479.

43. Hiramatsu, K., Sasagawa, S., Outani, H., Nakagawa, K., Yoshikawa, H., Tsumaki, N., 2011. Generation of hyaline cartilaginous tissue from mouse adult dermal fibroblast culture by defined factors. J Clin Invest 121, 640-657.

44. Holder, N., 1977. An experimental investigation into the early development of the chick elbow joint. Journal of embryology and experimental morphology 39, 115-127.

45. Hutmacher, D.W., Ng, K.W., Kaps, C., Sittinger, M., Kläring, S., 2003. Elastic cartilage engineering using novel scaffold architectures in combination with a biomimetic cell carrier. Biomaterials 24, 4445-4458.

46. Hyde, G., Boot-Handford, R.P., Wallis, G.A., 2008. Col2a1 lineage tracing reveals that the meniscus of the knee joint has a complex cellular origin. J Anat 213, 531-538.

47. Ichim, T.E., O'Heeron, P., Kesari, S., 2018. Fibroblasts as a practical alternative to mesenchymal stem cells. Journal of Translational Medicine 16, 212.

48. Ide, H., 2012. Bone pattern formation in mouse limbs after amputation at the forearm level. Dev Dyn 241, 435-441.

49. Ito, M.M., Kida, M.Y., 2000. Morphological and biochemical re-evaluation of the process of cavitation in the rat knee joint: cellular and cell strata alterations in the interzone. J Anat 197 Pt 4, 659-679.

50. Jacobi, M., Villa, V., Magnussen, R.A., Neyret, P., 2011. MACI - a new era? Sports Med Arthrosc Rehabil Ther Technol 3, 10.

51. James, A.W., Xu, Y., Lee, J.K., Wang, R., Longaker, M.T., 2009. Differential effects of TGF-beta1 and TGF-beta3 on chondrogenesis in posterofrontal cranial suture-derived mesenchymal cells in vitro. Plast Reconstr Surg 123, 31-43.

52. Jenner, F., A, I.J., Cleary, M., Heijsman, D., Narcisi, R., van der Spek, P.J., Kremer, A., van Weeren, R., Brama, P., van Osch, G.J., 2014. Differential gene expression of the intermediate and outer interzone layers of developing articular cartilage in murine embryos. Stem Cells Dev 23, 1883-1898.

53. Kang, Q., Sun, M.H., Cheng, H., Peng, Y., Montag, A.G., Deyrup, A.T., Jiang, W., Luu, H.H., Luo, J., Szatkowski, J.P., Vanichakarn, P., Park, J.Y., Li, Y., Haydon, R.C., He, T.C.,

2004. Characterization of the distinct orthotopic bone-forming activity of 14 BMPs using recombinant adenovirus-mediated gene delivery. Gene Ther 11, 1312-1320.

54. Karamboulas, K., Dranse, H.J., Underhill, T.M., 2010. Regulation of BMP-dependent chondrogenesis in early limb mesenchyme by TGFbeta signals. J Cell Sci 123, 2068-2076.

55. Kavanagh, E., Abiri, M., Bland, Y.S., Ashhurst, D.E., 2002. Division and death of cells in developing synovial joints and long bones. Cell Biol Int 26, 679-688.

56. Koga, H., Muneta, T., Nagase, T., Nimura, A., Ju, Y.J., Mochizuki, T., Sekiya, I., 2008. Comparison of mesenchymal tissues-derived stem cells for in vivo chondrogenesis: suitable conditions for cell therapy of cartilage defects in rabbit. Cell Tissue Res 333, 207-215.

57. Kozhemyakina, E., Zhang, M., Ionescu, A., Ayturk, U.M., Ono, N., Kobayashi, A., Kronenberg, H., Warman, M.L., Lassar, A.B., 2015. Identification of a Prg4-expressing articular cartilage progenitor cell population in mice. Arthritis Rheumatol 67, 1261-1273.

58. Kuo, A.C., Rodrigo, J.J., Reddi, A.H., Curtiss, S., Grotkopp, E., Chiu, M., 2006. Microfracture and bone morphogenetic protein 7 (BMP-7) synergistically stimulate articular cartilage repair. Osteoarthritis and Cartilage 14, 1126-1135.

59. Lamplot, J.D., Schafer, K.A., Matava, M.J., 2018. Treatment of Failed Articular Cartilage Reconstructive Procedures of the Knee: A Systematic Review. Orthop J Sports Med 6, 2325967118761871.

60. Lee, H.H., Chang, C.C., Shieh, M.J., Wang, J.P., Chen, Y.T., Young, T.H., Hung, S.C., 2013. Hypoxia enhances chondrogenesis and prevents terminal differentiation through PI3K/Akt/FoxO dependent anti-apoptotic effect. Sci Rep 3, 2683.

61. Li, L., Newton, P.T., Bouderlique, T., Sejnohova, M., Zikmund, T., Kozhemyakina, E., Xie, M., Krivanek, J., Kaiser, J., Qian, H., Dyachuk, V., Lassar, A.B., Warman, M.L., Barenius, B., Adameyko, I., Chagin, A.S., 2017. Superficial cells are self-renewing chondrocyte progenitors, which form the articular cartilage in juvenile mice. FASEB J 31, 1067-1084.

62. Li, Y., Wei, X., Zhou, J., Wei, L., 2013. The age-related changes in cartilage and osteoarthritis. Biomed Res Int 2013, 916530.

63. Lorenzo, P., Bayliss, M.T., Heinegård, D., 1998. A novel cartilage protein (CILP) present in the mid-zone of human articular cartilage increases with age. J Biol Chem 273, 23463-23468.

64. Makris, E.A., Hadidi, P., Athanasiou, K.A., 2011. The knee meniscus: structure-function, pathophysiology, current repair techniques, and prospects for regeneration. Biomaterials 32, 7411-7431.

65. Mankin, H.J., 1962. Localization of Tritiated Thymidine in Articular Cartilage of Rabbits: II. Repair in Immature Cartilage. JBJS 44, 688-698.

66. Markway, B.D., Tan, G.K., Brooke, G., Hudson, J.E., Cooper-White, J.J., Doran, M.R., 2010. Enhanced chondrogenic differentiation of human bone marrow-derived mesenchymal stem cells in low oxygen environment micropellet cultures. Cell Transplant 19, 29-42.

67. McCarthy, H.E., Bara, J.J., Brakspear, K., Singhrao, S.K., Archer, C.W., 2012. The comparison of equine articular cartilage progenitor cells and bone marrow-derived stromal cells as potential cell sources for cartilage repair in the horse. Vet J 192, 345-351.

68. Medvedeva, E.V., Grebenik, E.A., Gornostaeva, S.N., Telpuhov, V.I., Lychagin, A.V., Timashev, P.S., Chagin, A.S., 2018. Repair of Damaged Articular Cartilage: Current Approaches and Future Directions. Int J Mol Sci 19.

69. Mehlhorn, A.T., Niemeyer, P., Kaschte, K., Muller, L., Finkenzeller, G., Hartl, D., Sudkamp, N.P., Schmal, H., 2007. Differential effects of BMP-2 and TGF-beta1 on chondrogenic differentiation of adipose derived stem cells. Cell proliferation 40, 809-823.

70. Miljkovic, N.D., Cooper, G.M., Marra, K.G., 2008. Chondrogenesis, bone morphogenetic protein-4 and mesenchymal stem cells. Osteoarthritis Cartilage 16, 1121-1130.

71. Mithoefer, K., McAdams, T., Williams, R.J., Kreuz, P.C., Mandelbaum, B.R., 2009. Clinical efficacy of the microfracture technique for articular cartilage repair in the knee: an evidence-based systematic analysis. Am J Sports Med 37, 2053-2063.

72. Mitrovic, D., 1978. Development of the diarthrodial joints in the rat embryo. The American journal of anatomy 151, 475-485.

73. Mitrovic, D.R., 1977. Development of the metatarsophalangeal joint of the chick embryo: morphological, ultrastructural and histochemical studies. The American journal of anatomy 150, 333-347.

74. Morgan, B.J., Bauza-Mayol, G., Gardner, O.F.W., Zhang, Y., Levato, R., Archer, C.W., van Weeren, R., Malda, J., Conlan, R.S., Francis, L.W., Khan, I.M., 2020. Bone Morphogenetic Protein-9 Is a Potent Chondrogenic and Morphogenic Factor for Articular Cartilage Chondroprogenitors. Stem Cells Dev 29, 882-894.

75. Moskalewski, S., Hyc, A., Jankowska-Steifer, E., Osiecka-Iwan, A., 2013. Formation of synovial joints and articular cartilage. Folia Morphol (Warsz) 72, 181-187.

76. Mueller, M.B., Fischer, M., Zellner, J., Berner, A., Dienstknecht, T., Prantl, L., Kujat, R., Nerlich, M., Tuan, R.S., Angele, P., 2010. Hypertrophy in mesenchymal stem cell chondrogenesis: effect of TGF-beta isoforms and chondrogenic conditioning. Cells Tissues Organs 192, 158-166.

77. Muir, H., 1978. Proteoglycans of cartilage. J Clin Pathol Suppl (R Coll Pathol) 12, 67-81.

78. Murphy, M.P., Koepke, L.S., Lopez, M.T., Tong, X., Ambrosi, T.H., Gulati, G.S., Marecic, O., Wang, Y., Ransom, R.C., Hoover, M.Y., Steininger, H., Zhao, L., Walkiewicz, M.P., Quarto, N., Levi, B., Wan, D.C., Weissman, I.L., Goodman, S.B., Yang, F., Longaker,

M.T., Chan, C.K.F., 2020. Articular cartilage regeneration by activated skeletal stem cells. Nat Med 26, 1583-1592.

79. Ogata, Y., Mabuchi, Y., Yoshida, M., Suto, E.G., Suzuki, N., Muneta, T., Sekiya, I., Akazawa, C., 2015. Purified Human Synovium Mesenchymal Stem Cells as a Good Resource for Cartilage Regeneration. PLoS One 10, e0129096.

80. Outerbridge, R.E., 1961. The etiology of chondromalacia patellae. The Journal of bone and joint surgery. British volume 43-b, 752-757.

81. Pitsillides, A.A., Archer, C.W., Prehm, P., Bayliss, M.T., Edwards, J.C., 1995. Alterations in hyaluronan synthesis during developing joint cavitation. Journal of Histochemistry & Cytochemistry 43, 263-273.

82. Pitsillides, A.A., Ashhurst, D.E., 2008. A critical evaluation of specific aspects of joint development. Dev Dyn 237, 2284-2294.

83. Pittenger, M.F., Mackay, A.M., Beck, S.C., Jaiswal, R.K., Douglas, R., Mosca, J.D., Moorman, M.A., Simonetti, D.W., Craig, S., Marshak, D.R., 1999. Multilineage potential of adult human mesenchymal stem cells. Science 284, 143-147.

84. Poirier, O., Ciumas, M., Eyries, M., Montagne, K., Nadaud, S., Soubrier, F., 2012. Inhibition of apelin expression by BMP signaling in endothelial cells. Am J Physiol Cell Physiol 303, C1139-1145.

85. Rhee, D.K., Marcelino, J., Baker, M., Gong, Y., Smits, P., Lefebvre, V., Jay, G.D., Stewart, M., Wang, H., Warman, M.L., Carpten, J.D., 2005. The secreted glycoprotein lubricin protects cartilage surfaces and inhibits synovial cell overgrowth. J Clin Invest 115, 622-631.

86. Richter, A., Alexdottir, M.S., Magnus, S.H., Richter, T.R., Morikawa, M., Zwijsen, A., Valdimarsdottir, G., 2019. EGFL7 Mediates BMP9-Induced Sprouting Angiogenesis of Endothelial Cells Derived from Human Embryonic Stem Cells. Stem Cell Reports 12, 1250-1259.

87. Roelofs, A.J., Zupan, J., Riemen, A.H.K., Kania, K., Ansboro, S., White, N., Clark, S.M., De Bari, C., 2017. Joint morphogenetic cells in the adult mammalian synovium. Nat Commun 8, 15040.

88. Rux, D., Decker, R.S., Koyama, E., Pacifici, M., 2019. Joints in the appendicular skeleton: Developmental mechanisms and evolutionary influences. Curr Top Dev Biol 133, 119-151.

89. Schulze-Tanzil, G., de Souza, P., Villegas Castrejon, H., John, T., Merker, H.J., Scheid, A., Shakibaei, M., 2002. Redifferentiation of dedifferentiated human chondrocytes in high-density cultures. Cell Tissue Res 308, 371-379.

90. Sekiya, I., Larson, B.L., Vuoristo, J.T., Reger, R.L., Prockop, D.J., 2005. Comparison of effect of BMP-2, -4, and -6 on in vitro cartilage formation of human adult stem cells from bone marrow stroma. Cell Tissue Res 320, 269-276.

91. Sharff, K.A., Song, W.X., Luo, X., Tang, N., Luo, J., Chen, J., Bi, Y., He, B.C., Huang, J., Li, X., Jiang, W., Zhu, G.H., Su, Y., He, Y., Shen, J., Wang, Y., Chen, L., Zuo, G.W., Liu, B., Pan, X., Reid, R.R., Luu, H.H., Haydon, R.C., He, T.C., 2009. Hey1 basic helix-loop-helix protein plays an important role in mediating BMP9-induced osteogenic differentiation of mesenchymal progenitor cells. J Biol Chem 284, 649-659.

92. Shen, B., Wei, A., Whittaker, S., Williams, L.A., Tao, H., Ma, D.D., Diwan, A.D., 2010. The role of BMP-7 in chondrogenic and osteogenic differentiation of human bone marrow multipotent mesenchymal stromal cells in vitro. J Cell Biochem 109, 406-416.

93. Shintani, N., Hunziker, E.B., 2007. Chondrogenic differentiation of bovine synovium: bone morphogenetic proteins 2 and 7 and transforming growth factor beta1 induce the formation of different types of cartilaginous tissue. Arthritis Rheum 56, 1869-1879.

94. Shwartz, Y., Viukov, S., Krief, S., Zelzer, E., 2016. Joint Development Involves a Continuous Influx of Gdf5-Positive Cells. Cell Rep 15, 2577-2587.

95. Tiku, M.L., Sabaawy, H.E., 2015. Cartilage regeneration for treatment of osteoarthritis: a paradigm for nonsurgical intervention. Ther Adv Musculoskelet Dis 7, 76-87.

96. Toh, W.S., Liu, H., Heng, B.C., Rufaihah, A.J., Ye, C.P., Cao, T., 2005. Combined effects of TGFbeta1 and BMP2 in serum-free chondrogenic differentiation of mesenchymal stem cells induced hyaline-like cartilage formation. Growth Factors 23, 313-321.

97. Tong, W., Tower, R.J., Chen, C., Wang, L., Zhong, L., Wei, Y., Sun, H., Cao, G., Jia, H., Pacifici, M., Koyama, E., Enomoto-Iwamoto, M., Qin, L., 2019. Periarticular Mesenchymal Progenitors Initiate and Contribute to Secondary Ossification Center Formation During Mouse Long Bone Development. Stem Cells 37, 677-689.

98. Tsang, K.Y., Chan, D., Cheah, K.S., 2015. Fate of growth plate hypertrophic chondrocytes: death or lineage extension? Dev Growth Differ 57, 179-192.

99. Tummala, S., Bay-Jensen, A.C., Karsdal, M.A., Dam, E.B., 2011. Diagnosis of Osteoarthritis by Cartilage Surface Smoothness Quantified Automatically from Knee MRI. Cartilage 2, 50-59.

100. Valcourt, U., Gouttenoire, J., Moustakas, A., Herbage, D., Mallein-Gerin, F., 2002. Functions of transforming growth factor-beta family type I receptors and Smad proteins in the hypertrophic maturation and osteoblastic differentiation of chondrocytes. J Biol Chem 277, 33545-33558.

101. Valcourt, U., Ronzière, M.C., Winkler, P., Rosen, V., Herbage, D., Mallein-Gerin, F., 1999. Different effects of bone morphogenetic proteins 2, 4, 12, and 13 on the expression of cartilage and bone markers in the MC615 chondrocyte cell line. Experimental cell research 251, 264-274.

102. van Caam, A., Blaney Davidson, E., Garcia de Vinuesa, A., van Geffen, E., van den Berg, W., Goumans, M.J., ten Dijke, P., van der Kraan, P., 2015. The high affinity ALK1-ligand BMP9 induces a hypertrophy-like state in chondrocytes that is antagonized by TGFbeta1. Osteoarthritis Cartilage 23, 985-995.

103. van den Borne, M.P., Raijmakers, N.J., Vanlauwe, J., Victor, J., de Jong, S.N., Bellemans, J., Saris, D.B., International Cartilage Repair, S., 2007. International Cartilage Repair Society (ICRS) and Oswestry macroscopic cartilage evaluation scores validated for use in Autologous Chondrocyte Implantation (ACI) and microfracture. Osteoarthritis Cartilage 15, 1397-1402.

104. van der Kraan, P.M., van den Berg, W.B., 2012. Chondrocyte hypertrophy and osteoarthritis: role in initiation and progression of cartilage degeneration? Osteoarthritis Cartilage 20, 223-232.

105. Wang, L., Shen, H., Nie, J., Li, D., Fan, H., Jin, Z., Liu, C., 2018. Functional testing on engineered cartilage to identify the role played by shearing. Med Eng Phys 51, 17-23.

106. Wei, Y., Hu, Y., Lv, R., Li, D., 2006. Regulation of adipose-derived adult stem cells differentiating into chondrocytes with the use of rhBMP-2. Cytotherapy 8, 570-579.

107. Wu, M., Chen, G., Li, Y.P., 2016. TGF-beta and BMP signaling in osteoblast, skeletal development, and bone formation, homeostasis and disease. Bone Res 4, 16009.

108. Xiao, H., Wang, X., Wang, C., Dai, G., Zhu, Z., Gao, S., He, B., Liao, J., Huang, W., 2020. BMP9 exhibits dual and coupled roles in inducing osteogenic and angiogenic differentiation of mesenchymal stem cells. Biosci Rep 40.

109. Yang, X., Chen, L., Xu, X., Li, C., Huang, C., Deng, C.X., 2001. TGF-beta/Smad3 signals repress chondrocyte hypertrophic differentiation and are required for maintaining articular cartilage. J Cell Biol 153, 35-46.

110. Yu, D.-A., Han, J., Kim, B.-S., 2012a. Stimulation of Chondrogenic Differentiation of Mesenchymal Stem Cells. International journal of stem cells 5, 16-22.

111. Yu, L., Dawson, L.A., Yan, M., Zimmel, K., Lin, Y.-L., Dolan, C.P., Han, M., Muneoka, K., 2019. BMP9 stimulates joint regeneration at digit amputation wounds in mice. Nature Communications 10, 424.

112. Yu, L., Han, M., Yan, M., Lee, J., Muneoka, K., 2012b. BMP2 induces segment-specific skeletal regeneration from digit and limb amputations by establishing a new endochondral ossification center. Dev Biol 372, 263-273.

113. Yu, L., Lin, Y.-L., Yan, M., Li, T., Wu, E.Y., Zimmel, K., Qureshi, O., Falck, A., Sherman, K.M., Huggins, S.S., Hurtado, D.O., Suva, L.J., Gaddy, D., Cai, J., Brunauer, R., Dawson, L.A., Muneoka, K., 2022. Hyaline cartilage differentiation of fibroblasts in regeneration and regenerative medicine. Development 149.

114. Yu, L., Yan, M., Simkin, J., Ketcham, P.D., Leininger, E., Han, M., Muneoka, K., 2014a. Angiogenesis is inhibitory for mammalian digit regeneration. Regeneration (Oxf) 1, 33-46.

115. Yu, Y., Zheng, H., Buckwalter, J.A., Martin, J.A., 2014b. Single cell sorting identifies progenitor cell population from full thickness bovine articular cartilage. Osteoarthritis Cartilage 22, 1318-1326.

116. Zhang, P., Li, J., Tan, Z., Wang, C., Liu, T., Chen, L., Yong, J., Jiang, W., Sun, X., Du, L., Ding, M., Deng, H., 2008. Short-term BMP-4 treatment initiates mesoderm induction in human embryonic stem cells. Blood 111, 1933-1941.

117. Zhang, X., Ziran, N., Goater, J.J., Schwarz, E.M., Puzas, J.E., Rosier, R.N., Zuscik, M., Drissi, H., O'Keefe, R.J., 2004. Primary murine limb bud mesenchymal cells in long-term culture complete chondrocyte differentiation: TGF-beta delays hypertrophy and PGE2 inhibits terminal differentiation. Bone 34, 809-817.

2 HYALINE CARTILAGE DIFFERENTIATION OF FIBROBLASTS IN REGENERATION AND REGENERATIVE MEDICINE*

2.1 Abstract

Amputation injuries in mammals are typically non-regenerative, however joint regeneration is stimulated by BMP9 treatment (Yu et al., 2019) indicating the presence of latent articular chondrocyte progenitor cells. BMP9 induces a battery of chondrogenic genes in vivo, and a similar response is observed in cultures of amputation wound cells. Extended cultures of BMP9 treated cells results in differentiation of hyaline cartilage and single cell RNAseq analysis identified wound fibroblasts as BMP9 responsive. This culture model was used to identify a BMP9 responsive adult fibroblast cell line and a culture strategy was developed to engineer hyaline cartilage for engraftment into an acutely damaged joint. Transplanted hyaline cartilage survived engraftment and maintained a hyaline cartilage phenotype but did not form mature articular cartilage. In addition, individual hypertrophic chondrocytes were identified in some samples indicating that the acute joint injury site can promote osteogenic progression of engrafted hyaline cartilage. The findings identify fibroblasts as a cell source for engineering articular cartilage and establishes a novel experimental strategy that bridges the gap between regeneration biology and regenerative medicine.

2.2 Introduction

The synovial joint is a complex multi-tissue structure with articular cartilage (AC) covering the terminal surfaces of abutting bones. AC is composed of a highly specialized extracellular matrix (ECM) produced by articular chondrocytes (Firner et al., 2017; Luo et al., 2017) and after maturation, AC does not turn over and displays poor regenerative capabilities, thus damage from injury or disease is a major cause of disabilities worldwide (Medvedeva et al., 2018; Zhang et al., 2020). Cell-based engineering therapies involving expansion and differentiation of chondrocytes for transplantation (Brittberg et al., 1994) are complicated by a tendency to differentiate into fibrous cartilage and/or hypertrophic cartilage (Correa and Lietman, 2017). Mesenchymal stem cells (MSCs) from a variety of tissues are known to have chondrogenic potential and are employed as a cell source for engineering AC although clinical success is plagued by an instability of a stable AC phenotype (Demoor et al., 2014; Somoza et al., 2014). Promising results have been reported by following a development sequence to progressively differentiate induced pluripotent stem cells (Craft et al., 2015; Nakayama et al., 2020), or by direct differentiation of progenitor cells derived from healthy AC (Anderson et al., 2018).

In mammals, limb amputation injuries are non-regenerative however, growth factor treatment stimulates patterned skeletal regeneration when administered during wound healing (Dawson et al., 2017; Ide, 2012; Masaki and Ide, 2007; Yu et al., 2010; Yu et al., 2012). Recently, BMP9 was found to stimulate regeneration of synovial joint tissues that initiate with the formation of hyaline cartilage and results in AC regeneration (Yu et al., 2019). Joint tissue regeneration is also found to result from interactions between amputated bone and intact AC in neonatal digits (Miura et al., 2020). Since AC represents a non-regenerative tissue in mammals,

successful regeneration indicates the presence of endogenous AC progenitor cells within the non-regenerative amputation wound. Why would non-regenerative amputation wounds contain AC progenitor cells or, indeed, any progenitor cell involved in a regeneration response? A phylogenetic analysis of regenerative capabilities among vertebrates indicate that regenerative failure among mammals evolved by modification of a primitive pro-regenerative response (Sanchez Alvarado, 2000). Successful stimulation of regeneration supports the view that cells at non-regenerative amputation injuries possess an unrealized potential to participate in a regeneration response (Dolan et al., 2018; Muneoka and Dawson, 2020). In this model of evolved regenerative failure, the fibrotic healing response involves cells with a latent potential to regenerate tissues removed by amputation. In the case of BMP9 stimulated joint regeneration, this includes progenitor cells with the potential to differentiate to articular chondrocytes. The cell types involved in fibrosis during non-regenerative amputation healing are primarily fibroblasts and immune cells (Storer et al., 2020), and since immune cells do not contribute to regenerated tissues in either amphibians or mammals (Kragl et al., 2009; Rinkevich et al., 2011), amputation wound fibroblasts represent a likely source of progenitor cells.

Cartilage regeneration does not typically occur in adult mammals, so our understanding of how different types of cartilage form comes primarily from developmental studies. The ECM produced by chondrocytes identify the different types of cartilage found in the body, thus expression of matrix proteins (e.g. collagens, proteoglycans, and ECM binding proteins) plays a key role in defining cartilage regeneration. Three general types of cartilage are identified: hyaline cartilage, elastic cartilage and fibrocartilage, and the appendicular skeleton develops from a hyaline cartilage template that condenses within the limb bud mesenchyme. Condensation requires the expression of Sox9, and Collagen type II is the most prominent collagen expressed

by all chondrocytes (Aigner and Stove, 2003; Bi et al., 1999). Col2a1 cell lineage studies show that hyaline cartilage differentiates along two distinct paths: 1) endochondral ossification to form bone, and 2) AC development to form joints (Nakamura et al., 2006; Ono et al., 2014). Hyaline chondrocytes involved in endochondral ossification differentiate to hypertrophic chondrocytes and are identified as 'transient' hyaline cartilage, whereas AC development involves 'permanent' hyaline cartilage because hyaline characteristics are maintained by articular chondrocytes (Iwamoto et al., 2013). Hyaline cartilage and AC are often considered equivalent however, AC maturation is associated with the expression of genes not expressed by hyaline cartilage, e.g. Cilp (Lorenzo et al., 1998). Thus, hyaline cartilage represents an embryonic precursor to AC and hypertrophic cartilage. Prg4 cell lineage studies demonstrate that the superficial layer of AC contains stem cells that form all zonal layers of mature AC (Kozhemyakina et al., 2015; Li et al., 2017). In models of stimulated regeneration of non-regenerative digit amputation wounds, BMP2 stimulates endochondral ossification and hypertrophic chondrocyte differentiation, whereas BMP9 stimulates AC regeneration that initiates with formation of hyaline cartilage. Thus, induced regeneration displays characteristics reminiscent of cartilage formation during embryogenesis.

In this study, we investigated BMP9 induced hyaline cartilage regeneration in vivo and in vitro. Microarray analysis of BMP9-treated amputation wounds identified up-regulated genes linked to both hyaline cartilage and AC differentiation. Cells of the amputation wound were cultured and found to display a parallel response to BMP9, indicating that chondroprogenitor cells can be isolated from the amputation wound. Single-cell RNAseq (scRNAseq) analysis of cultured amputation wound cells identified BMP9 responsive cells as fibroblasts. The chondrogenic response to BMP9 was used to identify an adult digit fibroblast cell line (P3

fibroblasts) (Wu et al., 2013) as a chondroprogenitor cell source, and the P3 cell line was used to develop a novel strategy to engineer hyaline cartilage. P3-BMP9 engineered hyaline cartilage was characterized and evaluated in vivo by implantation into an acute joint injury. Following successful engraftment, hyaline cartilage was largely stable but did not mature to AC, indicating a requirement to differentiate AC prior to transplantation. Additionally, individual hypertrophic chondrocytes of both host and graft origin were observed suggesting that the stability of engrafted hyaline cartilage can be compromised by the injury site. These data identify fibroblasts as a novel source for hyaline cartilage regeneration, and BMP9 as a potent inducer of hyaline and articular chondrocyte differentiation. Overall, these studies establish an experimental strategy that bridges the current gap between regenerative biology and regenerative medicine of articular cartilage.

2.3 Materials and Methods

Animals and surgical procedures: Mouse strains used in this study included outbred CD1 purchased from Harlan Laboratories (Indianapolis, IN), C57BL/6-Tg(ACTBEGFP) 1Osb/J (EGFP) and NOD.CB17-Prkdcscid/J (SCID-NOD) mice purchased from Jackson lab. All mice were bred in house at the Texas Institute of Genomic Medicine. All digit amputations were carried out on hindlimbs of postnatal day 3 neonatal digits of each hindlimb at the level of the second phalangeal element (P2) as previously described (Yu et al., 2019; Yu et al., 2012), and are referred to as digit amputation. Amputations at this level are non-regenerative and complete wound closure within 4 days (Yu et al., 2012). CD1 neonates were used to isolate wound cells after the completion of wound closure following hindlimb P2-level digit amputation. EGFP mice were used to generate Egfp expressing fibroblasts from isolated third phalangeal elements (P3)

of adult hindlimb digits to establish the P3 fibroblast cell line (Egfp-P3 fibroblasts). SCID-NOD mice were used as hosts for transplantation studies of engineered cartilage into an acute defect of the metatarsal-phalangeal (MtP) joint.

The MtP joint defect was surgically created in adult SCID-NOD mice. Mice were anesthetized and maintained with isoflurane (1-5% in oxygen), and buprenorphine (0.1mg/kg) was used as a systemic analgesic. A tourniquet is placed on the hindlimb to minimize bleeding. Under a dissection microscope, the MtP joint is contracted ventrally and a 2-3 mm longitudinal skin incision was made to expose the joint capsule. A dorsal incision of the joint capsule allowed access to the proximal joint surface of the first phalangeal element (P1). An acute defect of approximately 0.5 mm diameter is created in the P1 joint surface with a scalpel (Type 11, EXELINT) at the central distal groove of MtP joint. The defect extends through the articular cartilage layer and subchondral bone into the P1 bone marrow. The acute defect is cleared of residual debris by flushing with PBS prior to tissue implantation. Samples to be implanted were prepared in advance to approximate the size of the MtP defect and maintained on ice. Unused samples were processed for histological analysis to validate the cartilage phenotype. Chondrogenic samples are hard and can be compressed to fit snuggly into the acute wound site. The surface of the implant is aligned with the surface of the P1 joint and straightening of the digit maintains the positioning of the implant. The joint capsule and the overlying skin is closed with 10.0 suture (Ethicon). All animals and techniques used are compliant with the standard operating procedures and approved by the Institutional Animal Care and Use Committees at the College of Veterinary Medicine and Biomedical Sciences at Texas A&M University.

Primary cultured amputation wound cells and P3 fibroblasts: Wound mesenchymal cells were isolated from non-regenerative digit amputation wounds following previously published

protocols (Lee et al., 2013; Wu et al., 2013). Briefly, neonatal postnatal day 3 hindlimb digits were amputated at a mid-phalangeal level of P2 and wound tissue was isolated on postnatal day 7 when wound closure is complete. Each primary culture was derived from amputation wound tissue collected from 18 amputated digits. The tissue was triturated to separate connective tissue from the epidermis and the epidermis was manually removed. Approximately 1 mm of the wound is isolated in dissection medium (DMEM supplemented with 2mM glutamine, 0.05 mg/ml gentamycin and 2% FBS), and digested in dissection medium containing 1.24U-2U/ml liberase blendenzyme (Roche, 5401054001) for 3 hours at 37ºC. 10% FBS is added to quench enzymatic activity and isolated cells are washed twice with PBS prior to plating onto a 10 cm cell culture dish coated with fibronectin (2-5 μg/cm2). Attached amputation wound cells were maintained in 2% FBS MSC medium supplemented with EGF, PDGF, LIF as described (Wu et al., 2013). The initial isolation and expansion of wound cells is designed passage 0 and all experiments were carried out with cells from passage 1 or 2. A total of 20 primary amputation wound cell cultures were used in this study. To detect cellular senescence, senescence-associated beta-galactosidase activity was assessed using a commercially available kit (BioVision, #K320) following the manufacturer's instructions. LacZ expressing P3 fibroblasts (LacZ-P3 fibroblasts) were generated previously, and the Egfp-P3 fibroblast line was generated from adult mice following an identical protocol (Wu et al., 2013).

Chondrogenic differentiation in vitro: Differentiation of amputation wound cells or P3 fibroblasts into hyaline cartilage is accomplished by treatment of centrifuged cell pellets or self-aggregated cell clusters in 2% FBS MSC medium supplemented only with BMP9 (100 ng/ml R&D). Cell pellets were created by suspending 2.5×10^5 cells in 0.5 ml of 2% FBS MSC medium in a 15 mL polypropylene culture tube and centrifuging at 150 x g for 5 minutes at room

temperature. Pellets were cultured with their caps loosened. Since cultured cell pellets frequently results in necrosis of cells in the center of the pellet in P3 fibroblasts, an alternative differentiation assay involving self-aggregation of cells was developed for P3 fibroblasts. Self-aggregation was accomplished by plating 4 X 10^5 cells onto petri dishes in 2% FBS MSC medium to minimize substrate attachment for 4 days. Under these conditions some cells form suspended aggregates that increase in size and fuse with one another with extended culture time. Media changes were carried out every 3-4 days for both differentiation assays and control cultures were treated identically but lacked BMP9 treatment.

Histology and Immunochemistry: In vitro differentiated tissues were fixed with Z-fix (Anatech 6269) followed by Decalcifier I (Surgipath, Leica 3800400) and processed for paraffin histology and immunohistochemistry. For histological analysis, the samples were stained with Mallory trichrome (Humason, 1962). Immunohistochemical staining for GFP, ColII, Acan, Prg4 and Cilp was carried out using heat retrieval (citrate buffer (pH 6) or ethylenediaminetetraacetic acid buffer (pH 8), 90ºC, 25 min) and antigen retrieval for ColX immunostaining used 1% hyaluronidase in PBS (Sigma-Aldrich H3506, room temperature, 30Min). Slides were treated in Protein Block Solution (Dako X0909; room temperature, 1 h). Primary antibodies included anti-GFP (Chicken polyclonal, Abcam 13970; 1:1000), anti-ColX (Rabbit polyclonal, Abcam 58632; 1:500), anti-ColII (Mouse monoclonal, Acris AF5710; 1:100), anti-Acan (Rabbit polyclonal, EMD Millipore, Billerica, MA; AB1030; 1:300), anti-Prg4 (Rabbit polyconol, LSbio LS-B8236; 1:200) and anti-Cilp (Rabbit polyclonal, Novus NBP1-81667; 1:100). Secondary antibody included Alexa Fluor 568 goat anti-rabbit IgG (Invitrogen; A11011, 1:500), Alexa Fluor 568 goat anti-Chicken IgG (Invitrogen, A11041, 1:500) or the Alexa Fluor goat anti-rabbit 488 IgG (Invitrogen, A11008, 1:500). Slides were counterstained with DAPI to label nuclei. Slides were

imaged with an Olympus BX61 fluorescence deconvolution microscope utilizing Slidebook software (Intelligent Imaging Innovations Inc., Denver, CO). Details of immunostaining procedures have been described previously (Dawson et al., 2019; Han et al., 2008; Yu et al., 2012).

RNA Analysis: In vivo microarrays were generated from 24 and 72 hour BMP9 or BSA treated amputated P2 digits (Yu et al., 2019) following a protocol previously described (Yu et al., 2014). Briefly, the wound mesenchyme between the P2 digit stump and wound epidermis was manually isolated under a dissection microscope and stored in RNAlater®-ICE at -20°C for total RNA isolation. For in vitro microarrays of P3 fibroblast aggregates, cells were aggregated for 96 hours then treated with BMP9 for 72 additional hours. Control untreated aggregates were prepared in parallel. Total RNA was extracted from in vivo or in vitro samples using the RNeasy Plus Micro Kit (Qiagen) following the manufacturer's recommended protocol. Each microarray analysis utilized the Agilent Mouse Gene Expression 8×60K G3 microarray format (G4852A) (Agilent Technologies) following manufacturer's recommended protocols. All analyses consisted of 3 independently collected BMP9 treated samples compared to 3 control samples. Data were obtained using the Agilent Feature Extraction software (v9.5) (Agilent Technologies) and were analyzed and normalized with the method described by Gene-Spring bioinformatics software (version 12.6). The unpaired unequal variance (Welch) t-test was used to determine significance. Genes identified as differentially expressed between BMP9 and untreated controls are based on greater than 1.5-fold change with a P value <0.05.

Quantitative reverse transcriptase polymerase chain reaction (qRT-PCR) was carried out in triplicate with the SuperScript™ III Platinum™ One-Step qRT-PCR Kit w/ROX on an Eppendorf Realplex machine according to the manufacturer's instruction. Total RNA extraction

was carried out as described above and quantified and quality-checked by using Nanodrop ratios of 260/280 and 260/310. For aggregation cultures at 14 and 36 days, samples were homogenized before RNA extraction. Applied Biosystem Taqman primer (Thermo Fisher) sets for the following cartilage-related genes are shown in Table 2.1. The expression levels of target genes were normalized to the housekeeping gene ribosomal protein L12 (RPL12) levels. Statistical significance was determined using a parametric unpaired T-test in Graphpad.

Table 2.1 Primer information for QRT-PCR

Name primer		Sequence information	Name primer		Sequence information
1	***Mouse Col2a1***	*Mm01309565_m1*	**2**	***Mouse Fmod***	Mm00491215-ml
3	***Mouse Col11a2***	Mm00487046_m1	**4**	***Mouse Cilp***	Mm00557687_m1
5	***Mouse Prg4***	Mm01284582_m1	**6**	***Mouse Scrg1***	Mm00485984_m1
7	***Mouse Acan***	Mm00545794_m1	**8**	***Mouse Runx2***	Mm00501584_m1
9	***Mouse Sox9***	Mm00448840_m1	**10**	***Mouse Col10a1***	Mm00487041_m1
11	***Mouse Chrdl2***	Mm01136674_m1	**12**	***Mouse Ucma***	Mm00546635_m1
13	***mouse Rpl12***	M02601627-gl			

Single-cell RNA-sequencing and data analysis: Neonatal cells from P2 non-regenerative digit amputation wounds were isolated as described above and $1x10^5$ passage 1 cells were plated in 10 cm culture dishes. Cells were collected after 24 hours by trypsin digestion (4 minutes, 37ºC), washed twice and resuspended in PBS with 0.08% BSA at concentration of 1x106 cells/ml. Single-cell sample preparation was conducted according to Sample Preparation Protocol provided by 10x Genomics. Cell viability was assessed by Trypan Blue staining (0.4%) and determined to be greater than 90%. Subsequently, single-cell GEMs (Gel bead in EMulsion) and

sequencing libraries were prepared using the 10x Genomics Chromium Controller in conjunction with the single-cell 3' kit (v3). Cell suspensions were diluted in nuclease-free water to achieve a targeted cell count of 10,000 for each sample. cDNA synthesis, barcoding, and library preparation were subsequently carried out according to the manufacturer's instructions. Libraries were sequenced in the Molecular Genomic Workspace of the Texas A&M Institute for Genome Sciences and Society (https://genomics.tamu.edu/) using a NovaSeq6000 sequencer (Illumina, San Diego). For the mapping of reads to transcripts and cells, sample demultiplexing, barcode processing, and unique molecular identifier (UMI) counts were performed using the 10x Genomics pipeline CellRanger v5.0.1 with default parameters. Specifically, raw reads were demultiplexed using the pipeline command 'cellranger mkfastq' in conjunction with 'bcl2fastq' (v2.17.1.14, Illumina) to produce two fastq files: the read-1 file containing 26-bp reads, consisting of a cell barcode and a unique molecule identifier (UMI), and the read-2 file containing 96-bp reads including cDNA sequences. Sequences were aligned to the mouse reference genome (mm10), filtered and counted using 'cellranger count' to generate the gene-barcode matrix. The resulting dataset generated 36,831 mean reads per cell, identified 4,070 median genes/cell, a sequencing saturation of 31.0%, and greater than 96% of reads mapped to the genome.

Dimension reduction of expression matrices was performed using UMAP. Marker gene expression and cell type assignment was performed manually using the SC_SCATTER function of scGEAToolbox (Cai, 2019). Differential gene expression was performed using MAST (Finak et al., 2015). Labeled cell-types were compared across experimental groups to quantify the differences in the level of expression. Genes with $|\log2(FC)| > 0.25$ and Benjamina-Hochberg

FDR < 0.05 were considered as differentially expressed. scRNA-seq data generated in this study are available at GEO with accession number GSE185197.

Isolation and differentiation of bone-derived mesenchymal stem cells: Bone-derived mesenchymal stem cells (bone MSC) were isolated and cultivated as described previously (Klepsch et al., 2013). Briefly, femurs and tibias from 6-8 week-old C57BL/6N mice were extracted. After flushing the bone marrow, femurs and tibias (diaphyses and epiphyses) were subjected to collagenase digestion for 3h at 37ºC, cells released from collagen-rich matrix were spun out, filtered through a cell strainer and seeded at a density of 50,000-100,000 cells/cm2 for propagation in bone MSC growth medium (alphaMEM supplemented with 10% FBS and Penicillin/Streptomycin). Cells were cultivated at 37ºC in 5% CO2 and atmospheric oxygen. Osteogenic differentiation was either induced by 50 µg/ml ascorbic acid and 10 mM beta-glycerol phosphate in growth medium (Gaddy-Kurten et al., 2002), or by StemXVivo mouse/rat osteogenic supplement (#CCM009, R&D systems) in StemXVivo adipogenic/osteogenic base media (#CCM007, R&D Systems) following the manufacturer's instructions. Adipogenic differentiation was induced by incubation in StemXVivo adipogenic supplement (#CCM011, R&D systems) in base media following the manufacturer's instructions. After 21 days, mineralized matrix was detected by Alizarin Red S for osteogenic differentiation, and lipid vacuoles were visualized with Oil Red O for adipogenic differentiation. P3 fibroblasts were subjected to identical adipogenic and osteogenic differentiation regimens for 21 days.

Flow cytometry: Flow cytometry was used to analyze P3 fibroblasts and bone MSCs. Cells were detached, filtered by 100 µm cell strainer (CORNING, REF431752), washed twice by flow buffer (0.5% FBS/PBS) and incubated with flow buffer at 4°C, 15 min for blocking. Cells were incubated in the dark with antibodies at the concentration of 1 µL antibody/2x105 cells/100 uL at

4°C, 30 min. Cells were then washed twice and re-suspended with flow buffer and kept at 4°C in the dark prior to running flow cytometry. Flow cytometry were performed using Gallios flow cytometer (Beckmen Coulter) and flow data was analyzed by Kaluza software (Beckmen Coulter). Antibodies used in this study include CD34 (Cat#: 48-0341-82, eBioscience), CD45 (Cat#: 47-0454-80, eBioscience), CD90 (Cat#: 47-0902-82, eBioscience), CD73 (Cat#: 12-0731-81, eBioscience), and CD105 (Cat#: 48-1051-80, eBioscience).

2.4 Results

BMP9 induces amputation-derived wound cells to differentiate into chondrocytes

BMP9 stimulated joint regeneration in mice involves a chondrogenic response coupled with the formation of a synovial cavity (Yu et al., 2019). To better define this response, microarrays of induced regenerates 24 and 72 hours after BMP9 treatment were generated and analyzed in comparison with control samples treated with BSA (N=3 for all samples). These timepoints were selected to correspond to previous in situ hybridization studies of the BMP9 response (Yu et al 19). At 24 hours, 1515 unique transcripts were differentially expressed ($P<0.05$; 1.5-fold change) that included 518 up-regulated and 383 down-regulated annotated genes, and 1021 unique transcripts were differentially expressed (432 up-regulated, 223 down-regulated genes) at 72 hours. To investigate the chondrogenic response, a list of 232 cartilage-related genes was compiled from the JAX MGI website (http://www.informatics.jax.org/mgihome/projects/aboutmgi.shtml) targeting genes associated with general cartilage development, AC, and hypertrophic cartilage. Based on a literature search,

this list was amended by adding 36 cartilage-related genes to generate a list of 268 cartilage-related genes which was used to screen the two microarray datasets (Table 2.2).

Table 2.2 Cartilage-Related Gene List

Acan, Adamts12, Adamts7, Anxa6, Arid5a, Atf2, Atp6v0d2[1], *Atp7a, Axin2, Barx2, Bbs1, Bbs2, Bgn, Bmp1, Bmp10, Bmp2, Bmp3, Bmp4, Bmp5, Bmp6, Bmp7, Bmp8a, Bmp8b, Bmpr1a, Bmpr1b, Bmpr2, Bpnt2, Carm1, Cbs, Ccl3, Ccn1, Ccn2, Ccn3, Ccn4, Cd44*[2], *Cfh, Chadl, Chrdl2, Chst11, Chsy1, Cilp*[3], *Clec3a, Cnmd, Col10a1, Col11a1, Col11a2, Col1a1, Col27a1, Col2a1, Col9a1, Col9a2*[4], *Col9a3*[5], *Comp, Cr2, Creb3l2, Crlf1*[6], *Csgalnact1, Csgalnact2, Cst10, Ctnnb1, Ctsk, Cytl1, Dcn*[7], *Ddrgk1, Dicer1, Dkk3, Dlk1, Dlk2, Dlx2, Dlx5*[8], *Dspp, Ecm1, Edn1, Efemp1, Eif2ak3, Enpp2*[9], *Ep300, Epyc, Ereg*[10], *Erg*[11], *Esrra, Ext1, Fam20b, Fbxw4, Fgf18, Fgf2, Fgf4, Fgf6, Fgf9, Fgfr1, Fgfr3, Fgfrl1*[12], *Fmod*[13], *Frzb, Fzd9*[14], *Gata3*[15], *Gdf2, Gdf5, Gdf6, Glg1, Gli2, Gli3, Gnas, Grem1, Gtf2ird1, Halpn1*[16], *Hand1, Hand2, Has1*[17], *Has2*[18], *Hes5, Hif1a, Hmga2, Hottip, Hoxa11, Hoxa3, Hoxa5, Hoxb3, Hoxc4, Hoxd11, Hoxd3, Hspg2, Htra1, Idua, Ift80, Igfbp5*[19], *Ihh, Il17f, Itgb8, Kat2a, Lep, Lnpk, Loxl2, Loxl3*[20], *Lrp1*[21], *Lrp6, Ltbp3, Maf, Mapk14, Mapk3, Matn1, Matn3, Matn4, Mboat2, Mdk, Mef2c, Mef2d, Mex3c, Mgp, Mia, Mia3, Mir140, Mir455, Mki67, Mkks, Mkx, Mmp13, Msx1, Msx2, Mustn1, Mycn, Myf5, Nfia*[22], *Nfib, Nkx3-2, Nog, Nov*[23], *Nppc, Opa3, Osmr, Osr1, Osr2, Otor, Pax7, Pbxip1, Pcna, Pcolce2*[24], *Pitx1, Pkd1, Pkdcc, Poc1a, Por, Prg4, Prkca, Prkg2*[25], *Prrx1, Prrx2, Ptger1*[26], *Pth, Pth1r, Pthlh, Ptpn11, Rara, Rarb, Rarg, Rb1, Rbp4*[27], *Rela, Rflna, Rflnb, Ror2, Rspo2, Runx1, Runx2, Runx3, Satb2, Scrg1*[28], *Scube2, Scx, Sdc3*[29], *Serpinh1, Sfrp2, Shox2, Sik3, Six2, Slc10a7, Slc29a1*[30], *Slc39a14, Smad1, Smad3, Smad5, Smad7, Smad9, Smpd3, Snai1, Snai2, Snorc, Snx19, Sost, Sox5, Sox6, Sox9, Sprx*[31], *Sprx2, Srf, Stc1, Stm, Sulf1, Sulf2, Tapt1, Tgfb1, Tgfb2, Tgfbr1, Tgfbr2, Thbs1, Thbs3, Thra, Thrb, Timp1, Timp2, Tnc, Trip11, Trps1, Trpv4, Ucma*[32], *Unc5c*[33], *Uncx, Wif1*[34], *Wnt5a, Wnt7a, Wnt7b, Wnt9a, Wwp2*[35], *Zbtb16, Zbtb7a, Zeb1, Zfp219, Zmpste24*

At 24 hours, 37 of the 267 chondrogenic genes were differentially expressed that included 28 up-regulated and 9 down-regulated genes (Table 2.3). The down-regulated gene list

included the joint development associated gene Osr2. The up-regulated genes included those induced during BMP9 stimulated joint regeneration (Acan, Fmod, Prg4, Ucma) (Yu et al., 2019), additional cartilage ECM genes (Col11a1, Sdc3), and AC related genes (Chrdl2, Cilp). Genes involved in BMP signaling (Chrdl2, Grem1) as well as other signaling pathways (Fgfrl1, Fxd9, Tgfb2, Wif1, Ptger1) were identified. A number of transcription factors (Prrx2, Runx1, Runx2, Six2, Snai1) were up regulated.

At 72 hours, 52 chondrogenic genes were differentially expressed including 42 up-regulated and 10 down-regulated genes (Table 2.3). 2 of the 10 down-regulated genes and 17 of the 42 up-regulated genes were identified at the 24-hour time point (Table 2.3) indicating maintenance of the initial BMP9 response. This list included 5 of the 6 induced chondrogenic genes identified by in situ hybridization during BMP9-stimulated joint regeneration (Ucma, Col2a1, Prg4, Acan, and Fmod) (Yu et al., 2019). In addition, the list of induced genes included major and minor collagens (Col9a3, Col9a2, Col9a1, Col11a2, Col11a1, Col27a1), collagen binding proteins (Matn3, Matn4), proteoglycans and proteoglycan binding proteins (Sdc3, Hapln1), and other cartilage ECM associated proteins (Comp, Scrg1, Chrdl2). Genes expressed during hyaline cartilage development include Col2a1 (Zhao et al., 1997), Col11a1 (Yoshioka, 1995), Acan (Li et al., 2018) and Ucma (Surmann-Schmitt et al., 2008). Genes expressed during AC formation include Prg4 (Kozhemyakina et al., 2015), Chrdl2 (Nakayama et al., 2004), Col11a2 (Lawrence et al., 2018), Scrg1 (Ochi et al., 2006) and Fmod (Murphy et al., 1999). Genes linked to hypertrophic cartilage Col10a1 (Zheng et al., 2003), Runx2 (Yoshida et al., 2004) and Dlx5 (Ferrari and Kosher, 2002) were notably absent. This microarray analysis confirms previous histological and in situ hybridization evidence that BMP9 induces a hyaline chondrogenic response in vivo (Yu et al., 2019), and identifies additional BMP9 target

chondrogenic genes. The data indicate that the chondrogenic response to BMP9 is rapid and progressive.

Table 2.3 In vivo Microarray Summary - Cartilage-related genes

BMP9 Treated Amputation Wound: 24-hours
Down-regulated: *Atp6v0d2, Bmp3, Cfh, Cr2, Gnas, Hoxd11, Mustn1, Osr2, Rarb*
Up-regulated: *Acan, Arid5a, Ccl3, Chrdl2, Cilp, Col11a1, Crlf1, Fgfrl1, Fmod, Fzd9, Grem1, Pcolce2, Prg4, Prrx2, Ptger1, Rbp4, Runx1, Runx2, Sdc3, Six2, Slc39a14, Snai1, Tgfb2, Thbs1, Timp1, Ucma, Wif1, Wwp2*
BMP9 Treated Amputation Wound: 72-hours
Down-regulated: *Atp6v0d2, Cd44, Dlk1, Ereg, Fgf9, Has1, Nov, Pthlh, Rarb, Wnt9a*
Up-regulated: *Acan, Chadl, Chrdl2, Clec3a, Col11a1, Col11a2, Col27a1, Col2a1, Col9a1, Col9a2, Col9a3, Comp, Crlf1, Cytl1, Epyc, Erg, Fgfrl1, Fmod, Foxa3, Frzb, Fzd9, Grem1, Ihh, Loxl3, Lrp1, Matn3, Matn4, Pcolce2, Prg4, Prkg2, Ptger1, Pth1r, Rbp4, Scrg1, Sdc3, Slc29a1, Snai1, Thbs1, Ucma, Wif1, Wwp2*
Underlined genes are differentially expressed at 24 and 72 hours

To determine whether the chondrogenic response to BMP9 can be recapitulated in vitro, mesenchymal cells were isolated from neonatal non-regenerative digit amputations after wound closure and cultured under conditions that maintain regenerative competence (Wu et al., 2013). Amputation wound mesenchymal cells (ampWMCs) appear similar to blastema cells derived from regenerating digit tips (Lee et al., 2013) and displayed a similar limited potential for expansion in culture (Figure 2.1). Thus, all experiments investigating gene expression changes associated with BMP9 treatment utilized cells derived from passage 1 or 2 cultures. The chondrogenic potential of ampWMCs was determined by differentiating cell pellets with or without BMP9. After 21 days of BMP9 treatment, ampWMC pellets displayed a robust response (N=6) forming a uniform layer of chondrocytes on the periphery of the pellet (Figure 2.2A).

Mallory's trichrome staining identified chondrocytes based on the presence of distinct lacunae and surrounded by Aniline blue positive matrix indicative of collagen production (Figure 2.2A). In contrast, control untreated ampWMC pellets (N=3) were smaller and contained isolated pockets of chondrocytes interspersed between non-chondrogenic cells (Figure 2.2B). Control cultures indicate the presence of chondroprogenitor cells in the non-regenerative digit amputation wound despite the absence of a chondrogenic response following digit amputation (Yu et al., 2012).

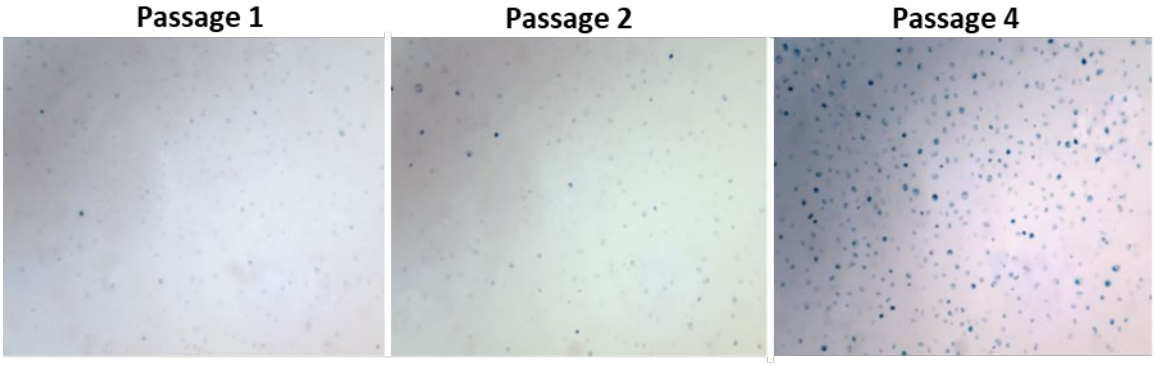

Figure 2.1 Senescence analysis of ampWMCs
Primary cultures of amputation wound mesenchymal cells derived from non-regenerative digit amputations were analyzed for senescence-associated beta-galactosidase activity at 3 different passage numbers (N=2). Senescent cells are present but not abundant after passage 1 and 2 when cells display rapid expansion. By passage 4 senescent cells are abundant and this correlates with reduced proliferation.

The BMP9-induced chondrogenic response of ampWMCs was analyzed by quantitative RT-PCR (qRT-PCR) in monolayer cultures focusing on chondrogenic genes identified in vivo (Table 2.3). Three different categories of chondrogenic genes were selected for analysis: 1) early chondrogenic genes associated with hyaline cartilage formation (Sox9, Col2a1, Col11a1, Acan, Ucma), 2) AC genes (Prg4, Chrld2, Fmod, Scrg1, Cilp, Col11a2) and 3) hypertrophic cartilage

genes (Col10a1, Runx2). Compared to untreated controls, 24 hours of BMP9 stimulation results in enhanced transcript levels of hyaline cartilage and AC genes, but not hypertrophic cartilage genes (Figure 2.2C). The possibility that the BMP9 response resulted solely from stimulated proliferation of endogenous chondroprogenitor cells cannot explain the level of enhanced gene expression within 24 hours, thus indicating that BMP9 induces chondrogenic gene expression. These studies indicate that 1) chondroprogenitor cells are present in the healing non-regenerative digit amputation wound, 2) BMP9 induces chondrogenesis of ampWMCs, and 3) BMP9-stimulated chondrogenic regeneration in vivo can be replicated in vitro.

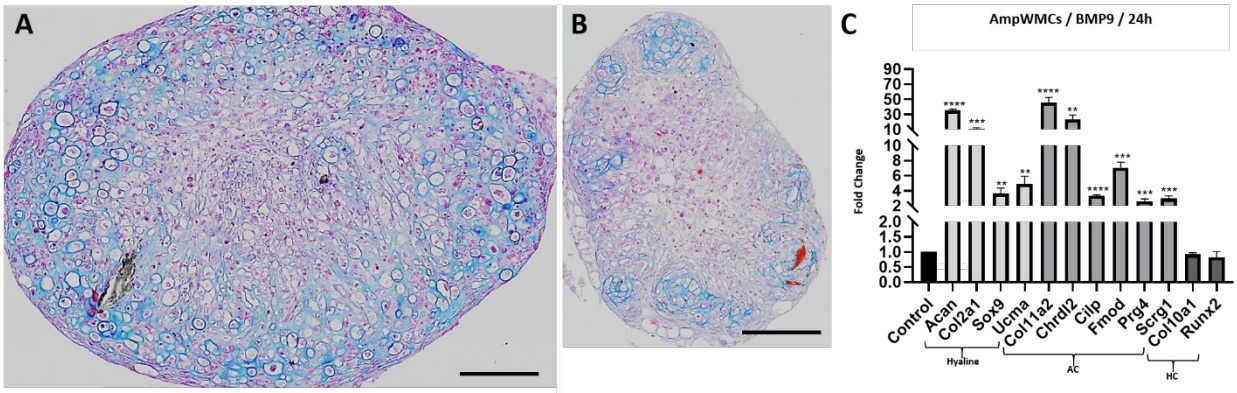

Figure 2.2 BMP9 stimulates chondrogenesis of cultured ampWMCs.
A-D) Chondrogenesis of ampWMCs cultures (passage 1). A) AmpWMC centrifuged cell pellets treated with BMP9 (100 ng/ml) for 21 days (N=6) differentiated cartilage with uniformly distributed chondrocytes. B) Control untreated ampWMC pellets cultured for 21 days (N=3) formed isolated pockets of chondrocytes. C) AmpWMC monolayer cultures treated with BMP9 (100 ng/ml; 24hrs; N=3) were analyzed by qRT-PCR for expression of chondrogenic genes. Hyaline cartilage (Hyaline) and articular cartilage (AC) genes were up-regulated while hypertrophic cartilage (HC) genes were unaffected. Statistical analysis: parametric unpaired T-test in Graphpad, ****=P<0.0001; ***=P<0.001; **=P<0.01; *=P<0.05. Scale bar in A and B= 200μm.

Amputation-derived mesenchymal wound cells are fibroblasts

These results led to the question of which cell type in the amputation wound responds to BMP9. To characterize BMP9 responsive cells, passage 1 ampWMCs were collected for scRNAseq analysis. The neonatal ampWMC scRNAseq dataset included transcriptomes from 13,474 cells and was analyzed using scGEAToolbox (Cai, 2019; Osorio et al., 2020) to determine cell type. Cell type determination utilized the PanglaoDB database of cell-type marker genes derived from published mouse scRNAseq studies (Franzen et al., 2019). The ampWMC dataset was analyzed with published amputation wound datasets for comparative analysis. Direct comparisons with published scRNAseq datasets of adult P2 level digit amputation wound cell transcriptomes (Storer et al., 2020) was carried out by establishing a combined dataset that included the ampWMC dataset with this published dataset. Adult amputation wound cell datasets were pooled from 10- and 14-days post-amputation digits which consisted of transcriptomes of 7,658 cells of which 1,654 cells were identified as fibroblasts. The combined digit amputation dataset included 21,132 total cell transcriptomes (7,658 adult cells and 13,474 neonatal ampWMCs). UMAP plots of this combined dataset identified macrophage, neutrophil, T-cell, keratinocyte, endothelial cell and 3 distinct fibroblast clusters derived from the adult dataset, whereas the cultured neonatal ampWMCs formed one large and one small fibroblast cluster (Figure 2.3A). The adult and neonatal fibroblast clusters were non-overlapping. The analysis of ampWMCs identified the vast majority of cells as fibroblasts, and this conclusion was supported by a high frequency of cells expressing the limb-specific fibroblast marker genes Prrx1 (95.06%) (Figure 2.3B) coupled with a paucity of cells expressing marker genes for other cell types known to be present at non-regenerative digit amputation wounds: epidermis (Krt14: 0.10%,), bone (Bglap: 0.71%), endothelial cells (Pecam1: 0.27%), Schwann cells (Plp1: 1.94%), monocytes

(Lyz2: 1.76%), vascular smooth muscle cells (Rgs5: 0.63%) and T cells (Cd3g: 0.00%) (Johnson et al., 2020; Storer et al., 2020).

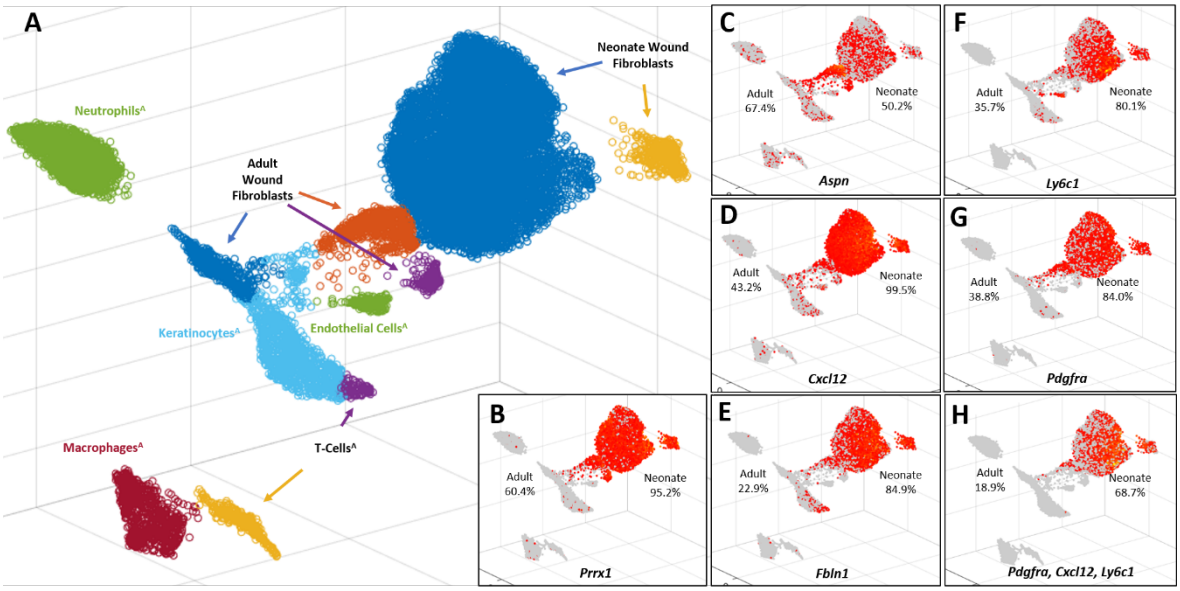

Figure 2.3 scRNAseq analysis of ampWMCs.
A) Uniform manifold approximation and projection (UMAP) plot of from 7,568 adult digit amputation wounds cells (Storer et al., 2020) and 13,470 neonatal ampWMCs. Each circle represents a single cell and cells assigned to the same cluster are similarly colored. Cell-type identities were assigned using the scGEAToolbox. Neonatal and adult (A) amputation wound cells are distinct and do not overlap. UMAP identifies ampWMCs as fibroblasts that form two distinct clusters and three clusters of adult wound fibroblasts. B) UMAP overlay identifying cells expressing Prrx1, a limb-specific fibroblast marker gene. C-G)) UMAP overlays identifying cells expressing key fibroblast marker genes from different adult tissues (Buechler et al., 2021): Aspn (C), Cxcl12 (D), Fbln1 (E), Ly6c1 (F), Pdgfra (G). H) UMAP overlay identifying cells co-expressing Pdgfra, Cxcl12 and Ly6c1. Each red circle identifies a cell expressing the gene(s) of interest, gray regions identify non-expressing cells. The frequency of adult and neonatal cell expression is indicated on the left and right side of each UMAP plot, respectively.

To further confirm the fibroblast identity of ampWMCs, the combined dataset was analyzed for expression of 23 key fibroblast marker genes identified from a whole body adult fibroblast scRNAseq atlas (Buechler et al., 2021). A dual analysis of differential gene expression coupled with the percentage of cells expressing key fibroblast marker genes was carried out for

adult and neonatal wound fibroblasts (15,074 total cells) using the scGEAToolbox. Differential expression analysis identified 10 key fibroblast marker genes expressed at higher levels in adult wound fibroblasts compared to neonatal wound fibroblasts, 4 genes not differentially expressed, and 9 genes expressed at higher levels in neonatal fibroblasts (Table 2.4). The top 4 differentially expressed genes based on expression frequency for adult wound fibroblasts are Aspn (67.4%), Cxcl12 (43.2%), Pdgfra (38,8%) and Ly6c1 (35.7%) and, of these genes, only Aspn was expressed at a higher level in adult wound fibroblasts compared to neonatal fibroblasts (Figure 2.3 B,C,D,F,G). The top 4 differentially expressed genes based on expression frequency for neonatal wound fibroblasts are Cxcl12 (99.4%), Fbln1 (84.7%), Pdgfra (83.7%) and Ly6c1 (80.6%) and all of these genes are enriched in neonatal fibroblasts compared to adult fibroblasts (Figure 2.3D,E,F,G). It is noteworthy that 3 of the 4 fibroblast marker genes expressed at high frequencies in neonatal and adult wound fibroblast populations are overlapping (Cxcl12, Pdgfra, Ly6c1), suggestive that these developmentally distinct digit fibroblast populations are related. The high frequency of fibroblasts expressing all 3 genes, especially in neonatal fibroblasts, suggests that individual fibroblasts are co-expressing multiple key tissue-specific fibroblast genes. Indeed, 68.7% of neonatal amputation wound fibroblasts co-express all 3 fibroblast marker genes whereas the level of co-expression in adult amputation fibroblasts was found to be 18.9% (Figure 2.3H). These results demonstrate that neonatal ampWMCs are fibroblasts and that these cells possess latent chondroprogenitor cell characteristics that can be activated by BMP9. Since neonatal and adult amputations display a similar chondrogenic response to BMP9 in vivo (Yu et al., 2019) and fibroblasts are the predominant non-inflammatory mesenchymal cell type present at the amputation wound (Storer et al., 2020), the results support the conclusion that

BMP9 stimulates chondrogenesis of fibroblasts involved in non-regenerative healing of digit amputation wounds.

BMP9 induces digit fibroblasts to differentiate into articular chondrocytes

Fibroblasts isolated from the unamputated terminal phalangeal element (P3 fibroblasts) can be expanded in culture while retaining position-specific characteristics and regenerative competence (Wu et al., 2013). We tested the BMP9 response of P3 fibroblasts using our chondrogenesis assays. Monolayer cultures of P3 fibroblasts were induced by BMP9 to up-regulated hyaline cartilage and AC genes, while transcripts of hypertrophic cartilage genes were minimally changed (Figure 2.4A). Thus, both neonate ampWMCs (Figure 2.4C) and adult P3 fibroblasts display a rapid chondrogenic respond to BMP9 that is directed toward hyaline cartilage and AC but not hypertrophic cartilage.

MSCs are known precursors for bone, cartilage and adipose tissue (Dominici et al., 2006) and since P3 fibroblasts are heterogenous, MSCs are likely present. BMP9 treated P3 fibroblast cell pellets differentiated chondrocytes indicating chondrogenic potential (Figure 2.4B), however P3 fibroblasts failed to differentiate all other MSC phenotypes when tested using commercially available assays (Figure 2.5A-D) and did not display a cell surface phenotype characteristic of MSCs based on flow cytometry (Figure 2.6E,F), thus P3 fibroblasts cannot be characterized as MSCs (Dominici et al., 2006).

Table 2.4 scRNAseq: Differential Expression and Expression Frequency

				Expression Frequency	Expression Frequency
	Gene	**LogFC**	**Adj P Value**	**Neonate**	**Adult**
Adult>Neonate	*Ccl21a*	Inf	0	0.0%	27.1%
	Sp7	6.43	4.00E-85	0.1%	3.8%
	Ccl19	6.16	3.78E-48	0.1%	2.5%
	Fmod	4.85	7.56E-135	13.4%	34.2%
	Hhip	3.54	6.28E-13	0.3%	1.5%
	Col15a1	3.47	7.68e-320	5.5%	32.8%
	Aspn	3.19	5.14E-153	50.2%	67.4%
	Lepr	2.01	9.76E-10	1.0%	2.7%
	Pi16	1.84	0.656	14.8%	13.4%
	Dpp4	0.98	1.76E-05	1.7%	3.3%
Unchanged	*Npnt*	0.26	0.594	2.1%	2.4%
	Bst1	0.22	0.448	1.6%	1.9%
	Ces1d	Inf	0.297	0.1%	0.0%
	Wt1	Inf	0.163	0.2%	0.0%
Neonate>Adult	*Penk*	6.85	0	71.6%	5.5%
	Coch	4.07	8.00E-47	13.3%	1.0%
	Fbln1	3.70	0	84.9%	22.9%
	Cxcl12	3.50	0	99.5%	43.2%
	Sfrp1	3.27	0	75.7%	25.2%
	Bmp4	2.34	1.49E-90	36.0%	11.8%
	Ly6c1	2.25	1.49E-275	80.7%	35.7%
	Pdgfra	1.63	7.13E-280	84.0%	38.8%
	Comp	1.42	9.73E-228	75.2%	28.4%

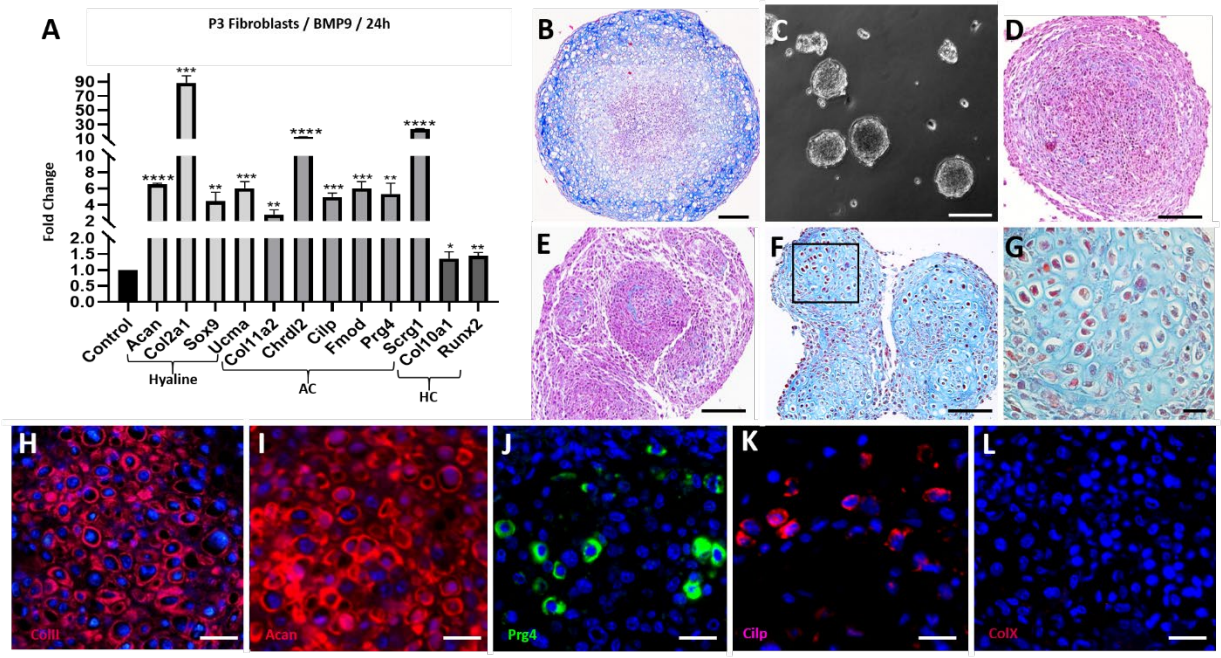

Figure 2.4 P3-BMP9 cultures differentiate hyaline cartilage.
A) P3 monolayer cultures treated with BMP9 (100 ng/ml; 24 hr; N=3) and analyzed by qRT-PCR for chondrogenic gene expression. Hyaline cartilage (Hyaline) and articular cartilage (AC) genes were up-regulated while hypertrophic cartilage (HC) genes were largely unaffected. Statistical analysis: parametric unpaired T-test in Graphpad, ****=P<0.0001; ***=P<0.001; **=P<0.01; *=P<0.05. B) P3-BMP9 pellet cultures (21 days; N=2) differentiate chondrocytes along the periphery but central cells are necrotic. C) P3 SA cultures form cell aggregates after 4-days. D) P3 Control SA cultures (36 days; N=6) enlarge to a size similar to pellet cultures with no evidence of central necrosis. E) P3-BMP2 SA cultures (100 ng/ml; 36 days; N=2) fail to differentiate chondrocytes. F) P3-BMP9 SA cultures (100 ng/ml; 36 days; N=6) differentiate hyaline cartilage. G) High magnification of BMP9 stimulated hyaline cartilage showing chondrocyte doublets surrounded by a collagen rich matrix. H-L) P3-BMP9 SA cultures (100 ng/ml; 36-days; N=2) immunostained for chondrogenic markers. H,I) Hyaline cartilage markers ColII (H) and Acan (I) are expressed by the majority of cells. J,K) AC markers Prg4 (J) and Cilp (K) are expressed by cells scattered throughout the cartilage. L) ColX is not expressed by any cells. Scale bars: B= 200μm; C-F=100μm; G= 20μm; H-L= 25μm.

Cultures of centrifuged P3 fibroblast pellets displayed BMP9-stimulated chondrogenesis of peripheral cells with extensive necrosis in the central region (Figure 2.4B), and this warranted the development of an alternative approach to differentiate cartilage. A 4-day self-aggregation

(SA) protocol in petri dishes was established to promote formation of cell clusters prior to BMP9 treatment (Figure 2.4C). Untreated SA cultures enlarged to form aggregates that approximate the size of cell pellets and after 36 days, histological analysis indicated healthy undifferentiated cells and an absence of necrosis (Figure 2.4D). SA cultures treated with BMP2 (100 ng/ml) also failed to stimulate a chondrogenic response (Figure 2.4E), whereas SA cultures treated with BMP9 (100 ng/ml) formed large cartilage tissue networks that are histologically indistinguishable from hyaline cartilage (Figure 2.4F,G). Immunostaining studies of P3-BMP9 treated aggregates indicate high level expression of Col II (Figure 2.4H) and Aggrecan (Figure 2.4I) confirming chondrocyte differentiation. In addition, cells expressing AC markers, Prg4 (Figure 2.4J) and Cilp (Figure 2.4K) were scattered throughout the cartilage indicating differentiation of articular chondrocytes. Cells expressing Col X were absent indicating that hypertrophic chondrocytes did not differentiate (Figure 2.4AL). Control untreated P3 fibroblast aggregates cultured for 36 days were immuno-negative for ColII, Acan, Prg4, Cilp and ColX (Figure 2.6).

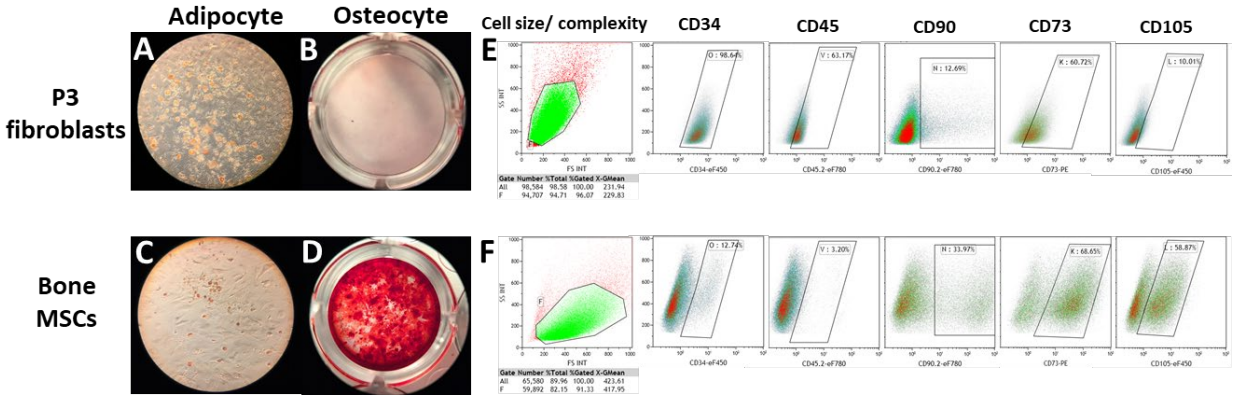

Figure 2.5 Comparison of P3 fibroblasts and bone MSCs with multi-lineage differentiation ability and surface marker profiles.
P3 fibroblasts can differentiate to adipocytes (A) but not osteoblasts (B). Bone MSCs, as a positive control, differentiate both adipocytes (C) and osteoblasts (D). The adipogenic differentiation was

determined by Oil Red O staining and the osteogenic differentiation was identified by Alizarin Red staining. Differentiation experiments were done in triplicate wells. (E) Representative MSC surface marker phenotype by flow cytometry of P3 fibroblasts (N=2) showing that they are positive for CD73, CD34, CD45, and negative to CD90 and CD105. F) MSC surface marker phenotype of bone MSCs showing that they are positive for CD90, CD73, CD105 and negative to CD34 and CD45. The black boxes in E and F identify positive sub-populations with the percentage of cells indicated.

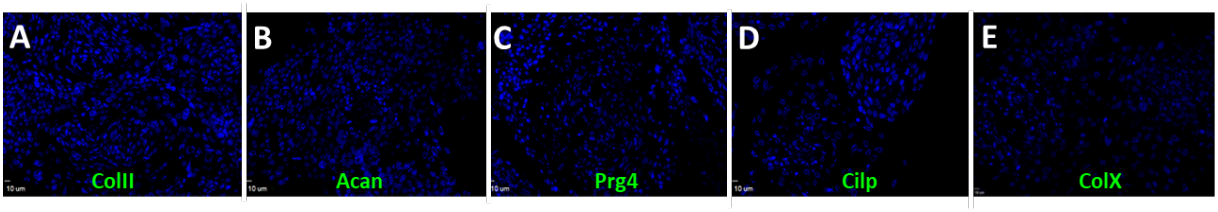

Figure 2.6 Immunofluorescence staining for chondrogenic marker proteins of P3-fibroblast control self-aggregation cultures after 36 days of culture.
Control cultures are immune-negative for ColII (A), Acan (B), Prg4 (C), Cilp (D) and ColX (E) confirming histological studies showing that chondrogenesis is not stimulated in control cultures (N=2). Immuno-stained sections were counterstained with DAPI to label nuclei (blue). Scale bars A-E= 10μm.

The temporal response of P3-BMP9 treated aggregates was analyzed by qRT-PCR for expression of chondrocyte transcripts after different culture times (1, 14 and 36 days). 1 day after BMP9 treatment, hyaline cartilage and AC genes were up regulated whereas hypertrophic cartilage genes were not (Fig 2.7A). This chondrogenic response was similar to that of monolayer cultures of ampWMCs (Figure 2.2C) and P3 fibroblasts (Figure 2.4A) and indicate that culture conditions (i.e. 2-D versus 3-D) do not modify the P3 fibroblast response. At later timepoints this expression profile was qualitatively similar but differed quantitatively (Figure 2.4B-C). All of the hyaline cartilage genes displayed their highest relative level of expression at 14 days with transcript levels declining by 36 days, and most of the AC genes displayed a similar pattern with the exception of Prg4 which showed a continuous increase in transcript levels during

the 36-day timeline. Hypertrophic cartilage transcripts (Col10a1 and Runx2) were largely unaffected by BMP9 treatment at all timepoints analyzed.

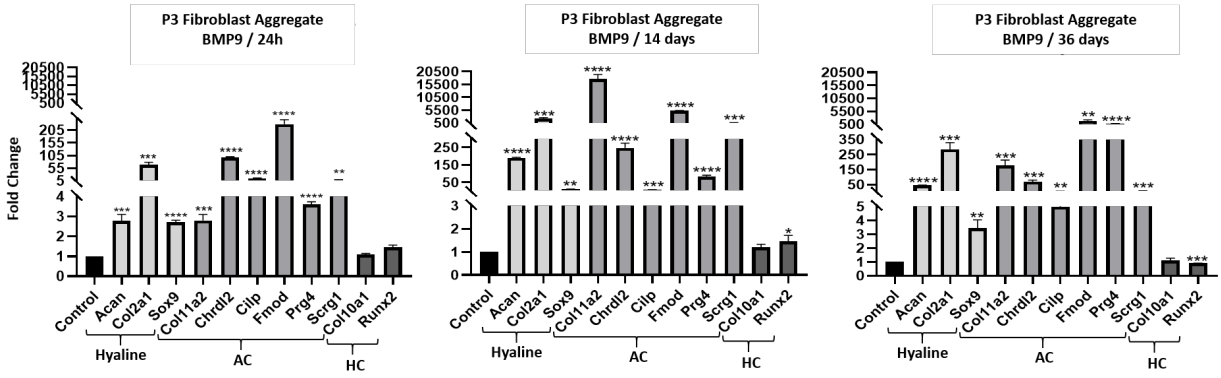

Figure 2.7 BMP9 stimulates chondrogenic gene expression in SA cultures.
qRT-PCR analysis of P3-BMP9 SA cultures treated with BMP9 for 1 (A), 14 (B) and 36 (C) days. At all timepoints, hyaline cartilage (Hyaline) and articular cartilage (AC) genes were up-regulated while hypertrophic cartilage (HC) genes were largely unaffected. Statistical analysis: parametric unpaired T-test in Graphpad, ****=P<0.0001; ***=P<0.001; **=P<0.01; *=P<0.05.

The similarity of the chondrogenic responses between ampWMCs and P3 fibroblasts suggests that the two are related. To explore this hypothesis, microarray analysis of P3-BMP9 treated aggregates was preformed after 3 days of treatment and compared to untreated control aggregates. A total of 6016 differentially expressed transcripts were identified when compared to untreated controls (N=3) (P<0.05; 1.5-fold change). This included 2,428 up-regulated and 3,177 down-regulated transcripts. An analysis of differentially expressed cartilage-related genes (Table 2.2) identified 109 (39 down-regulated and 71 up-regulated) genes (Table 2.3). The list of down-regulated genes included genes associated with joint development (Ors1, Ors2, Cd44), developmentally important transcription factors (Hoxb3, Hoxd3, Scx), and signaling pathways (Bmp2, Bmp4, Bmp6, Fgf18, Prhlh, Rarb, Smad3, Tgfbr2, Wnt7a, Wnt7b, Wnt9a). 8 of the 39

down-regulated chondrogenic genes were also down-regulated by BMP9 in in vivo microarrays, and there were 4 ambiguous genes that were down-regulated by BMP9 in P3-BMP9 treated aggregates but up-regulated by BMP9 in vivo (Ccl3, Chadl, Runx1, Thbs1) (Table 2.3). The list of 71 up regulated chondrogenic genes was remarkable because 43.7% of the genes (31/71) overlapped with BMP9 induced genes in vivo (Table 2.3). Many of the genes are associated with hyaline cartilage and AC, but notably absent were genes associated with hypertrophic cartilage. Overall, the data shows that P3 fibroblasts and ampWMCs respond similarly to BMP9 by differentiating into hyaline cartilage that contains articular chondrocytes.

Amputation wound fibroblasts and P3 fibroblasts both display a similar chondrogenic response to BMP9 yet, wound fibroblasts are derived from non-regenerative digit amputations whereas P3 fibroblasts are expanded from uninjured digit tissue. The role of wound healing in the BMP9 response was investigated by implanting a BMP9 bead into an uninjured adult digit to determine if uninjured fibroblasts displayed a chondrogenic response in vivo. In contrast with the response of wound fibroblasts in neonates and adults that display a robust chondrogenic response to BMP9 (Yu et al., 2019), no chondrogenic response was observed by fibroblasts of uninjured digits (Figure 2.8). These results suggest that digit fibroblasts acquire chondroprogenitor characteristics during the process of amputation injury healing in vivo and, also by enzymatic dissociation and expansion in a 2-dimensional cell culture environment.

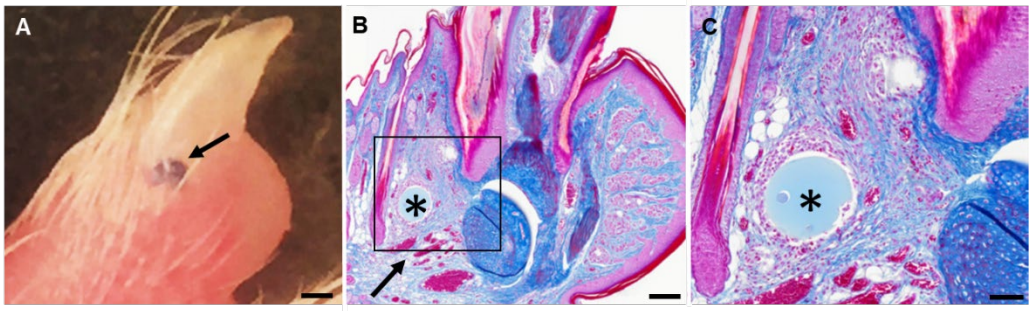

Figure 2.8 in vivo response to BMP9 of injured digit cells.
To test the in vivo response to BMP9 of injured digit cells BMP9 releasing microcarrier beads (500 ng/µl) were implanted into the adult digit in proximity of the P2-P3 joint (N=6). A) External image showing an implanted BMP9 bead (arrow). B) Histological section stained with Mallory's trichome of the P2-P3 joint showing the bead (asterisk) and surrounding tissue 7 days after bead implantation. The BMP9 bead appears to elicit an angiogenic response (arrow) but no chondrocytes are induced. C) High magnification of the box in (B) showing chondrocytes of the endogenous joint but no chondrocytes associated with the BMP9 bead (asterisk). Scale bars: A,B= 200 µm, C= 50µm.

Chondrogenic Stability of P3-BMP9 engineered hyaline cartilage

The cell culture model described here can serve as a foundation to engineer AC for joint repair. To investigate in vivo stability of engineered cartilage, we established an acute joint defect model in the metatarsal-phalangeal (MtP) joint of immunodeficient (NOD/Scid) host mice. The MtP joint consists of the distal end of the metatarsus (Mt) and the proximal end of the first phalangeal (P1) element (Figure 2.9A). Abutting AC surfaces are histologically similar: each consists of two prominent zones that are identified as middle and deep (Figure 2.9B). Scattered flattened cells are observed on the AC surface but these cells do not form a contiguous superficial cell layer and are not immuno-positive for Prg4. Subchondral bone separates the AC layers from the bone marrow. Acan immuno-positive cells are specific to both middle and deep layers and identify the AC (Figure 2.9C). A defect in the P1 AC is created surgically by removing the central segment and subchondral bone thereby exposing the joint cavity to the bone marrow (Figure 2.9D). Control joint defects in which excised tissue was immediately

transplanted back into the defect demonstrates that implanted tissue survives and retains a differentiated phenotype after a 90-day engraftment period (Figure 2.9E,F).

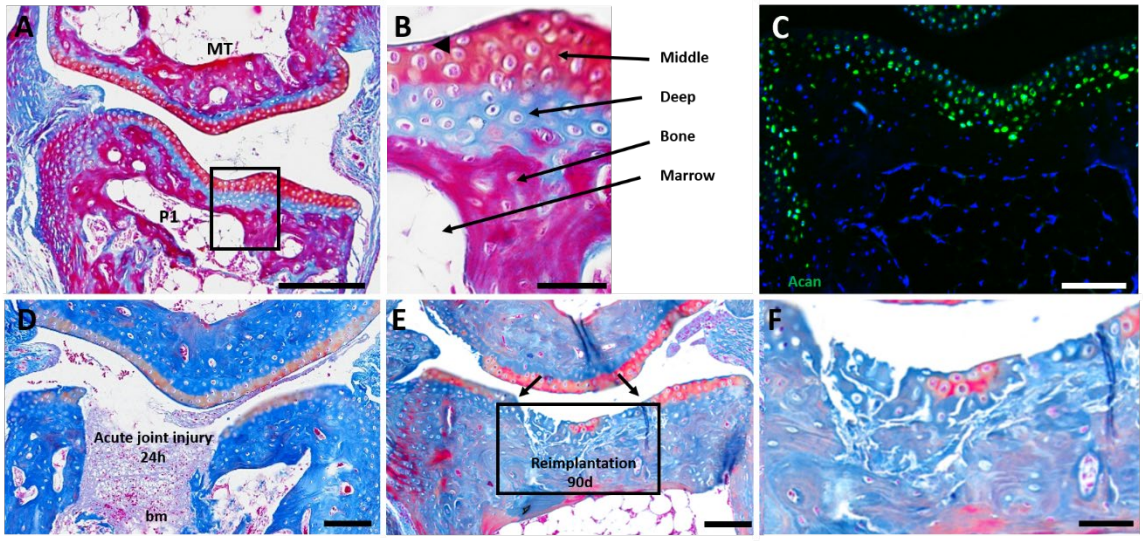

Figure 2.9 Metatarsal-phalangeal (MtP) joint defect.
A-B) Abutting AC surfaces each display a layered organization consisting of a middle layer and a deep layer (N=2). A single flattened superficial cell is shown in B (arrowhead) but these cells are infrequent and do not form a continuous cell layer. C) Articular chondrocytes of the middle and deep layers are characterized by the expression of Acan (N=3). D) An acute defect of the phalangeal surface removes the AC and underlying bone exposing the joint to the bone marrow (bm). 24 hours after injury the acute defect is filled with cells contiguous with the bone marrow (N=4). E-F) Re-engrafted excised AC after 3 months contained cells that retained staining characteristics of articular chondrocytes (N=3). Scale bars: A= 200μm; B=40μm; C-E= 100μm; F= 50μm.

The stability of P3-BMP9 engineered hyaline cartilage was tested by implantation into the joint defect. Hyaline cartilage was engineered using Gfp expressing P3 fibroblasts (Gfp-P3) and after 36 days in culture the resulting tissue was engrafted into the joint defect. Histological and immunohistochemical analyses (GFP, Acan and ColX) after 28 and 90 days determined implant survival, integration with host tissues, and retention of cartilage characteristics. Control implants engineered without BMP9 treatment (n=7) (see Figure 2.4D and Figure 2.6) did not

form cartilage after implantation (Figure 2.10A) but filled the defect with matrix that was largely acellular (Figure 2.10B-D) indicating that cell survival was compromised.

Implants of P3-BMP9 engineered hyaline cartilage analyzed at 28-days (n=6) and 90 days (n=12) were equivocal. All samples survived and maintained a hyaline chondrogenic phenotype, but no samples were found to completely integrate with host tissues (Figure 2.10E,I). Implanted cartilage adhered tightly with host bone tissue, but not with host AC where gaps between host and implanted cartilage are apparent. GFP immunostaining confirmed implanted cartilage survival and demonstrated continuity within the implant as well as sharp boundaries with unlabeled host cells (Figure 2.10F,J). Overall, there was little evidence of cell invasion into host tissues or vice versa, although individual GFP positive cells were occasionally observed in neighboring host tissue (Figure 2.10F). Immunostaining identified Acan expression by chondrocytes throughout the implanted tissue indicating that engrafted cells maintained chondrogenic characteristics (Figure 2.10G,K). Double immunostaining for GFP and Acan identified numerous double-labeled cells within the engrafted tissue confirmed that many implanted cells retained a chondrogenic phenotype although the level of co-expression was not 100% (Figure 2.10H,L). These studies indicate that the chondrogenic phenotype of BMP9 engineered hyaline cartilage from P3 fibroblast aggregates was maintained following engraftment into an acute joint defect.

Implants of P3-BMP9 engineered hyaline cartilage analyzed at 28-days (n=6) and 90 days (n=12) were equivocal. All samples survived and maintained a hyaline chondrogenic phenotype, but no samples were found to completely integrate with host tissues (Figure 2.10E,I). Implanted cartilage adhered tightly with host bone tissue, but not with host AC where gaps between host and implanted cartilage are apparent. GFP immunostaining confirmed implanted

cartilage survival and demonstrated continuity within the implant as well as sharp boundaries with unlabeled host cells (Figure 2.10F,J). Overall, there was little evidence of cell invasion into host tissues or vice versa, although individual GFP positive cells were occasionally observed in neighboring host tissue (Figure 2.10F). Immunostaining identified Acan expression by chondrocytes throughout the implanted tissue indicating that engrafted cells maintained chondrogenic characteristics (Figure 2.10G,K). Double immunostaining for GFP and Acan identified numerous double-labeled cells within the engrafted tissue confirmed that many implanted cells retained a chondrogenic phenotype although the level of co-expression was not 100% (Figure 2.10H,L). These studies indicate that the chondrogenic phenotype of BMP9 engineered hyaline cartilage from P3 fibroblast aggregates was maintained following engraftment into an acute joint defect.

A major concern of AC engineering is that implanted cartilage can undergo endochondral ossification leading to pathological osteogenesis (Ripmeester et al., 2018). To determine if pathological progression of engrafted tissue or surrounding host tissue occurred, 90-day samples were analyzed for ColX expression to determine the presence of hypertrophic chondrocytes. Hypertrophic chondrocytes are not observed in the intact MtP joint or in engineered hyaline cartilage prior to transplantation, so their presence following engraftment would suggest in vivo conditions that promoted pathological osteogenesis. Hypertrophic chondrocytes were not found in 4 of the 12 (33.3%) samples (Figure 2.10M), but 8 samples (66.6%) contained individual hypertrophic chondrocytes. 3 of the 8 positive samples contained only host-derived hypertrophic chondrocytes (Figure 2.10N), 3 samples contained only graft-derived cells (Figure 2.10O), and 2 samples contained both host- and graft-derived cells. The presence of graft-derived hypertrophic chondrocytes indicated that P3-BMP9 engineered hyaline cartilage maintains a potential for

hypertrophic chondrocyte differentiation. To test this, P3-BMP9 engineered hyaline cartilage (36-day cultures) were cultured an additional 20 days in BMP2 (P3-BMP9-BMP2) or, as a control, in BMP9. Control P3-BMP9 cultures (56 days) maintained a hyaline cartilage phenotype that was confirmed based on histology, qRT-PCR, and ColX immunostaining (Figure 2.11A,B,D), whereas P3-BMP9-BMP2 cultures were found to contain numerous ColX positive hypertrophic chondrocytes (Figure 2.11C). These studies indicate that P3-BMP9 engineered hyaline cartilage retain a potential for hypertrophic chondrocyte differentiation and suggest that the acute joint defect can promote pathological osteogenesis of engrafted hyaline cartilage. These engraftment studies indicate that the differentiative state of engineered AC prior to engraftment will be important to minimize post engraftment osteogenesis.

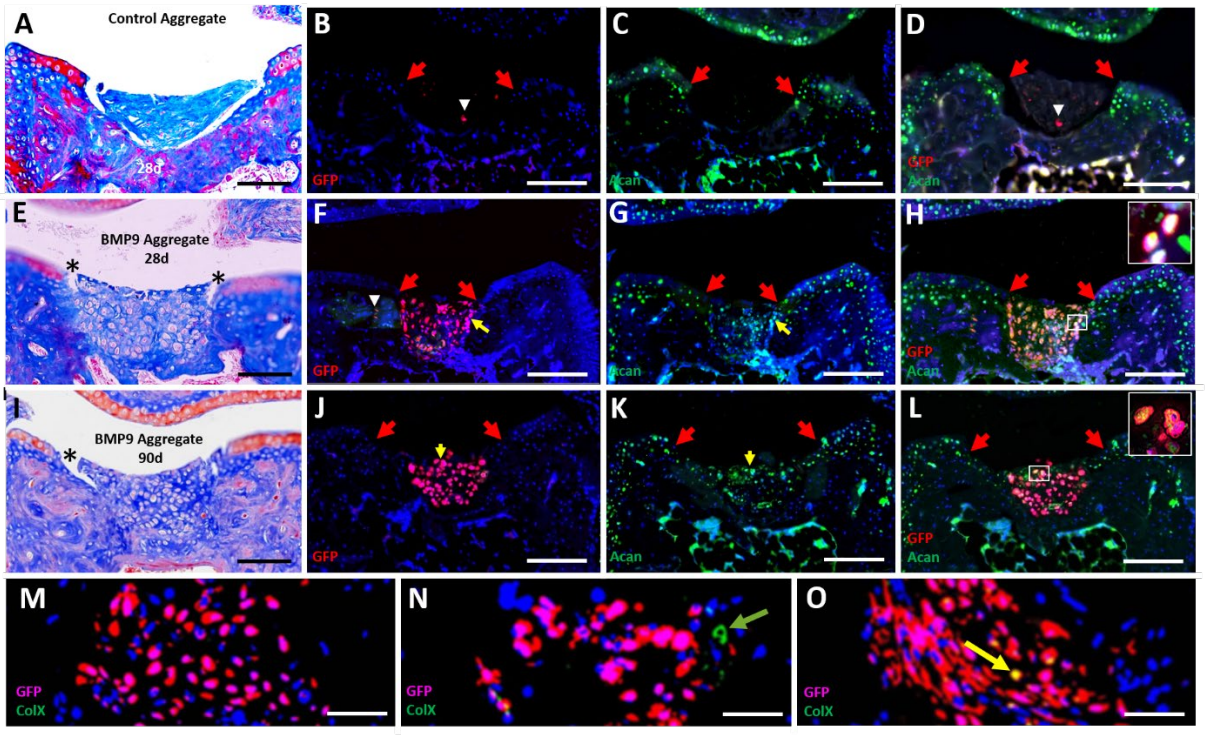

Figure 2.10 Engraftment of P3-BMP9 engineered hyaline cartilage into the MtP joint defect.

Red arrows identify the boundary of the injury in immuno-stained sections in C-D; F-H; J-L. A-D) Engrafted control tissue from untreated P3 SA cultures (36 days) after 28 days. A) Histological assessment: engrafted tissue appears acellular and not integrated with host tissues. B) GFP immunostaining identified few positive cells (white arrowhead) associated with the implant. C) Acan immunostaining indicates the implanted tissue is devoid of Acan positive cells. D) Overlay of GFP and Acan immuno-staining shows that GFP positive cells (white arrowhead) are negative for Acan. E-H) Hyaline cartilage implants from P3-BMP9 SA cultures (36 days; N=6)) analyzed after 28 days. E) Histological assessment: the MtP defect contains cartilage tissue that is tightly adherent to surrounding bone tissue but not adherent to surface AC (*). F) GFP immunostaining is localized to the joint defect with a few GFP positive cells (white arrowhead) invading neighboring host tissue. G) Acan immunostaining identifies immuno-positive chondrocytes within the implanted tissue. H) Overlay of GFP and Acan immunostaining demonstrates Acan expression by implanted cells. Inset shows a double labeled cell cluster at high resolution. Yellow arrows in F and G identify the cell cluster shown at high resolution. I-L) Hyaline cartilage implants from P3-BMP9 SA cultures (36 days; N=12) analyzed after 90 days. I) Histological assessment: the MtP defect contains cartilage tissue that is tightly adherent to surrounding bone tissue but not adherent to surface AC (*). J) GFP immunostaining is localized to the joint defect. K) Immunostaining identifies Acan positive cells spanning the joint defect. L) Overlay of GFP and Acan immunostaining shows that implanted cells maintain expression of Acan. Inset shows a double labeled cell cluster at high resolution. Yellow arrows in J and K identify the cell cluster shown at high resolution. M-O) Double immunostaining for GFP and ColX. M) ColX positive cells were not found in 4 of 12 samples. N) ColX positive/GFP negative cells (green arrow) were found in 5 of 12 samples. O) ColX positive/GFP positive cells (yellow arrow) were found in 5 of 12 samples. Scale bars: A,E,I= 100µm,B-D, F-H, J-L= 200□m, M-O= 50µm.

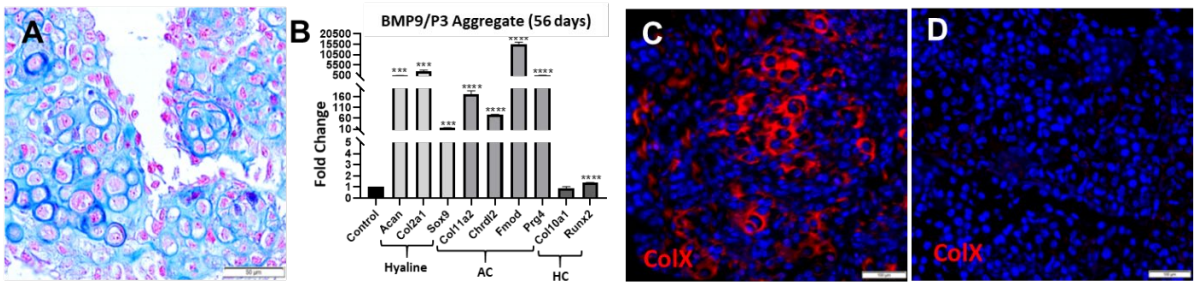

Figure 2.11 P3 aggregates cultured with BMP9 for 56 days can be induced to differentiate hypertrophic chondrocytes by BMP2 treatment.
A) P3 aggregates cultured with BMP9 for 56 days maintain a chondrogenic phenotype based on histological staining with Mallory's trichrome. B) qRT-PCR analysis of 56-day BMP9 treated cultures indicate that hyaline cartilage and articular cartilage specific genes are expressed at levels comparable to 36-day cultures and that hypertrophic cartilage specific genes are not minimally expressed. C) When 36-day BMP9 treated chondrogenic aggregates were treated with BMP2 instead of BMP9 for the 20 day period from 36 days to 56 days, many chondrocytes were found to be immuno-positive for ColX indicating hypertrophic chondrocyte differentiation (N=2). D) Control aggregates treated continuously with BMP9 for 56 days were immuno-negative for ColX (N=2). Immuno-stained sections were counterstained with DAPI to label nuclei (blue). Scale bar in A=50µm, C,D=100µm.

2.5 Discussion

Endogenous joint repair and AC regeneration in mammals does not readily occur so the demonstration that BMP9 stimulates joint and AC regeneration at a non-regenerative amputation wound in mice warrants further mechanistic investigation. There are two distinct outcomes from these studies. The first involves the biological response to BMP9 as a regeneration-inducing agent in vivo, and the second involves exploration of a regenerative medicine strategy aimed at engineering AC. While regeneration biology and regenerative medicine share a common interest, i.e. regeneration, these two fields remain largely separate. Regeneration biology is focused on models that display a high level of endogenous regenerative capabilities, for example invertebrates, fish and amphibians, whereas regenerative medicine is focused on mammals, particularly humans, that display relatively poor regenerative capabilities. The development of mammalian models of endogenous regenerative responses (Seifert and Muneoka, 2018) and the demonstration that regeneration can be stimulated at non-regenerative injury sites in mice (Dawson et al., 2017; Han et al., 2003; Ide, 2012; Masaki and Ide, 2007; Yu et al., 2019; Yu et al., 2010; Yu et al., 2012) provide an opportunity to bridge these two disparate but related fields. By focusing on BMP9 stimulated AC regeneration in vivo and in vitro we have established a novel strategy for investigating regeneration and regenerative failure in mammals that can impact therapeutic strategies for regenerative medicine.

Regeneration Biology

Following amputation, the mammalian digit is non-regenerative with the exception that the digit tip possesses endogenous regenerative ability (Muneoka et al., 2008; Simkin et al., 2015; Storer and Miller, 2020). This regenerative response in mice represents a rare example of blastema-mediated epimorphic regeneration in mammals. Canonical BMP signaling is required

for regeneration (Han et al., 2003; Yu et al., 2010) but surprisingly, BMP9 treatment also inhibits digit tip regeneration by precociously stimulating Vegfa-mediated angiogenesis during blastema formation (Yu et al., 2014). Alternatively, BMP9 stimulates joint regeneration at non-regenerative amputation wounds but this response is not associated with enhanced angiogenesis (Yu et al., 2019) nor enhanced Vegfa expression (see Supplemental Excel files 1 and 2). Stimulation of non-regenerative amputation wounds by BMP9 or BMP2 (Yu et al., 2012) directly stimulates chondroprogenitor cells and does not involve blastema formation, so amputation level dependent BMP9 effects reflect differences in BMP9 responsive cells present at regenerating versus non-regenerative wounds. Supporting this conclusion, BMP9 either enhances or inhibits angiogenesis in different experimental model systems (Scharpfenecker et al., 2007; Xiao et al., 2020), and is known to display a context-dependent response on vascular development (Chen et al., 2013). Thus, the stimulatory and inhibitory effects of BMP9 in different regeneration models can be explained by its role in regulating angiogenesis during blastema formation on the one hand and stimulating chondroprogenitor cells on the other.

Amputation at the level of the second phalanx is a model of fibrotic healing and regenerative failure that can be stimulated to regenerate (Dawson et al., 2016; Turner et al., 2010; Yu et al., 2012). Treatment of the amputation wound with BMP2 or BMP7 stimulates skeletal regeneration by endochondral ossification where differentiating hypertrophic chondrocytes mediate the regeneration of new bone (Dawson et al., 2017; Yu et al., 2010; Yu et al., 2012). Alternatively, BMP9 stimulates joint regeneration inducing ectopic hyaline cartilage coupled with a synovial cavity that articulates with the stump bone (Yu et al., 2019). Both responses initiate with induced early chondrogenic genes (i.e. Col2a1, Sox9) but with distinct outcomes; hypertrophic cartilage precedes skeletal regeneration, whereas hyaline cartilage

precedes AC regeneration. BMP9 stimulates a rapid up-regulation of genes specifically associated with AC and not hypertrophic cartilage indicating that BMP9 directs chondroprogenitor cell differentiation toward articular chondrocytes and not hypertrophic chondrocytes. It is noteworthy that hypertrophic chondrocytes can be induced in P3-BMP9 engineered hyaline cartilage in vivo, and in vitro following treatment with BMP2, indicating a differentiation potential that is actively inhibited by BMP9. Thus, BMP9 represents an inducer of AC differentiation during joint regeneration.

The cells responding to BMP9 are the fibroblasts of the amputation wound. P2 amputation undergoes non-regenerative wound healing and fibroblasts are the principal mesenchymal cell type involved in the response (Storer et al., 2020). Amputation wound fibroblasts are stimulated by BMP9 to initiate a chondrogenic program that results in the differentiation hyaline cartilage in vivo and in vitro. Fibroblast re-programming into chondrocytes has been demonstrated by ectopic gene expression (Hiramatsu et al., 2011) indicating chondrogenic potential. In amphibian limb regeneration, amputation wound fibroblasts over-contribute to blastema formation and undergo chondrogenesis to form the hyaline cartilage anlagen of the regenerating limb (Dunis and Namenwirth, 1977; Kragl et al., 2009; Muneoka et al., 1986). Thus, the presence of wound fibroblasts at non-regenerating mammalian amputations with chondroprogenitor characteristics is predicted based on an evolved regenerative failure model (Muneoka and Dawson, 2020; Sanchez Alvarado, 2000). How chondroprogenitor fibroblasts arise at the mammalian amputation wound remains unclear since chondrogenesis is not stimulated by treatment of uninjured or immediately amputated digits with either BMP9 (Supplemental Figure 4) or BMP2 (Dawson et al., 2017). One explanation is that fibroblasts respond to amputation injury by dedifferentiation to a developmentally immature

phenotype thereby acquiring a chondroprogenitor phenotype (Gerber et al., 2018). In mammals, this idea is supported by the demonstration that non-regenerative fibroblasts can participate in regeneration and display epithelial-mesenchymal signaling characteristics reminiscent of early development (Wu et al., 2013).

Regenerative Medicine

The successful stimulation of AC regeneration in vivo provides the impetus to explore the potential for translational repair in humans. A clinically successful approach to engineering AC is a complex problem that includes 1) identification of a cell source, 2) establishing a differentiation protocol, and 3) post-transplantation assessment of tissue survival, integration, and maintenance of differentiation (Iwamoto et al., 2013). Most approaches to engineering AC utilize stem cells because they represent a plentiful cell source and a differentiation protocol involving high density cell cultures treated with TGF (Correa and Lietman, 2017). Unfortunately, a common clinical outcome of implanted cartilage engineered using this approach is a transient repair response with chondrocytes eventually differentiating into fibrocartilage or hypertrophic cartilage (Demoor et al., 2014; Somoza et al., 2014). The current study establishes a completely novel approach to AC engineering that exploits the chondrogenic response of an in vivo joint regenerative response (Yu et al., 2019). Fibroblasts of the amputation wound represent a BMP9 responsive chondroprogenitor cell type, and the P3 fibroblast cell line (Wu et al., 2013) displays an analogous chondrogenic response that establishes a limitless cell source for AC differentiation studies. A novel self-aggregation protocol was developed to maximize hyaline cartilage differentiation, and an acute joint defect model was established to evaluate the quality of engineered cartilage. Overall, these studies establish a comprehensive regenerative engineering strategy for AC that is rooted in an endogenous regenerative response.

Mammalian cartilage is not inherently regenerative so strategies to engineer cartilage have been established empirically. Historically, spontaneous chondrogenic differentiation was observed when dissociated limb bud cells are cultured at high density to mimic chondrogenic condensation (Gay and Kosher, 1984). Stem cells cultured at high density are inherently non-chondrogenic however, chondrocytes differentiate when cultures of MSCs are treated with TGFβ1 or TGFβ3 (Johnstone et al., 1998; Mackay et al., 1998). TGFβ signaling involves binding and activation of the TGFβR1/TGFβRII receptor complex, but disruption of this signaling pathway does not influence embryonic chondrogenesis suggesting that induced chondrogenesis by TGFβ signaling is indirect (Wang et al., 2020). TGFβR1 was found to repress formation of the high affinity receptor complex for BMP9, Alk1/ActRIIb, (Townson et al., 2012), thus implicating BMP9 signaling in embryonic chondrogenesis (Wang et al., 2019). The current findings coupled with previous findings that BMP9 induces chondrogenesis in a number of different cell culture models (Cheng et al., 2016; Majumdar et al., 2001; Morgan et al., 2020; Seemann et al., 2009) support the conclusion that BMP9 is a highly effective inducer of chondrogenesis, particularly articular chondrocytes.

The BMP9 chondrogenic response of P3 fibroblasts is rapid and robust, and represents an empirical assay, both in vivo and in vitro, for chondroprogenitor cells. Direct application of BMP9 to the uninjured digit fails to elicit a chondrogenic response indicating an absence of BMP9 responsive chondroprogenitor cells. The chondrogenic response of P3 fibroblasts in vitro suggests that the sourcing of cells for culture transitions them from a non-chondroprogenitor state to chondroprogenitor cells, and a similar transition occurs during the healing response following digit amputation. This suggests that sourcing of fibroblasts for culture mimics the amputation healing response in vivo; both acquire chondroprogenitor characteristics that are

absent in the uninjured digit. What does cell sourcing and amputation wound healing have in common that might be responsible for transitioning chondrogenic potential of fibroblasts? The answer to this question has implications for regenerative engineering in general since many strategies begin with the isolation and expansion of a cell source. One potential answer to this question centers around enzymatic digestion of tissues to release individual cells for culture. An in vivo equivalent is the histolytic response of tissues undergoing regenerative and non-regenerative wound healing following digit amputation (Dawson et al., 2016; Fernando et al., 2011), which correlates with amputation enhanced expression of ECM degrading enzymes, e.g. matrix metalloproteases (Johnson et al., 2020; Storer et al., 2020). The suggests that enzymatic ECM digestion can serve as a general activator of latent progenitor cell characteristics that are otherwise masked in uninjured tissues.

The technique of centrifugation to create 3-D high-density cell cultures that initiate chondrogenesis is widely used however, the chondrogenic response is attenuated in central regions of the pellet that become necrotic. Central necrosis is likely attributed to reduced oxygen and/or nutrient availability. As a tissue, cartilage is avascular so chondrocytes are expected to be adaptive to hypoxic conditions (Anderson et al., 2018), however progenitor cells prior to induction are potentially sensitive to hypoxic conditions. The strategy of self-aggregation was employed to encourage cells to establish high density culture conditions progressively and this protocol was found to prevent regional necrosis while allowing cultures to enlarge to sizes comparable to cell pellets. BMP9 treatment of cell aggregates stimulates chondrogenic gene expression within 24 hours indicating a rapid onset of chondrogenesis and, under conditions of continuous BMP9 treatment, aggregate size progressively increases along with a quantitative enhancement of chondrogenic genes expression. The increase in aggregate size is, in part, due to

chondrocyte proliferation since there is clear histological evidence of isogenous chondrocyte groups within P3-BMP9 engineered hyaline cartilage (see Fig 3G). Self-aggregation represents a simple culture model to explore mechanisms guiding the growth and differentiation of hyaline cartilage and has the potential for engineering tissue to sizes that are clinically relevant.

Given the clinical importance of joint disabilities and the potential for cell-based regenerative strategies, there are few transplantation models that allow for critical evaluation of transplanted tissue survival, stability, and integration with injured host tissues. Ectopic implantation of engineered cartilage demonstrates graft survival and stability (Craft et al., 2015; Hiramatsu et al., 2011), but not tissue integration or the influence host tissues. Large animal models are clinically relevant (Frisbie et al., 2015) but reduced sample size and a lack of cell lineage markers compromise detailed assessment of transplanted tissue. We have developed an acute MtP joint defect in immunodeficient hosts coupled with genetically labeling (GFP) of engineered cartilage for accessing graft survival, stability, integration and injury site effects. Following engraftment, engineered hyaline cartilage does not mature into AC indicating a need to improve articular chondrocyte differentiation prior to engraftment. Engineered hyaline cartilage integrate with host bone but there is little integration with host articular cartilage consistent with previous studies (Bhumiratana et al., 2014). Differentiation of hypertrophic chondrocytes indicate that the injury site can be detrimental to the long-term stability of engrafted cells. Future studies are required to determine whether the hypertrophic chondrocytes are derived from hyaline chondrocytes versus undifferentiated chondroprogenitor cells of the engineered cartilage. Answering this question will be important for understanding the pathological progression of transplanted cartilage. Since digit joints are not predicted to be subjected to significant mechanical load, the variability of the hypertrophic chondrocyte response

may reflect the importance of load for osteophyte development following acute joint damage. The MtP joint injury model represents a simple and economical way to assess and improve engraftment outcomes of future regenerative engineering strategies.

2.6 References

118. Aigner, T., Stove, J., 2003. Collagens--major component of the physiological cartilage matrix, major target of cartilage degeneration, major tool in cartilage repair. Adv Drug Deliv Rev 55, 1569-1593.
119. Anderson, D.E., Markway, B.D., Weekes, K.J., McCarthy, H.E., Johnstone, B., 2018. Physioxia Promotes the Articular Chondrocyte-Like Phenotype in Human Chondroprogenitor-Derived Self-Organized Tissue. Tissue Eng Part A 24, 264-274.
120. Bhumiratana, S., Eton, R.E., Oungoulian, S.R., Wan, L.Q., Ateshian, G.A., Vunjak-Novakovic, G., 2014. Large, stratified, and mechanically functional human cartilage grown in vitro by mesenchymal condensation. Proc Natl Acad Sci U S A 111, 6940-6945.
121. Bi, W., Deng, J.M., Zhang, Z., Behringer, R.R., de Crombrugghe, B., 1999. Sox9 is required for cartilage formation. Nat Genet 22, 85-89.
122. Brittberg, M., Lindahl, A., Nilsson, A., Ohlsson, C., Isaksson, O., Peterson, L., 1994. Treatment of deep cartilage defects in the knee with autologous chondrocyte transplantation. N Engl J Med 331, 889-895.
123. Buechler, M.B., Pradhan, R.N., Krishnamurty, A.T., Cox, C., Calviello, A.K., Wang, A.W., Yang, Y.A., Tam, L., Caothien, R., Roose-Girma, M., Modrusan, Z., Arron, J.R., Bourgon, R., Muller, S., Turley, S.J., 2021. Cross-tissue organization of the fibroblast lineage. Nature 593, 575-579.
124. Cai, J.J., 2019. scGEAToolbox: a Matlab toolbox for single-cell RNA sequencing data analysis. Bioinformatics.
125. Chen, H., Brady Ridgway, J., Sai, T., Lai, J., Warming, S., Roose-Girma, M., Zhang, G., Shou, W., Yan, M., 2013. Context-dependent signaling defines roles of BMP9 and BMP10 in embryonic and postnatal development. Proc Natl Acad Sci U S A 110, 11887-11892.
126. Cheng, A., Gustafson, A.R., Schaner Tooley, C.E., Zhang, M., 2016. BMP-9 dependent pathways required for the chondrogenic differentiation of pluripotent stem cells. Differentiation 92, 298-305.

127. Correa, D., Lietman, S.A., 2017. Articular cartilage repair: Current needs, methods and research directions. Semin Cell Dev Biol 62, 67-77.

128. Craft, A.M., Rockel, J.S., Nartiss, Y., Kandel, R.A., Alman, B.A., Keller, G.M., 2015. Generation of articular chondrocytes from human pluripotent stem cells. Nat Biotechnol 33, 638-645.

129. Dawson, L.A., Brunauer, R., Zimmel, K.N., Qureshi, O., Falck, A.R., Kim, P., Dolan, C.P., Yu, L., Lin, Y.L., Daniel, B., Yan, M., Muneoka, K., 2019. Adult Mouse Digit Amputation and Regeneration: A Simple Model to Investigate Mammalian Blastema Formation and Intramembranous Ossification. J Vis Exp.

130. Dawson, L.A., Simkin, J., Sauque, M., Pela, M., Palkowski, T., Muneoka, K., 2016. Analogous cellular contribution and healing mechanisms following digit amputation and phalangeal fracture in mice. Regeneration (Oxf) 3, 39-51.

131. Dawson, L.A., Yu, L., Yan, M., Marrero, L., Schanes, P.P., Dolan, C., Pela, M., Peterson, B., Han, M., Muneoka, K., 2017. The periosteal requirement and temporal dynamics of BMP2-induced middle phalanx regeneration in the adult mouse. Regeneration 4.

132. Demoor, M., Ollitrault, D., Gomez-Leduc, T., Bouyoucef, M., Hervieu, M., Fabre, H., Lafont, J., Denoix, J.M., Audigie, F., Mallein-Gerin, F., Legendre, F., Galera, P., 2014. Cartilage tissue engineering: molecular control of chondrocyte differentiation for proper cartilage matrix reconstruction. Biochim Biophys Acta 1840, 2414-2440.

133. Dolan, C.P., Dawson, L.A., Muneoka, K., 2018. Digit Tip Regeneration: Merging Regeneration Biology with Regenerative Medicine. Stem Cells Transl Med 7, 262-270.

134. Dominici, M., Le Blanc, K., Mueller, I., Slaper-Cortenbach, I., Marini, F., Krause, D., Deans, R., Keating, A., Prockop, D., Horwitz, E., 2006. Minimal criteria for defining multipotent mesenchymal stromal cells. The International Society for Cellular Therapy position statement. Cytotherapy 8, 315-317.

135. Dunis, D.A., Namenwirth, M., 1977. The role of grafted skin in the regeneration of x-irradiated axolotl limbs. Dev Biol 56, 97-109.

136. Fernando, W.A., Leininger, E., Simkin, J., Li, N., Malcom, C.A., Sathyamoorthi, S., Han, M., Muneoka, K., 2011. Wound healing and blastema formation in regenerating digit tips of adult mice. Dev Biol 350, 301-310.

137. Ferrari, D., Kosher, R.A., 2002. Dlx5 is a positive regulator of chondrocyte differentiation during endochondral ossification. Dev Biol 252, 257-270.

138. Finak, G., McDavid, A., Yajima, M., Deng, J., Gersuk, V., Shalek, A.K., Slichter, C.K., Miller, H.W., McElrath, M.J., Prlic, M., Linsley, P.S., Gottardo, R., 2015. MAST: a flexible statistical framework for assessing transcriptional changes and characterizing heterogeneity in single-cell RNA sequencing data. Genome Biol 16, 278.

139. Firner, S., Zaucke, F., Michael, J., Dargel, J., Schiwy-Bochat, K.H., Heilig, J., Rothschild, M.A., Eysel, P., Bruggemann, G.P., Niehoff, A., 2017. Extracellular

Distribution of Collagen II and Perifibrillar Adapter Proteins in Healthy and Osteoarthritic Human Knee Joint Cartilage. J Histochem Cytochem 65, 593-606.

140. Franzen, O., Gan, L.M., Bjorkegren, J.L.M., 2019. PanglaoDB: a web server for exploration of mouse and human single-cell RNA sequencing data. Database (Oxford) 2019.

141. Frisbie, D.D., McCarthy, H.E., Archer, C.W., Barrett, M.F., McIlwraith, C.W., 2015. Evaluation of articular cartilage progenitor cells for the repair of articular defects in an equine model. J Bone Joint Surg Am 97, 484-493.

142. Gaddy-Kurten, D., Coker, J.K., Abe, E., Jilka, R.L., Manolagas, S.C., 2002. Inhibin suppresses and activin stimulates osteoblastogenesis and osteoclastogenesis in murine bone marrow cultures. Endocrinology 143, 74-83.

143. Gay, S.W., Kosher, R.A., 1984. Uniform cartilage differentiation in micromass cultures prepared from a relatively homogeneous population of chondrogenic progenitor cells of the chick limb bud: effect of prostaglandins. J Exp Zool 232, 317-326.

144. Gerber, T., Murawala, P., Knapp, D., Masselink, W., Schuez, M., Hermann, S., Gac-Santel, M., Nowoshilow, S., Kageyama, J., Khattak, S., Currie, J.D., Camp, J.G., Tanaka, E.M., Treutlein, B., 2018. Single-cell analysis uncovers convergence of cell identities during axolotl limb regeneration. Science 362.

145. Han, M., Yang, X., Farrington, J.E., Muneoka, K., 2003. Digit regeneration is regulated by Msx1 and BMP4 in fetal mice. Development 130, 5123-5132.

146. Han, M., Yang, X., Lee, J., Allan, C.H., Muneoka, K., 2008. Development and regeneration of the neonatal digit tip in mice. Dev Biol 315, 125-135.

147. Hiramatsu, K., Sasagawa, S., Outani, H., Nakagawa, K., Yoshikawa, H., Tsumaki, N., 2011. Generation of hyaline cartilaginous tissue from mouse adult dermal fibroblast culture by defined factors. J Clin Invest 121, 640-657.

148. Humason, G.L., 1962. Animal tissue techniques. W.H. Freeman, San Francisco,.

149. Ide, H., 2012. Bone pattern formation in mouse limbs after amputation at the forearm level. Dev Dyn 241, 435-441.

150. Iwamoto, M., Ohta, Y., Larmour, C., Enomoto-Iwamoto, M., 2013. Toward regeneration of articular cartilage. Birth Defects Res C Embryo Today 99, 192-202.

151. Johnson, G.L., Masias, E.J., Lehoczky, J.A., 2020. Cellular Heterogeneity and Lineage Restriction during Mouse Digit Tip Regeneration at Single-Cell Resolution. Dev Cell 52, 525-540 e525.

152. Johnstone, B., Hering, T.M., Caplan, A.I., Goldberg, V.M., Yoo, J.U., 1998. In vitro chondrogenesis of bone marrow-derived mesenchymal progenitor cells. Exp Cell Res 238, 265-272.

153. Klepsch, S., Jamnig, A., Trimmel, D., Schimke, M., Kapferer, W., Brunauer, R., Singh, S., Reitinger, S., Lepperdinger, G., 2013. Isolation of mesenchymal stem cells from human bone and long-term cultivation under physiologic oxygen conditions. Methods Mol Biol 976, 99-109.

154. Kozhemyakina, E., Zhang, M., Ionescu, A., Ayturk, U.M., Ono, N., Kobayashi, A., Kronenberg, H., Warman, M.L., Lassar, A.B., 2015. Identification of a Prg4-expressing articular cartilage progenitor cell population in mice. Arthritis Rheumatol 67, 1261-1273.

155. Kragl, M., Knapp, D., Nacu, E., Khattak, S., Maden, M., Epperlein, H.H., Tanaka, E.M., 2009. Cells keep a memory of their tissue origin during axolotl limb regeneration. Nature 460, 60-65.

156. Lawrence, E.A., Kague, E., Aggleton, J.A., Harniman, R.L., Roddy, K.A., Hammond, C.L., 2018. The mechanical impact of col11a2 loss on joints; col11a2 mutant zebrafish show changes to joint development and function, which leads to early-onset osteoarthritis. Philos Trans R Soc Lond B Biol Sci 373.

157. Lee, J., Marrero, L., Yu, L., Dawson, L.A., Muneoka, K., Han, M., 2013. SDF-1alpha/CXCR4 signaling mediates digit tip regeneration promoted by BMP-2. Dev Biol 382, 98-109.

158. Li, I.M.H., Liu, K., Neal, A., Clegg, P.D., De Val, S., Bou-Gharios, G., 2018. Differential tissue specific, temporal and spatial expression patterns of the Aggrecan gene is modulated by independent enhancer elements. Sci Rep 8, 950.

159. Li, L., Newton, P.T., Bouderlique, T., Sejnohova, M., Zikmund, T., Kozhemyakina, E., Xie, M., Krivanek, J., Kaiser, J., Qian, H., Dyachuk, V., Lassar, A.B., Warman, M.L., Barenius, B., Adameyko, I., Chagin, A.S., 2017. Superficial cells are self-renewing chondrocyte progenitors, which form the articular cartilage in juvenile mice. FASEB J 31, 1067-1084.

160. Lorenzo, P., Bayliss, M.T., Heinegard, D., 1998. A novel cartilage protein (CILP) present in the mid-zone of human articular cartilage increases with age. J Biol Chem 273, 23463-23468.

161. Luo, Y., Sinkeviciute, D., He, Y., Karsdal, M., Henrotin, Y., Mobasheri, A., Onnerfjord, P., Bay-Jensen, A., 2017. The minor collagens in articular cartilage. Protein Cell 8, 560-572.

162. Mackay, A.M., Beck, S.C., Murphy, J.M., Barry, F.P., Chichester, C.O., Pittenger, M.F., 1998. Chondrogenic differentiation of cultured human mesenchymal stem cells from marrow. Tissue Eng 4, 415-428.

163. Majumdar, M.K., Wang, E., Morris, E.A., 2001. BMP-2 and BMP-9 promotes chondrogenic differentiation of human multipotential mesenchymal cells and overcomes the inhibitory effect of IL-1. J Cell Physiol 189, 275-284.

164. Masaki, H., Ide, H., 2007. Regeneration potency of mouse limbs. Dev Growth Differ 49, 89-98.

165. Medvedeva, E.V., Grebenik, E.A., Gornostaeva, S.N., Telpuhov, V.I., Lychagin, A.V., Timashev, P.S., Chagin, A.S., 2018. Repair of Damaged Articular Cartilage: Current Approaches and Future Directions. Int J Mol Sci 19.

166. Miura, S., Tsutsumi, R., Agata, K., Endo, T., 2020. Maturating Articular Cartilage Can Induce Ectopic Joint-Like Structures in Neonatal Mice. Regen Eng Transl Med 6, 373-382.

167. Morgan, B.J., Bauza-Mayol, G., Gardner, O.F.W., Zhang, Y., Levato, R., Archer, C.W., van Weeren, R., Malda, J., Conlan, R.S., Francis, L.W., Khan, I.M., 2020. Bone Morphogenetic Protein-9 Is a Potent Chondrogenic and Morphogenic Factor for Articular Cartilage Chondroprogenitors. Stem Cells Dev 29, 882-894.

168. Muneoka, K., Allan, C.H., Yang, X., Lee, J., Han, M., 2008. Mammalian regeneration and regenerative medicine. Birth Defects Res C Embryo Today 84, 265-280.

169. Muneoka, K., Dawson, L.A., 2020. Evolution of epimorphosis in mammals. J Exp Zool B Mol Dev Evol.

170. Muneoka, K., Fox, W.F., Bryant, S.V., 1986. Cellular contribution from dermis and cartilage to the regenerating limb blastema in axolotls. Dev Biol 116, 256-260.

171. Murphy, J.M., Heinegard, R., McIntosh, A., Sterchi, D., Barry, F.P., 1999. Distribution of cartilage molecules in the developing mouse joint. Matrix Biol 18, 487-497.

172. Nakamura, E., Nguyen, M.T., Mackem, S., 2006. Kinetics of tamoxifen-regulated Cre activity in mice using a cartilage-specific CreER(T) to assay temporal activity windows along the proximodistal limb skeleton. Dev Dyn 235, 2603-2612.

173. Nakayama, N., Han, C.Y., Cam, L., Lee, J.I., Pretorius, J., Fisher, S., Rosenfeld, R., Scully, S., Nishinakamura, R., Duryea, D., Van, G., Bolon, B., Yokota, T., Zhang, K., 2004. A novel chordin-like BMP inhibitor, CHL2, expressed preferentially in chondrocytes of developing cartilage and osteoarthritic joint cartilage. Development 131, 229-240.

174. Nakayama, N., Pothiawala, A., Lee, J.Y., Matthias, N., Umeda, K., Ang, B.K., Huard, J., Huang, Y., Sun, D., 2020. Human pluripotent stem cell-derived chondroprogenitors for cartilage tissue engineering. Cell Mol Life Sci 77, 2543-2563.

175. Ochi, K., Derfoul, A., Tuan, R.S., 2006. A predominantly articular cartilage-associated gene, SCRG1, is induced by glucocorticoid and stimulates chondrogenesis in vitro. Osteoarthritis Cartilage 14, 30-38.

176. Ono, N., Ono, W., Nagasawa, T., Kronenberg, H.M., 2014. A subset of chondrogenic cells provides early mesenchymal progenitors in growing bones. Nat Cell Biol 16, 1157-1167.

177. Osorio, D., Zhong, Y., Li, G., Huang, J.Z., Cai, J.J., 2020. scTenifoldNet: A Machine Learning Workflow for Constructing and Comparing Transcriptome-wide Gene Regulatory Networks from Single-Cell Data. Patterns (N Y) 1, 100139.

178. Rinkevich, Y., Lindau, P., Ueno, H., Longaker, M.T., Weissman, I.L., 2011. Germ-layer and lineage-restricted stem/progenitors regenerate the mouse digit tip. Nature 476, 409-413.

179. Ripmeester, E.G.J., Timur, U.T., Caron, M.M.J., Welting, T.J.M., 2018. Recent Insights into the Contribution of the Changing Hypertrophic Chondrocyte Phenotype in the Development and Progression of Osteoarthritis. Front Bioeng Biotechnol 6, 18.

180. Sanchez Alvarado, A., 2000. Regeneration in the metazoans: why does it happen? Bioessays 22, 578-590.

181. Scharpfenecker, M., van Dinther, M., Liu, Z., van Bezooijen, R.L., Zhao, Q., Pukac, L., Lowik, C.W., ten Dijke, P., 2007. BMP-9 signals via ALK1 and inhibits bFGF-induced endothelial cell proliferation and VEGF-stimulated angiogenesis. J Cell Sci 120, 964-972.

182. Seemann, P., Brehm, A., Konig, J., Reissner, C., Stricker, S., Kuss, P., Haupt, J., Renninger, S., Nickel, J., Sebald, W., Groppe, J.C., Ploger, F., Pohl, J., Schmidt-von Kegler, M., Walther, M., Gassner, I., Rusu, C., Janecke, A.R., Dathe, K., Mundlos, S., 2009. Mutations in GDF5 reveal a key residue mediating BMP inhibition by NOGGIN. PLoS Genet 5, e1000747.

183. Seifert, A.W., Muneoka, K., 2018. The blastema and epimorphic regeneration in mammals. Dev Biol 433, 190-199.

184. Simkin, J., Sammarco, M.C., Dawson, L.A., Schanes, P.P., Yu, L., Muneoka, K., 2015. The mammalian blastema: regeneration at our fingertips. Regeneration (Oxf) 2, 93-105.

185. Somoza, R.A., Welter, J.F., Correa, D., Caplan, A.I., 2014. Chondrogenic differentiation of mesenchymal stem cells: challenges and unfulfilled expectations. Tissue Eng Part B Rev 20, 596-608.

186. Storer, M.A., Mahmud, N., Karamboulas, K., Borrett, M.J., Yuzwa, S.A., Gont, A., Androschuk, A., Sefton, M.V., Kaplan, D.R., Miller, F.D., 2020. Acquisition of a Unique Mesenchymal Precursor-like Blastema State Underlies Successful Adult Mammalian Digit Tip Regeneration. Dev Cell 52, 509-524 e509.

187. Storer, M.A., Miller, F.D., 2020. Cellular and molecular mechanisms that regulate mammalian digit tip regeneration. Open Biol 10, 200194.

188. Surmann-Schmitt, C., Dietz, U., Kireva, T., Adam, N., Park, J., Tagariello, A., Onnerfjord, P., Heinegard, D., Schlotzer-Schrehardt, U., Deutzmann, R., von der Mark, K., Stock, M., 2008. Ucma, a novel secreted cartilage-specific protein with implications in osteogenesis. J Biol Chem 283, 7082-7093.

189. Townson, S.A., Martinez-Hackert, E., Greppi, C., Lowden, P., Sako, D., Liu, J., Ucran, J.A., Liharska, K., Underwood, K.W., Seehra, J., Kumar, R., Grinberg, A.V., 2012. Specificity and structure of a high affinity activin receptor-like kinase 1 (ALK1) signaling complex. J Biol Chem 287, 27313-27325.

190. Turner, N.J., Johnson, S.A., Badylak, S.F., 2010. A histomorphologic study of the normal healing response following digit amputation in C57bl/6 and MRL/MpJ mice. Arch Histol Cytol 73, 103-111.

191. Wang, W., Chun, H., Baek, J., Sadik, J.E., Shirazyan, A., Razavi, P., Lopez, N., Lyons, K.M., 2019. The TGFbeta type I receptor TGFbetaRI functions as an inhibitor of BMP signaling in cartilage. Proc Natl Acad Sci U S A 116, 15570-15579.

192. Wang, W., Rigueur, D., Lyons, K.M., 2020. TGFbeta as a gatekeeper of BMP action in the developing growth plate. Bone 137, 115439.

193. Wu, Y., Wang, K., Karapetyan, A., Fernando, W.A., Simkin, J., Han, M., Rugg, E.L., Muneoka, K., 2013. Connective Tissue Fibroblast Properties Are Position-Dependent during Mouse Digit Tip Regeneration. PLoS One 8, e54764.

194. Xiao, H., Wang, X., Wang, C., Dai, G., Zhu, Z., Gao, S., He, B., Liao, J., Huang, W., 2020. BMP9 exhibits dual and coupled roles in inducing osteogenic and angiogenic differentiation of mesenchymal stem cells. Biosci Rep 40.

195. Yoshida, C.A., Yamamoto, H., Fujita, T., Furuichi, T., Ito, K., Inoue, K., Yamana, K., Zanma, A., Takada, K., Ito, Y., Komori, T., 2004. Runx2 and Runx3 are essential for chondrocyte maturation, and Runx2 regulates limb growth through induction of Indian hedgehog. Genes Dev 18, 952-963.

196. Yu, L., Dawson, L.A., Yan, M., Zimmel, K., Lin, Y.L., Dolan, C.P., Han, M., Muneoka, K., 2019. BMP9 stimulates joint regeneration at digit amputation wounds in mice. Nat Commun 10, 424.

197. Yu, L., Han, M., Yan, M., Lee, E.C., Lee, J., Muneoka, K., 2010. BMP signaling induces digit regeneration in neonatal mice. Development 137, 551-559.

198. Yu, L., Han, M., Yan, M., Lee, J., Muneoka, K., 2012. BMP2 induces segment-specific skeletal regeneration from digit and limb amputations by establishing a new endochondral ossification center. Dev Biol 372, 263-273.

199. Yu, L., Yan, M., Simkin, J., Ketcham, P.D., Leininger, E., Han, M., Muneoka, K., 2014. Angiogenesis is inhibitory for mammalian digit regeneration. Regeneration 1, 14.

200. Zhang, S., Hu, B., Liu, W., Wang, P., Lv, X., Chen, S., Liu, H., Shao, Z., 2020. Articular cartilage regeneration: The role of endogenous mesenchymal stem/progenitor cell recruitment and migration. Semin Arthritis Rheum 50, 198-208.

201. Zhao, Q., Eberspaecher, H., Lefebvre, V., De Crombrugghe, B., 1997. Parallel expression of Sox9 and Col2a1 in cells undergoing chondrogenesis. Dev Dyn 209, 377-386.

202. Zheng, Q., Zhou, G., Morello, R., Chen, Y., Garcia-Rojas, X., Lee, B., 2003. Type X collagen gene regulation by Runx2 contributes directly to its hypertrophic chondrocyte-specific expression in vivo. J Cell Biol 162, 833-842.

3 ISOLATION AND CHARACTERIZATION OF ARTICULAR CHONDROCYTE PROGENITOR LINE EXISTS IN P3 FIBROBLASTS

3.1 Introduction

Articular cartilage (AC) is a highly specialized tissue composed of hyaline chondrocytes that are responsible for maintaining proper function and homeostasis of this tissue by producing specific extracellular matrix components. Unfortunately, damaged AC cannot regenerate spontaneously and can lead to osteoarthritis (OA), a degenerative disease characterized by the progressive loss of AC. Cell-based joint regenerative studies aim to repair damaged AC by differentiating stem/progenitor cells into articular chondrocytes for transplantation but the effective outcome is still limited. The significant challenges include 1) the identification of stem/progenitor cells that can maintain chondrogenic characteristics during expansion; and 2) an efficient methodology for differentiating articular chondrocytes; and 3) maintaining AC characteristics following transplantation to repair a joint defect. The studies done by our lab have identified BMP9 as a potent growth factor that can stimulate joint regeneration, that includes AC, at digit amputation wounds in vivo (Yu et al., 2019a). Based on these regeneration studies, we have determined that the responsive cell type are fibroblasts and have identified a fibroblast cell line (P3 fibroblasts) that can be induced to form stable hyaline cartilage in culture utilizing a novel self-aggregation protocol coupled with BMP9 treatment. In this chapter I present studies that expand these findings to differentiate stable articular chondrocytes rather than hypertrophic chondrocytes (HC) or fibrocartilages.

The major goal of regenerative medicine is to regenerate tissues, damaged by traumatic injury, that lack the ability to regenerate or self-renew. The salamander limb is one of the best models for studying epimorphic regeneration due to its ability to regenerate an entire limb that is lost by amputation (Kragl et al., 2009). Among mammals, regenerative capacity is restricted to the distal tip of the terminal phalangeal element (P3) in both human fingers and mouse digits (Borgens, 1982; Douglas, 1972; Han et al., 2008; Illingworth, 1974; Muneoka et al., 2008). Amputation of the tip of the mouse digit results in blastemal formation and the successful regeneration of amputated tissues. Whereas, amputation at a more proximal level, for example, the sub-terminal phalangeal element (P2), fails to regenerate and the amputated wound is healed by scar formation (Muller et al., 1999). Since the regenerative potency in mammalian digits is level-dependent, it provides an opportunity to study the mechanism underlying regenerative events and the possibility to stimulate regeneration at regenerative incompetent tissues. Using this amputation model of non-regeneration competent P2 digit, our lab has revealed that BMP2 stimulates an endochondral ossification event to regenerate new bone (Dawson et al., 2017; Yu et al., 2010; Yu et al., 2012). Moreover, treating BMP9 in P2 digit amputation model induces complete joint regeneration, including the synovial cavity, articular cartilage, and tendon/ligament attachments (Yu et al., 2019a). This result indicates that BMP9 is a remarkable inducer for joint regeneration, and the regenerative competent cells are present in the digit. In chapter II we showed evidence that cells isolated from amputation wounds (AmpWMCs) display a parallel response to BMP9 when compared with the in vivo studies (Yu et al., 2022). These studies indicate that chondroprogenitor cells are present in the healing non-regenerative digit amputation wound and the BMP9-stimulated chondrogenic regeneration in vivo can be replicated in vitro.

The cells in connective tissue that surround the endogenous regenerative P3 skeletal element (named P3 fibroblast) and the non-regeneration competent P2 skeletal element (named P2 fibroblast) have been isolated and studied. Both P2 and P3 fibroblasts can be maintained and expanded over 22 passages in monolayer culture with 2%FBS/MSC medium and successfully frozen and thawed, thus representing stable cell lines. P2 and P3 fibroblasts also shared similar surface marker profile used to identify stem cells. However, the mRNA expression level of a few stem cell-related genes, such as Msx1, Rex1 and Sox2, showed differences between P2 and P3 fibroblasts, indicating they are different from each other (Wu et al., 2013). In addition, when cells are cultured using a self-aggregation protocol with BMP9 treatment (SA/BMP9), P3 fibroblast exhibit better self-aggregation and chondrogenic abilities, while P2 fibroblast fail to aggregate thus making it difficult to determine its chondrogenic potential (Yu et al., 2022); unpublished data). Although this result suggests that P3 fibroblast displays a good cell source, compared to P2 fibroblast, for in vitro AC regeneration, the challenge of P3 fibroblast chondrogenesis lies in its heterogeneity. The connective tissue isolated from P3 skeletal elements contains multiple cell types including fibroblast, endothelial cells, vascular smooth muscle cells and pericytes (Wu et al., 2013). Therefore, identifying articular chondrocyte progenitor cells from heterogeneous P3 fibroblast is needed to further study its potential for AC regeneration.

The cartilage regenerated from P3 fibroblasts displays plasticity for hyaline chondrocyte differentiation and hypertrophic chondrocyte differentiation. Using an established SA/BMP9 protocol, the chondrogenic response of P3 fibroblasts is rapid and robust. Within 24 hours of culture, P3 fibroblasts express hyaline and articular cartilage-related genes but no HC-specific genes were observed. During extended culture (36 days) several hyaline and articular cartilage-related genes are expressed in higher levels and the HC-specific genes remain unchanged. In

addition, immunohistochemical studies of P3 fibroblast differentiated cartilage shows results consistent with gene expression studies, indicating that BMP9 stimulates P3 fibroblasts to differentiate stable hyaline cartilage that contains articular chondrocytes. However, an immunohistochemical analysis of implanted P3 fibroblast differentiated cartilage into an acute metatarsal-phalangeal (MtP) joint defect identified ColX expressing HC indicating that hyaline chondrocyte stability was compromised. A study of P3 fibroblast differentiated cartilage in culture found that ColX expressing hypertrophic chondrocytes was induced by BMP2 (100 ng/ml) indicating a potential for HC differentiation (Yu et al., 2022). Together, these results suggest two possibilities: 1) hyaline chondrocytes differentiated from P3 fibroblasts have the plasticity to undergo hypertrophic differentiation when treating proper inducer; or 2) P3 fibroblasts contain HC progenitor cells that are distinct from AC progenitor cells.

To address these questions, in this chapter we cloned cells from this heterogeneous P3 fibroblastic population and identified a clonal cell line (P3_D8 clone) that exhibits a hyaline chondrogenic response to BMP9 treatment, while the P3_E3 clone differentiates to HC under identical culture condition. By modifying SA/BMP9 protocol with sequentially treatments of BMP2 and BMP9 (BMP2/SA/BMP9), the P3_D8 clone differentiates into AC while self-renewing during in vitro chondrogenesis. In addition, P3_D8 clone differentiated AC maintains hyaline chondrocyte phenotype in vitro when treating with the osteogenic inducer (BMP2) and in vivo when implanting into joint defects. Overall, this study identified a promising cloned cell line and modified an effective differentiation protocol for in vitro AC regeneration.

3.2 Materials and Methods

Cell Culture: P3 fibroblasts were cultured and expanded on fibronectin coated dishes in 2% FBS MSC medium supplemented with EGF, PDGF, LIF (growth medium) as described (Wu et al., 2013). Passage 9 LacZ-expressing P3 fibroblasts were used for clonal study and conditioned medium from these cells was collected and used in the cloning process. To generate single cell-derived clones, P3 fibroblasts were serial diluted to the concentration of 5 cells/ml and 200 μl aliquots were plated into each well of a 96-well plate (#08-772-2C, Fisher Scientific) to generate single cell cultures. Cells were cultured using a 1:1 mixture of growth medium and conditioned medium. The wells that contain a single cell were identified visually, expanded and store in liquid Nitrogen for future use. The single cell-derived clones on 96-well plate were designated as clonal passage 0 (Cpassage 0) and all experiments were carried out with cells less than Cpassage 6. The self-renewal studies to obtain cells for in vitro chondrogenesis were carried out by enzymatic dissociation. Briefly, in vitro differentiated cartilage was treated with trypsin for 2 minutes, filtered with a 100 μm cell strainer (CORNING, REF431752) and plated onto fibronectin coated dishes in growth medium. After achieved 70-80% confluence, cells were detached for future studies or stored in liquid Nitrogen. The remaining undigested cartilage tissue was fixed, sectioned and stained to determine the effects of the brief trypsin treatment.

Differentiation Assay: For chondrogenesis studies, cells were expanded in growth medium then transferred to 2% FBS MSC medium (basal medium) supplemented with or without BMP9 (50 ng/mL, R&D) (BMP9 medium). Cell pellets were generated out by centrifugation as follows: 2.5×10^5 cells in basal medium (0.5 ml) of were centrifuged (150 x g / 5 minutes at room temperature) in a 15 mL polypropylene tube to form a cell pellet. Cell pellets were incubated for 21 days in the polypropylene tube with the cap loosed for gas exchange. Medium was changed

twice a week until the end of culture period. For chondrogenesis studies using the SA culture protocol, cells were expanded in growth medium, collected and resuspended in basal medium (1.0×10^5 cells/ml). 2.5×10^5 cells in 2.5 ml of basal medium was transferred into a petri dish (45 mm diameter) for 4 day and allowed to self-aggregate to form cell aggregates. During the SA culture period (day 0 - day 4), BMP9 (50 ng/mL), BMP2 (50 ng/mL) or TGFβ3 (50 ng/mL) were supplemented to promote cell aggregation. After self-aggregation, the aggregates were differentiated using BMP9 medium until the end of the culture period. The sectioned pellets were visualized by Mallory's trichrome staining (Humason, 1962) to identify collagens or Safranin O/fast green staining (Schmitz et al., 2010) to detect mucopolysaccharides including proteoglycans. Osteogenic differentiation was tested by culturing monolayer cells (4,800 cells/mL) in adipogenic/osteogenic base media (#CCM007, R&D Systems) supplemented with StemXVivo mouse/rat osteogenic supplement (#CCM009, R&D systems) for 14 days and assaying mineralized matrix based on Alizarin Red S staining (Yu et al., 2022). Adipogenic differentiation was tested by culturing monolayer cells (20,000 cells/mL) in adipogenic/osteogenic base media (#CCM007, R&D Systems) supplemented with StemXVivo adipogenic supplement (#CCM011, R&D systems) for 21 days and assaying lipid vacuoles based on Oil Red O staining.

Flow Cytometry: Cells for flow cytometry studies were detached by trypsin, filtered using a 100 μm cell strainer, and incubated in flow buffer (0.5% FBS/PBS) at 4°C, 15 min for blocking. Cells were incubated in the dark with antibodies at the concentration of 1 μL antibody/2×10^5 cells/100 μL at 4°C, 30 min. Cells were then washed twice and re-suspended with flow buffer and kept at 4°C in the dark prior to running flow cytometry. In multi-colors studies, fluorescent compensation was performed by UltraComp eBeads (#01-2222, invitrogen). Flow cytometry

were conducted using Gallios flow cytometer (Beckmen Coulter) and flow data was analyzed by Kaluza software (Beckmen Coulter). Antibodies used in this study include CD34 (#48-0341-82, eBioscience), CD45 (#47-0454-80 and #11-0454-82, eBioscience), CD90 (#47-0902-82, eBioscience), CD73 (#12-0731-81, eBioscience), CD105 (#48-1051-80, eBioscience), CD51 (#12-0512-81, eBioscience), Tie2 (#566716, BD), 6C3 (#46-5891-82, eBioscience), TER-119 (#11-5921-82, eBioscience) and 7-AAD viability staining solution (00-6993, eBioscience).

Histology and Immunochemistry: In vitro differentiated cultures were fixed with Z-fix (Anatech 6269) and in vivo implanted tissues were fixed with Z-fix followed by Decalcifier I (Surgipath, Leica 3800400). Samples then processed for paraffin histology and immunohistochemistry. For histological analysis, the samples were stained with Mallory trichrome (Humason, 1962) or Safranin O/fast green (Schmitz et al., 2010). Immunohistochemical staining for LacZ, Sox9, ColI, Acan, Prg4 and Cilp was carried out using heat retrieval (citrate buffer (pH 6), 65°C, 20 hours) and antigen retrieval for ColX immunostaining used 1% hyaluronidase in PBS (Sigma-Aldrich H3506, room temperature, 30Min). Slides were treated in Protein Block Solution (Dako X0909; room temperature, 1 h). Primary antibodies included anti-LacZ (Chicken polyclonal, Abcam ab9361; 1:500), anti-Sox9 (Rabbit polyclonal, Abcam ab26414; 1:500), anti-ColX (Rabbit polyclonal, Abcam 58632; 1:500), anti-ColI (Rabbit Polyclonal, Origene R1038; 1:200), anti-Acan (Rabbit polyclonal, Millipore AB1030; 1:300), anti-Prg4 (Rabbit polyconol, LSbio LS-B8236; 1:200) and anti-Cilp (Rabbit polyclonal, Novus NBP1-81667; 1:100). Secondary antibody included Alexa Fluor 568 goat anti-rabbit IgG (Invitrogen; A11011, 1:500), Alexa Fluor 568 goat anti-Chicken IgG (Invitrogen, A11041, 1:500) or the Alexa Fluor goat anti-rabbit 488 IgG (Invitrogen, A11008, 1:500). Slides were counterstained with DAPI to label nuclei. Slides were imaged with an

Olympus BX61 fluorescence deconvolution microscope utilizing Slidebook software (Intelligent Imaging Innovations Inc., Denver, CO). Details of immunostaining procedures have been described previously (Dawson et al., 2019; Han et al., 2008; Yu et al., 2012). **RNA Extraction, RT-qPCR and RNA-seq:** Total RNA was extracted from cultures using the RNeasy Plus Micro Kit (Qiagen) following the manufacturer's recommended protocol. The aggregation cultured samples were homogenized before RNA extraction. The quantity and quality of total RNAs were checked by Nanodrop ratios of 260/280 and 260/310. Quantitative reverse transcriptase polymerase chain reaction (qRT-PCR) was carried out in triplicate with the SuperScript™ III Platinum™ One-Step qRT-PCR Kit w/ROX on an Eppendorf Realplex machine according to the manufacturer's instruction. The expression levels of target genes were normalized to the housekeeping gene ribosomal protein L12 (RPL12) levels. Statistical significance was determined using a parametric unpaired T-test in "Graphpad". Primers used in this study include mouse Prg4 (Mm01284582_m1), mouse Cilp (Mm00557687_m1), mouse Sox9 (Mm00448840_m1), mouse Enpp2 (Mm00516572_m1), mouse Scrg1 (Mm00485984_m1), mouse Col2a1 (Mm01309565_m1), and mouse Rpl12 (Mm02601627_g1).

For RNA-seq samples, the quantity and quality of total RNAs were further checked with concentration, RIN, and 28S/18S ratio by Agilent 2100 at BGI Genomics. The 100-bp length paired-end reads from cultures were generated using BGISEQ-500 at BGI Genomics, while the SRA shared datasets are downloaded from NCBI website (Primary ACs: SRR9317861-SRR9317863, (Bekki et al., 2020) and Primary GP: SRR5036053-SRR5036056, (Sabik et al., 2017). All reads are aligned and referenced against the Mus musculus genome (UCSC version mm10) using "HTSAT2" and counted using "htseq-count". The normalization and DE analysis were processed by "DESeq2" running under a Galaxy instance. The significant differentially

expressed genes were defined by a cutoff of log2(FC) ≥ │1.5│ and FDR P-value < 0.05. The volcano plot, correlation analysis, and heatmap couple with clustering analysis were performed and visualized by R/R studio with packages of "gplots", "ggplot2", "corrplot", "heatmap.plus", and "RColorBrewer". The functional annotation was conducted by "DAVID" software (Huang da et al., 2009a, b).

Animal Studies: Mouse strain used in this study was NOD.CB17-Prkdcscid/J (SCID-NOD) mice purchased from Jackson lab or bred in house at the Texas Institute of Genomic Medicine. The MtP joint defect was surgically created in adult SCID-NOD mice as previously described (Yu et al., 2022). Mice were anesthetized and maintained with isoflurane (1-5% in oxygen), and buprenorphine (0.1 mg/kg) was used as a systemic analgesic. A tourniquet is placed on the hindlimb to minimize bleeding. Under a dissection microscope, the MtP joint is contracted ventrally and a 2-3 mm longitudinal skin incision was made to expose the joint capsule. A dorsal incision of the joint capsule allowed access to the proximal joint surface of the first phalangeal element (P1). An acute defect of approximately 0.5 mm diameter is created in the P1 joint surface with a scalpel (Type 11, EXELINT) at the central distal groove of MtP joint. The defect extends through the articular cartilage layer and subchondral bone into the P1 bone marrow. The acute defect is cleared of residual debris by flushing with PBS prior to tissue implantation. Samples to be implanted were prepared in advance to approximate the size of the MtP defect and maintained on ice. Unused samples were processed for histological analysis to validate the cartilage phenotype. Chondrogenic samples are hard and can be compressed to fit snuggly into the acute wound site. The surface of the implant is aligned with the surface of the P1 joint and straightening of the digit maintains the positioning of the implant. The joint capsule and the overlying skin is closed with 10.0 suture (Ethicon). All animals and techniques used are

compliant with the standard operating procedures and approved by the Institutional Animal Care and Use Committees at the College of Veterinary Medicine and Biomedical Sciences at Texas A&M University.

Single-cell RNA-seq: P3 fibroblast and P3_D8 clone cells were collected by trypsin digestion, washed twice and resuspended in PBS with 0.08% BSA at concentration of $1x10^6$ cells/ml. Single-cell sample preparation was conducted according to Sample Preparation Protocol provided by 10x Genomics. Cell viability was assessed by Trypan Blue staining (0.4%) and determined to be greater than 90%. Subsequently, single-cell GEMs (Gel bead in EMulsion) and sequencing libraries were prepared using the 10x Genomics Chromium Controller in conjunction with the single-cell 3' kit (v3). Cell suspensions were diluted in nuclease-free water to achieve a targeted cell count of 10,000 for each sample. cDNA synthesis, barcoding, and library preparation were subsequently carried out according to the manufacturer's instructions. Libraries were sequenced in the Molecular Genomic Workspace of the Texas A&M Institute for Genome Sciences and Society (https://genomics.tamu.edu/) using a NovaSeq6000 sequencer (Illumina, San Diego). For the mapping of reads to transcripts and cells, sample demultiplexing, barcode processing, and unique molecular identifier (UMI) counts were performed using the 10x Genomics pipeline CellRanger v5.0.1 with default parameters. Specifically, raw reads were demultiplexed using the pipeline command 'cellranger mkfastq' in conjunction with 'bcl2fastq' (v2.17.1.14, Illumina) to produce two fastq files: the read-1 file containing 26-bp reads, consisting of a cell barcode and a unique molecule identifier (UMI), and the read-2 file containing 96-bp reads including cDNA sequences. Sequences were aligned to the mouse reference genome (mm10), filtered and counted using 'cellranger count' to generate the gene-barcode matrix. Dimension reduction of expression matrices was performed using tSNE. Marker

gene expression and cell type assignment was performed manually using the SC_SCATTER function of scGEAToolbox (Cai, 2019). Differential gene expression was performed using MAST (Finak et al., 2015a; Finak et al., 2015b).

3.3 Results

Characteristics of Single Cell-derived Clones Isolated from P3 Fibroblasts

BMP9 stimulates joint regeneration after digit amputation and the primary cells isolated from the amputation wound can be induced to differentiate hyaline cartilage by BMP9 treatment in vitro (Yu et al., 2019b). Similarly, fibroblasts isolated from the unamputated mouse digit (P3 fibroblasts) exhibit an identical chondrogenic response to BMP9 treatment (Wu et al., 2013), indicating that chondrocyte progenitor cells exist among fibroblasts of the mouse digit. To study chondrocyte progenitor cells, we cloned P3 fibroblasts by dilution and tested the chondrogenic potential of clonally derived P3 fibroblasts. A total of 51 P3 fibroblast clones were isolated, expanded and stored. As a test of chondrogenic differentiation, P3 fibroblast clonal lines were cultured as centrifuged cell pellets, treated with BMP9 (50 ng/mL) for 21 days and assayed based on histological staining with Safranin O, a cationic stain routinely used to identify mucopolysaccharides prevalent in articular cartilage based on orange to red staining of cartilage matrix (Schmitz et al., 2010). An analysis of 18 fibroblast clones treated with BMP9 identified 2 clones (2/18, 11%) that failed to form chondrocytes (Figure 3.1A) and 16 clones (16/18, 89%) that formed clusters of chondrocytes identified based on cell morphology (spherical cells with lacuna) and matrix rich in mucopolysaccharides (Figure 3.1B and C). Seven of the 16 chondrogenic clones (44%) formed cartilage containing small chondrocytes that appeared similar

to hyaline cartilage (Figure3.1 B), whereas 9 chondrogenic clones (56%) formed cartilage containing large chondrocytes that appeared similar to hypertrophic cartilage (Figure 3.1C). These clonal studies indicate that P3 fibroblasts are a heterogeneous cell population containing progenitor cells that display distinct chondrogenic responses when cultured under identical conditions. Two clonal cell lines were selected from both chondrocyte forming groups for further studies: 1) a hyaline cartilage line (P3_D8), and 2) a hypertrophic cartilage line (P3_E3) (Figure 3.1B and C). The two selected clones exhibit different cell morphology when plated on tissue culture plastic. P3_D8 cells remain rounded and do not readily attach to the surface, whereas P3_E3 cells attach and spread as stellate cells (Figure 3.2A and E). Immunostaining studies focusing on BMP9 induced chondrocytes with hyaline chondrocyte marker, Acan, and hypertrophic chondrocyte marker, ColX, revealed that P3_D8 clone differentiated chondrocytes were positive for Acan but not ColX, while P3_E3 clone differentiated chondrocytes were positive for both (Figure 3.2B-D and F-H). These data support the histological results that BMP9 treatment induces P3_D8 clone differentiated to hyaline chondrocytes, while P3_E3 clone was induced to form hypertrophic chondrocytes. Taken together, the evidence suggests that adult digit fibroblasts contain chondrocyte progenitor cells for hyaline cartilage that are distinct from progenitor cells for hypertrophic cartilage.

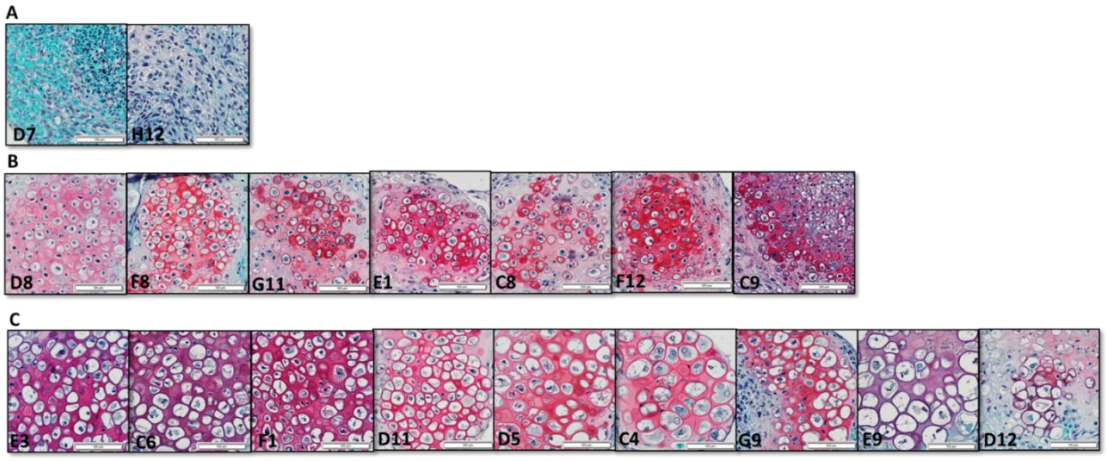

Figure 3.1 Characterization of BMP9 induced chondrogenesis of clones isolated from P3 fibroblasts.
18 clones were centrifuged as a pellet and cultured with BMP9 treatment for 21 days. Pellets were analyzed histologically based on Safranin O/ fast green staining. A) 2 clones failed to differentiate histologically identifiable chondrocytes. B) 7 clones differentiated to cartilage containing small chondrocytes. C) 9 clones differentiated to cartilage containing large chondrocytes. Scale bars: 100 μM.

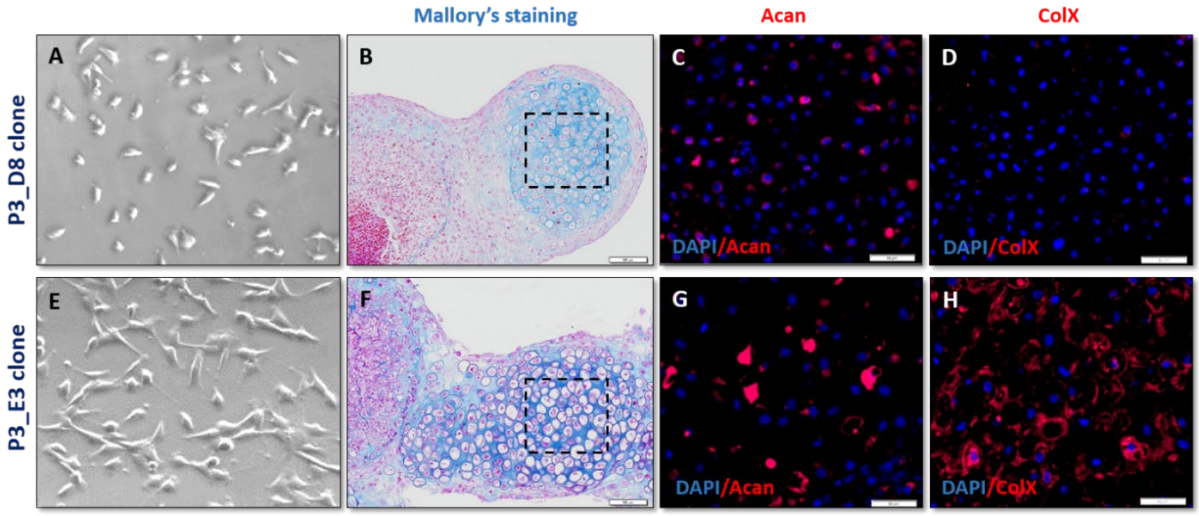

Figure 3.2 BMP9 induces P3_D8 clone differentiate to hyaline chondrocytes while P3_E3 clone differentiate to hypertrophic chondrocytes.
P3_D8 clone was cultured in monolayer (A) or centrifuged as a pellet, cultured with BMP9 treatment for 21 days, and stained by Mallory's trichrome staining (B). P3_D8 clone differentiated chondrocytes were stained with Acan (C) and ColX (D). P3_E3 clone was cultured in monolayer (E) or centrifuged as a pellet, cultured with BMP9 treatment for 21 days and stained by Mallory's trichrome staining (F). P3_D8 clone differentiated chondrocytes were stained with Acan (G) and ColX (H). Black boxes indicate the focusing areas for immunostaining studies. Scale bars: 100 μM for B and F; 50 μM for C, D, G and H.

To characterize the hyaline cartilage clonal line, the P3_D8 clone was selected for cell-type determination. The single cell RNA sequencing (scRNA-seq) were performed for the P3_D8 clone and P3 fibroblast and the datasets were analyzed using scGEAToolbox (Cai, 2019; Osorio et al., 2020). When merged 14,949 P3_D8 clonal cells with 13,142 P3 fibroblasts, the tSNE three-dimensional map separated cells to two populations (Figure 3.3A). Since P3 fibroblast has been defined as a fibroblast cell type with the ability to differentiate to chondrocyte and adipocyte (Yu et al., 2022), we next compared P3_D8 clone and P3 fibroblast with differentiation potency and fibroblast marker (Col1a1), limb-specific fibroblast marker (Prrx1), and three key fibroblast markers (Pdgfra, Cxcl12, and Penk). The expression level analysis indicated that P3_D8 clone displays higher differentiation potency and lower fibroblast marker genes expression when compared to P3 fibroblast (Figure 3.3B-G), suggesting that P3_D8 clone, as a subpopulation of P3 fibroblast, represents a cell type with higher stemness but lower fibroblast features. Mesenchymal stromal/stem cells (MSCs) and skeletal stem cells (SSCs) have been reported with chondrogenic potential, we therefore tested whether the P3_D8 clone is MSCs or SCCs. MSCs are known to be positive for CD90, CD73 and CD105, negative to CD34 and CD45, and can differentiate to multiple tissues including cartilage, bone and fat (Dominici et al., 2006), while SSCs have been defined as CD45-/TER119-/TIE2-/CD51+/CD90-/6C3-/CD105- cell type with the ability to differentiate to cartilage and bone, but not fat (Chan et al., 2015; Murphy et al., 2020). The differentiation assay results revealed that the P3_D8 clone can differentiate to chondrocytes and osteocytes, but not adipocytes (Figure 3.3H). The flow cytometry analysis with MSCs markers indicated that the P3_D8 clone is positive for CD34, CD73 and negative to CD45, CD90, and CD105 (Figure 3.3I). Thus, the P3_D8 clone cannot be

characterized as MSCs. When testing the P3_D8 clone with SSCs surface markers, there are 94.2% of P3_D8 clonal cells express SSCs markers and only 53.3% of P3 fibroblasts shared SSCs surface marker profile (Figure 3.3J). Taken together, these results led to the conclusion that the P3_D8 clone represents a high differentiation potency cell line within P3 fibroblasts that displays SSCs characteristics.

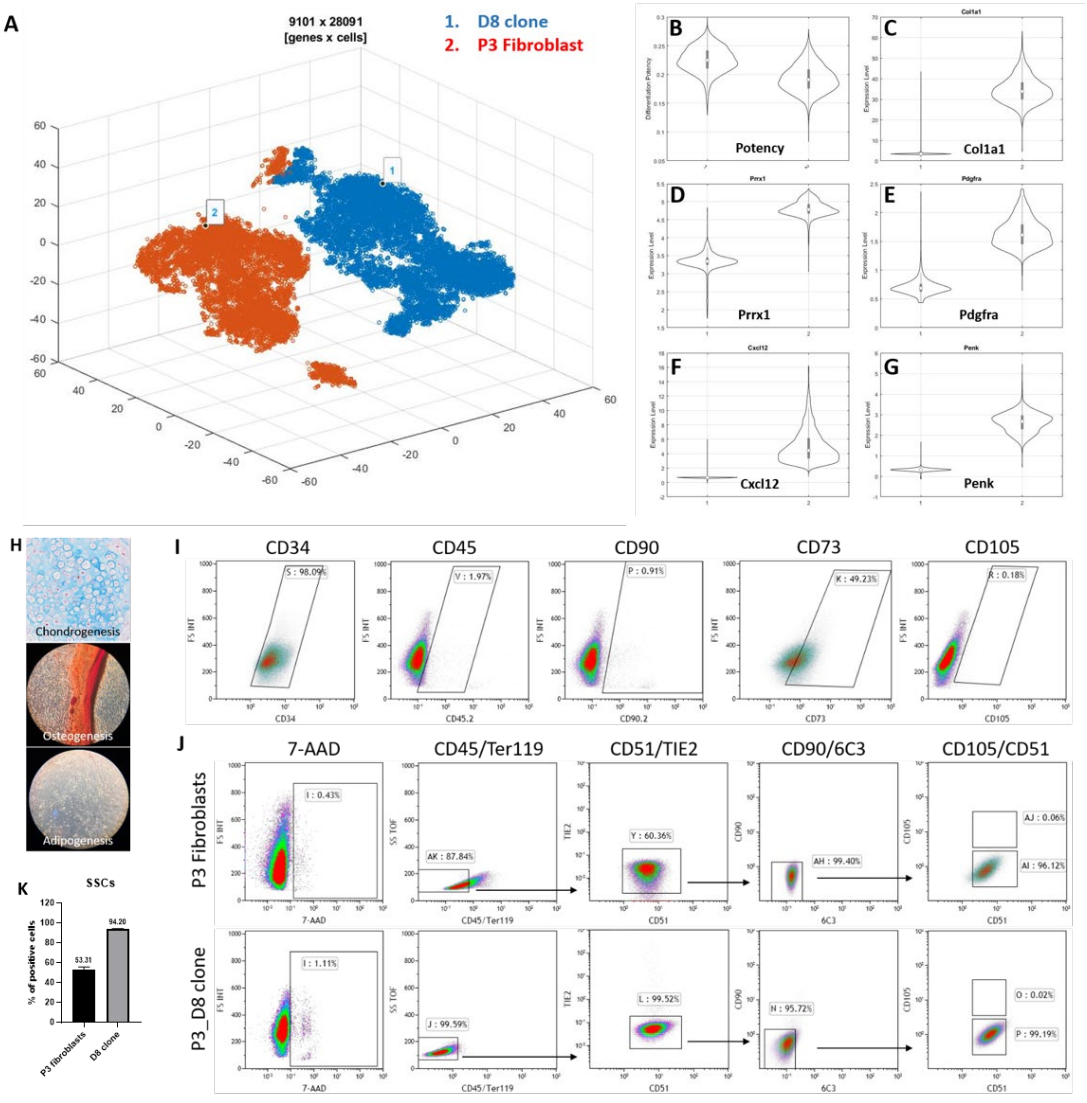

Figure 3.3 Characterization of P3_D8 clone.

scRNA-seq analysis with merged datasets of P3 fibroblast and P3_D8 clone visualizing by t-SNE three-dimensional map (A). The blue spots represent P3_D8 clone and red spots represent P3 fibroblasts. The comparison of P3_D8 clone (labeled by 1) and P3 fibroblast (labeled by 2) in differentiation potency (B), and expression levels of fibroblast markers: *Col1a1* (C), *Prrx1* (D), *Pdgfra* (E), *Cxcl12* (F) and *Penk* (G). H) Differentiation assay of P3_D8 clone was stained by Mallory's trichrome staining for chondrogenesis (Top), Alizarin Red S for osteogenesis (Middle) and Oil Red O for adipogenesis (Bottom). I) Phenotype study of P3_D8 clone with MSCs markers. J) Phenotype study with SSCs markers of P3 fibroblast (Up panels), P3_D8 clone (Bottom panels) and the quantification analysis (K). N=3 for differentiation assay and phenotype studies.

Since centrifugation-induced chondrogenesis results in cell necrosis in the central region of the pellet (Figure 3.2B), the P3_D8 clone was differentiated using a self-aggregation (SA) protocol developed previously for P3 fibroblasts (Yu et al., 2022). Briefly, cells are cultured in a petri dish for 4 days to minimize adherence to the culture dish and allow cells to self-aggregate, then treated with BMP9 (50 ng/mL) to stimulate chondrogenesis. During this 4 days self-aggregation period, the P3_D8 clone displayed varying levels of self-aggregation forming both large and small aggregates (Figure 3.4A). After a culture period of 18 days (4 days for SA and 14 days of BMP9 treatment) the P3_D8 clonal aggregates formed spherical structures of varying size (Figure 3.4E) and when large aggregates were assayed histologically, they contained cartilaginous tissue composed of chondrocytes surrounded by mucopolysaccharide rich matrix similar to hyaline cartilage (Figure 3.4I). This result indicated that the SA/BMP9 protocol was well suited for differentiating cartilage tissue in the form of large chondrospheres from the P3_D8 clone. However, the formation of chondrospheres using the SA/BMP9 protocol appeared to be limited by the initial aggregation response; small aggregates differentiate small chondrospheres and large aggregates differentiate large chondrospheres. Ideally, we sought to establish a protocol that produced large chondrospheres for cartilage regeneration studies and the formation of large chondrospheres in SA/BMP9 cultures was somewhat variable. During

cartilage development, hyaline cartilage forms in vivo by a self-aggregation process called condensation and this dynamic process is initiated by various growth factors including BMP2 and TGFβ (Giffin et al., 2019). To determine whether growth factor treatment improved the initial self-aggregation response in vitro, suspension cultures of P3_D8 fibroblasts were treated with BMP2, BMP9 or TGFβ3 during the 4 day self-aggregation period. Each growth factor treatment enhanced the initial size of cell aggregates by comparison to untreated control (Figure 3.4A-D). When these aggregate cultures were treated with BMP9 for an additional 14 days they all formed multiple large chondrospheres (Figure 3.4E-H) indicating that growth factor treatment during the self-aggregation period enhanced the formation of large chondrospheres. However, when the chondrospheres were assayed histologically, only the BMP2/SA/BMP9 protocol differentiated cartilage rich in mucopolysaccharides based on Safranin O/fast green staining. The other treatment protocols (BMP9/SA/BMP9 and TGFβ3/SA/BMP9) differentiated large chondrospheres but the cartilage matrix contained reduced levels of mucopolysaccharides (Figure 3.4I-L). Based on these results we adopted a BMP2/SA/BMP9 protocol for further studies on cartilage regeneration in vitro.

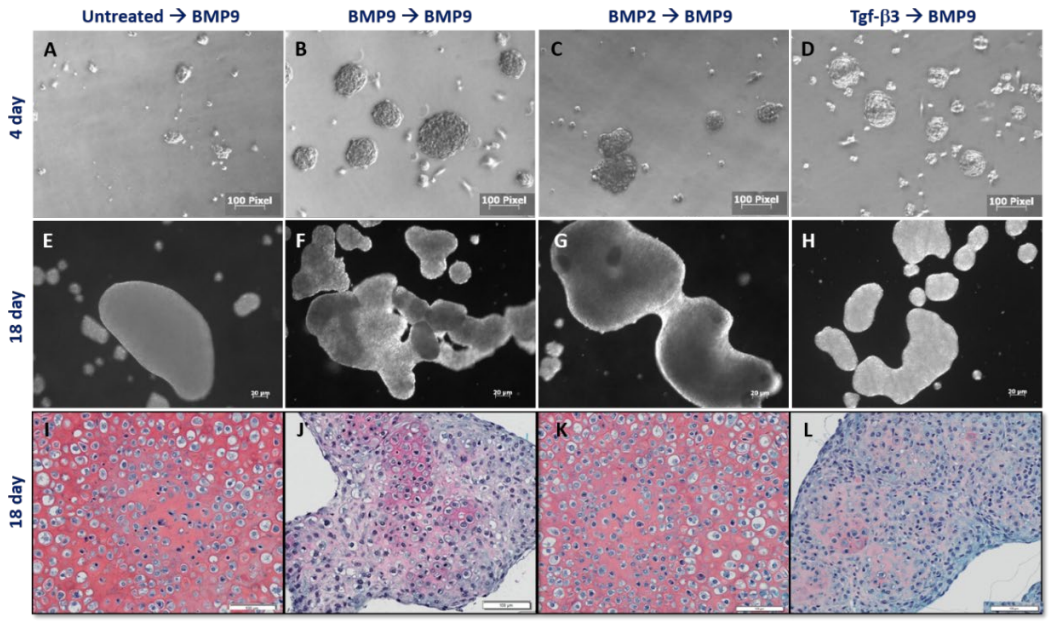

Figure 3.4 Treating BMP2 during self-aggregation period enhances the size of P3_D8 aggregate and maintains P3_D8 chondrocyte differentiation with mucopolysaccharides rich matrix.
At day 4, the size of P3_D8 aggregate in untreated control (A), BMP9 treated (B), BMP2 treated (C) and TGFb3 treated (D). After 14 days of BMP9 treatment, the size and number of P3_D8 chondrospheres in no pre-treatment control (E), BMP9 pre-treatment (F), BMP2 pre-treatment (G) and TGFb3 pre-treatment (H). Safranin O/fast green staining of large P3_D8 chondrospheres in no pre-treatment control (I), BMP9 pre-treatment (J), BMP2 pre-treatment (K) and TGFb3 pre-treatment (L). Scale bars: 200 μM for E-H; 100 μM for A-D and I-L.

BMP9 Differentiates P3_D8 clone toward Articular Cartilage

To investigate the P3_D8 chondrogenic response using the BMP2/SA/BMP9 protocol, a genome-wide transcriptome study was performed using RNA-seq. P3_D8 clone was differentiated for 18 days and total RNA was extracted from cartilage aggregates for RNA-seq (P3_D8_B2B9). Monolayer culture of the P3_D8 clone was used for comparison (P3_D8_control). Using a cutoff of $\log2(FC) \geq |1.5|$ and FDR P-value < 0.05, the differential expressed gene analysis identified 2365 up-regulated and 812 down-regulated genes (Figure 3.5A). Functional annotation analysis identified the top 6 associated biological activities of up-regulated genes (cell adhesion, biological adhesion, skeletal system development, extracellular

structure organization, cartilage development and ECM organization) and all have obvious links with induced chondrogenesis (Figure 2.5B). To study the differentiation of cartilage from the P3_D8 clone, we compared our datasets to RNA-seq datasets of mature murine (5 month old) articular cartilage (Bekki et al., 2020) and developing (PN21) mouse growth plate cartilage (Sabik et al., 2017) from NCBI shared resource. A genome-wide analysis of articular cartilage and growth plate cartilage indicated a strong positive correlation (r = 0.78) as anticipated given that both contain chondrocytes with a similar origin. Expressed genes between articular cartilage and growth plate cartilage were analyzed and the top 30 differentially expressed genes were used as a model for comparing chondrogenic tissues (Figure 3.5C and D). Analysis of the relationship between articular cartilage and growth plate cartilage indicated a negative correlation (r = -0.33), suggesting that these 60 genes can separate these two types of cartilage (Figure 3.5C). When the P3_D8_B2B9 RNAseq dataset is compared, the correlation analysis indicates a positive relationship with mature articular cartilage (r = 0.5) and a negative correlation with growth plate cartilage (r = -0.21; Figure 3.5C), suggesting that the chondrogenic response of the P3_D8 clone is more similar to articular cartilage than it is to growth plate cartilage. A similar heatmap clustering analysis based on the 60 differentially expressed chondrogenic genes was carried out with the P3_D8_control dataset (Figure 3.5C and D) and this analysis found a positive correlation with P3_D8_B2B9 cartilage (r = 0.63), a neutral relationship with articular cartilage (r = 0.11) and a negative relationship with growth plate cartilage (r = -0.35). Together with the histological evidence of cartilage formation from the P3_D8 clone, this unbiased analysis suggests that the BMP2/SA/BMP9 protocol induces the P3_D8 clone to differentiate toward an articular chondrocyte phenotype.

A more targeted heatmap analysis was carried out focusing on genes known to be associated with the differentiation of hyaline cartilage (Acan, Col2a1, Col9a2, Comp, and Sox9), articular cartilage (Prg4, Cilp, Chrdl2, Enpp2, and Scrg1), hypertrophic cartilage (Col10a1 and mmp13), and fibrocartilage (Col1a1) (Figure 3.5E; Yu et al., 2022). Focusing first on changes in gene expression associated with the differentiation of P3_D8_control to P3_D8_B2B9 cartilage, the analysis found that the expression of all target chondrogenic genes was at a low level in the P3_D8 clone prior to BMP2/SA/BMP9 treatment, and expression was enhanced for all target genes with the exception of Prg4. To confirm these RNA-seq results, quantitative RT-PCR (qRT-PCR) was used to compare the expression of 6 target genes (Col2a1, Sox9, Prg4, Cilp, Enpp2, and Scrg1) between P3_D8_B2B9 cartilage RNA and P3_D8 control RNA (Figure 3.5F). This analysis validated the RNAseq results in 5 of the 6 genes tested with the one exception involving the articular cartilage-specific gene Prg4 which displayed enhanced expression in contrast to the RNAseq data. The heatmap analysis revealed a general trend in which P3_D8_B2B9 chondrogenic gene expression levels were positioned intermediate between P3_D8 control and mature articular cartilage for most target genes. The exception to this rule included Col2a1, Enpp2 and Col1a1 all of which were expressed in P3/D8_B2B9 cartilage at a higher level than mature articular cartilage. Overall, this analysis provides further support for the hypothesis that the P3_D8 clone is stimulated to differentiate into articular chondrocytes by the BMP2/SA/BMP9 protocol.

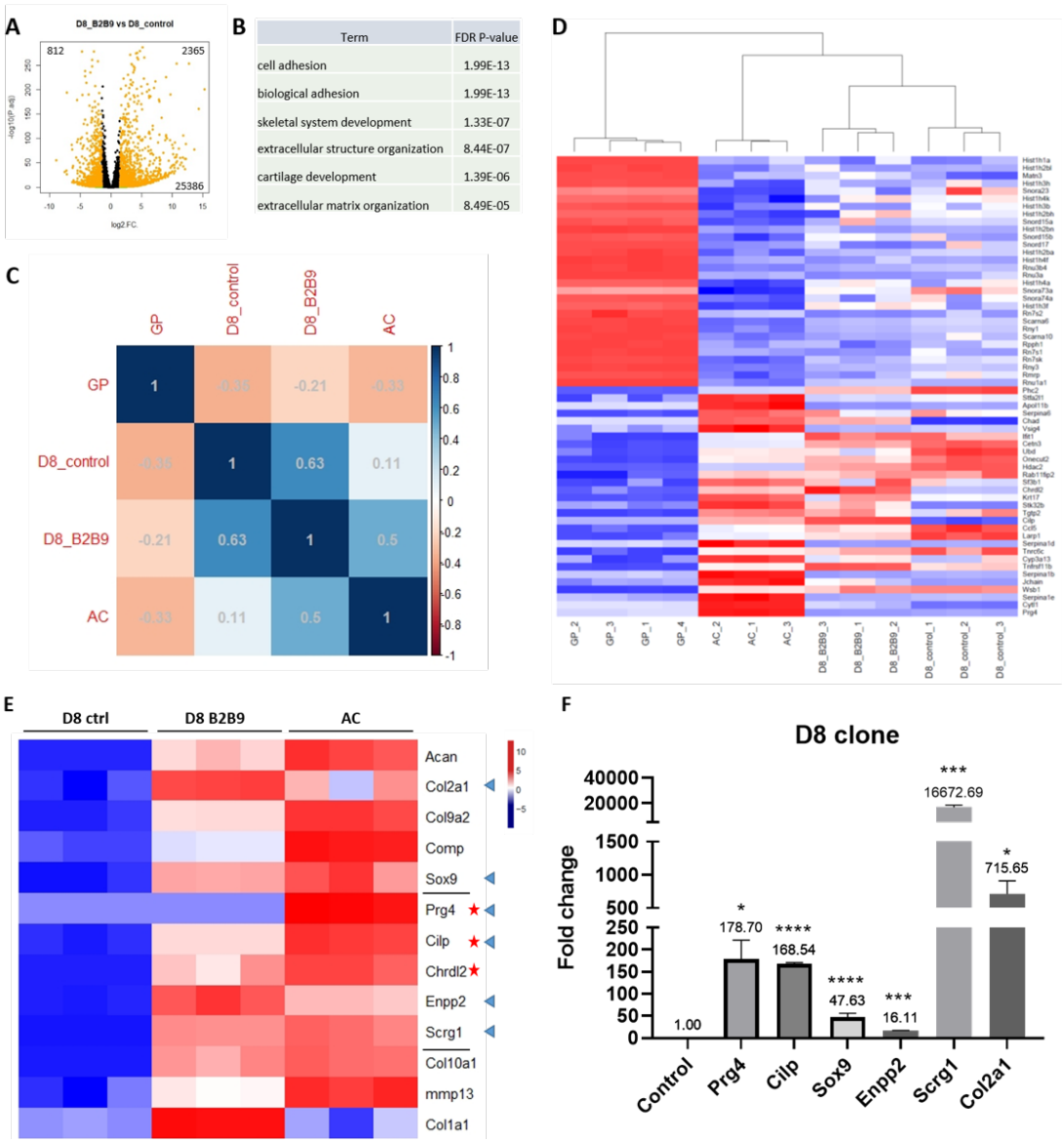

Figure 3.5: Genome-wide RNA-seq analysis and chondrocyte-related gene expression analysis of P3_D8 clone differentiated cartilage.
Comparison of P3_D8 cartilage differentiated by 18 days culture of BMP2/SA/BMP9 protocol (D8_B2B9) and monolayer culture control (D8_control) by volcano plot (A) and functional annotation (B). Comparison of GP, AC, D8_control, and D8_B2B9 with the top 30 GP highest expression genes compared to AC and the top 30 AC highest expression genes compared to GP: correlation analysis (C); heatmap couple with clustering analysis (D). Heatmap analysis with chondrocyte-related genes was used to compare gene expression levels of AC, D8_control, and D8_B2B9 (E). The red stars indicate genes that present in the top 30 AC highest expression genes compared to GP. The blue arrowheads indicate the selected genes for qRT-PCR analysis. The qRT-PCR result of D8_B2B9 gene expression levels normalized by individual D8_controls (F). AC: Articular Cartilage; GP: Growth Plate cartilage. Statistical analysis: default adjusted analysis for RNA-seq results and unpaired t test for qPT-PCR, N=3 for all analysis.

P3_D8 clone Organized Differentiate into Articular Cartilage but Not Hypertrophic Chondrocyte or Fibrocartilage

To further confirm P3_D8 clone was differentiated into articular cartilage at the protein level, the P3_D8 clone was cultured for an extended period (44 days: BMP2/self-aggregation for 4 days followed by BMP9 for 40 days) and the resulting chondrospheres were analyzed using histology and immunohistochemistry. For comparison, we analyzed the articular cartilage of the PN7 knee joint as an example of maturing articular cartilage. Safranin O/fast green stained sections of the knee identified high mucopolysaccharide content throughout the articular cartilage matrix and a gradient of chondrocyte size with small chondrocytes associated with the superficial layer and progressively larger chondrocytes in the deeper layers (Figure 3.6A and E). Immunohistochemical analyses indicate that many, but not all, cells of PN7 knee articular cartilage express Sox9 whereas ColX expression is restricted to the growth plate and ColI is expressed in bone and fibrous tissues surrounding the joint (Figure 3.6B-D and F-H). By comparison, cartilage differentiated by P3_D8 clone after 44 days of culture appeared well differentiated. Safranin O/fast green stained histological samples identified cartilage with high mucopolysaccharide content in the matrix surrounding the chondrocytes and the cartilage was encapsulated by a fibrous layer of cells (Figure 3.7A). The cartilage contains chondrocytes of varying sizes that do not appear to be randomly distributed with small chondrocytes in the center and larger chondrocytes in the periphery (Figure 3.7B). Immunohistochemical staining for Sox9 indicates expression by many, but not all cells, of the regenerated cartilage similar to postnatal articular cartilage. Alternatively, ColI expression is restricted to the fibrous cell layer, as is ColX

expression, although we found no histological evidence of hypertrophic chondrocytes in this layer (Figure 3.7C-E).

We next investigated the structural similarity between P3_D8 differentiated cartilage and the PN7 knee articular cartilage. Histological analysis using Mallory's trichrome staining to identify collagens present in cartilage matrix differentiates an upper zone of dark blue stained tissue from the light blue stained deep zone of the PN7 knee articular cartilage (Figure 3.6I). There is a clear change in chondrocyte density and the presence of lacunae based on safranin O/fast green staining (Figure 3.6E) that correlates with this staining pattern. The immunohistochemical analysis identifies expression of the superficial zone marker, Prg4, and the middle zone marker, Cilp (Lorenzo et al., 1998), as associated with the dark blue upper zone of articular cartilage (Figure 3.6J and K). We also find that Acan expression is primarily associated with the light blue deep zone indicating differential expression by cells within distinct articular cartilage layers of the PN7 knee (Figure 3.6L). These expression domains in maturing articular cartilage have been previously described (Di Bella et al., 2015). A similar analysis of the P3_D8 differentiated cartilage identifies a clear histological separation of the dark blue stained central cells from the light blue stained peripheral cells based on Mallory's trichrome staining (Figure 3.7F). This transition appears to correlate with a change in chondrocyte size evident in Safranin O/fast green stained sections (Figure 3.7B and G). Immunostaining for Cilp identifies cells scattered throughout the regenerated cartilage and appeared to be a region-specific expression that is regionally restricted to the small chondrocytes of the central cartilage (Figure 3.7I). Alternatively, Acan immunopositive cells are found throughout the regenerated cartilage (and in the fibrous layer), however the Acan expressing cells are mostly localized to the larger chondrocytes in the periphery of the cartilage (Figure 3.7J). A similar analysis of Prg4

expressing cells shows that they are scattered throughout the regenerated cartilage and fibrous layer and not regionally localized (Figure 3.7H). These results suggest that the BMP2/SA/BMP9 protocol establishes culture conditions that promote the differentiation of chondrocytes into distinct layers that parallel maturing articular cartilage. The data also support the conclusion that the P3_D8 clone represents an articular chondrocyte progenitor cell.

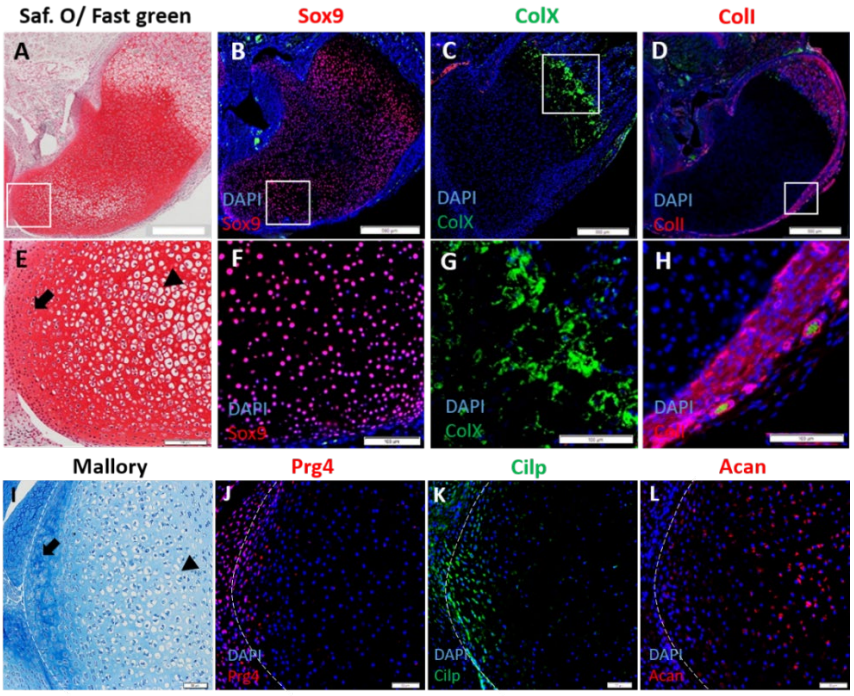

Figure 3.6 Stained mouse PN7 knee joint with markers associated to distinct types of chondrocyte. For chondrocyte type study, sectioned PN7 knee samples were stained with Safranin O/fast green staining in low magnification (A) and high magnification (E), Sox9 in low magnification (B) and high magnification (F), ColX in low magnification (C) and high magnification (G), and ColI in low magnification (D) and high magnification (H). For chondrocyte structure study, PN7 knee was stained with Mallory's trichrome staining (I), Prg4 (J), Cilp (K), and Acan (L). The white line indicates the surface of joint, the black arrow indicates small chondrocytes, and the black arrowhead indicates the enlarged chondrocytes. Scale bars: 500 μM for A-D; 100 μM for E-H and 50 μM for I-L.

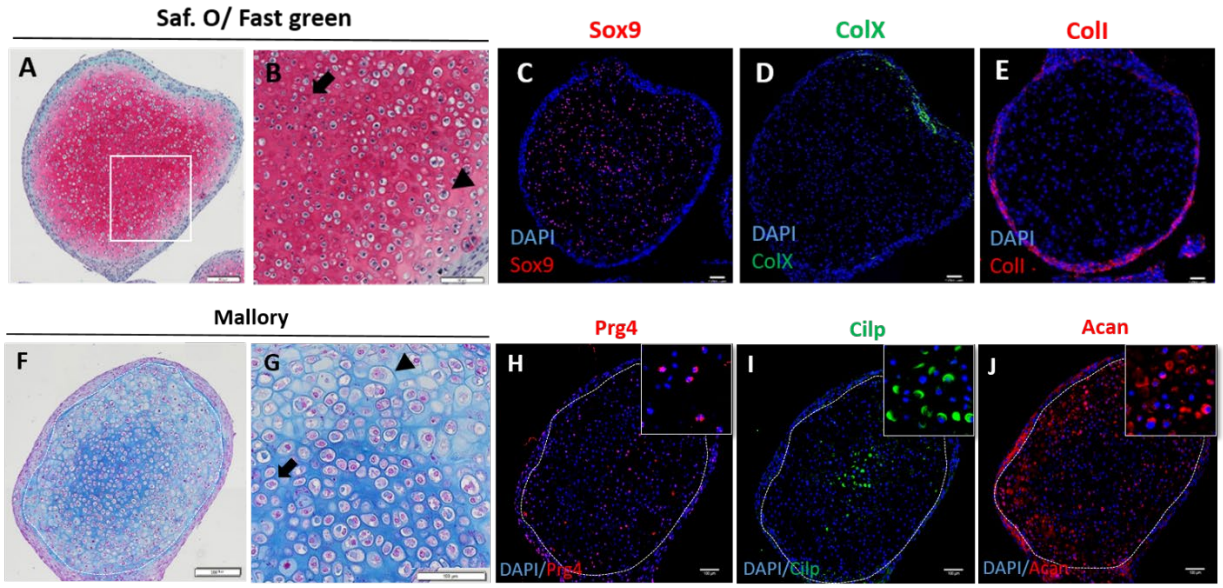

Figure 3.7 P3_D8 clone differentiated chondrocytes express articular cartilage markers but not hypertrophic and fibrous cartilage markers.
For chondrocyte type study, P3_D8 clone was differentiated by BMP2/SA/BMP9 protocol for 44 days and the sectioned samples were stained with Safranin O/fast green staining in low magnification (A) and high magnification (B), Sox9 (C), ColX (D), and ColI (E). For chondrocyte structure study, sectioned samples were stained with Mallory's trichrome staining in low magnification (F) and high magnification (G), Prg4 in low magnification (H) and high magnification (H'), Cilp in low magnification (I) and high magnification (I'), and Acan in low magnification (J) and high magnification (J'). The white line indicates the interface of chondrocyte region and fibrous tissue, the black arrow indicates small chondrocytes, and the black arrowhead indicates the enlarged chondrocytes. Scale bars: 200 μM for A and F; 100 μM for B-E and G-J. N=3 for all analysis.

Another similarity between P3_D8 differentiated cartilage and the maturing knee articular cartilage is the fibrous layer – both surround the cartilage tissues and are positive for ColI and ColX. The fibrous layer of developing epiphyseal cartilage has been reported containing mesenchymal progenitor cells (Tong et al., 2019), we therefore tested whether progenitor cells are also present in the fibrous layer of P3_D8 differentiated cartilage. The cells within the P3_D8 fibrous layer (D8_edge cells) were isolated by enzymatic dissociation (Figure 3.8A-B), and when expensed in monolayer culture they appeared rounded cell morphology

similar to the P3_D8 clone (Figure 3.8C and Figure 3.2A). Chondrogenic differentiation result indicated that the D8_edge cells can be differentiated into chondrocytes by BMP2/SA/BMP9 protocol in 18 days (Figure 3.8D). After 44 days of culture, Mallory's trichrome stained D8_edge cell differentiated cartilage displayed the dark blue central region, the light blue peripheral region and a fibrous layer, which is histologically similar to P3_D8 differentiated cartilage (Figure 3.8F). The immunohistochemical analysis identified that the D8_edge cell differentiated chondrocytes are composed of Cilp and Acan positive cells with few Prg4 positive cells, while the cells in the fibrous layer are positive for Prg4, ColX and ColI (Figure 3.8G-K). These results indicated that the P3_D8 clone has the ability to self-renew during in vitro chondrogenesis, and the renewal cells are niched in the fibrous layer. To further confirm this, the fibrous layer cells (D8_edge_R2 cells) were enzymatically dissociated from D8_edge cell differentiated cartilage and the chondrogenic potential was tested. Using BMP2/SA/BMP9 protocol, D8_edge_R2 cells successfully differentiated into chondrocytes (Figure 3.8E). In addition, when test cells with SSCs characters, both D8_edge cells and D8_edge_R2 cells can be differentiated to osteocytes but not adipocytes, and expressed SSCs surface markers (94.4% and 93.2% respectively, N=3; Figure 3.8L and M). These results support the conclusion that the P3_D8 clone is an SSCs-like cell type and can self-renew during BMP2/SA/BMP9 protocol induced in vitro chondrogenic differentiation.

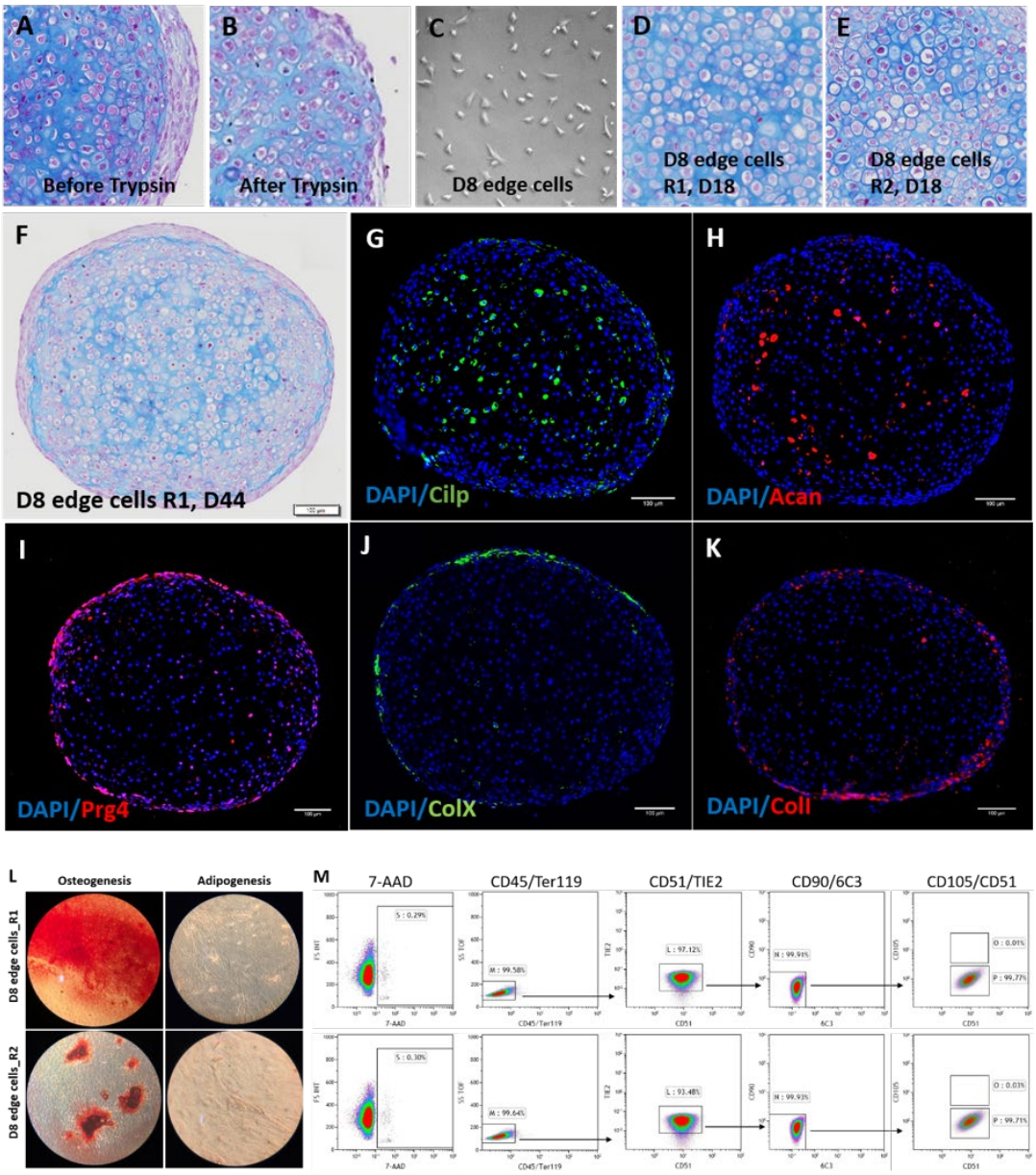

Figure 3.8: P3_D8 clone has ability to self-renew during in vitro chondrogenic differentiation. The fibrous layer of P3_D8 differentiated cartilage was enzymatic dissociated to obtain D8_edge cells: before trypsin (A) and after trypsin (B). Cell morphology of D8_edge cells in monolayer culture (C). Mallory's trichrome staining of D8_edge cell differentiated by BMP2/SA/BMP9 protocol for 18 days (D) and 44 days (F). Immunostaining studies of D8_edge cell differentiated cartilage with Cilp (G), Acan (H), Prg4 (I), ColX (J) and ColI (K). The fibrous layer of D8_edge cell differentiated cartilage was enzymatic dissociated to obtain D8_edge R2 cells, and the chondrogenic potential was determined by 18 days culture of BMP2/SA/BMP9 protocol. The D8_edge R2 cell differentiated chondrocytes were indicated by Mallory's trichrome staining (E). L) Osteogenic and adipogenic differentiations were tested using D8_edge cells (Top panels) and D8_edge R2 cells (Bottom panels). M) Phenotype studies with SSCs markers of D8_edge cells (Up panels), D8_edge R2 cells (Bottom panels). N=3 for immunostaining, differentiation assay and phenotype studies.

P3_D8 clone differentiated chondrocytes retained hyaline chondrocyte phenotype

One of the critical differences between articular cartilage and growth plate cartilage is that hyaline chondrocytes are maintained within articular cartilage, while in growth plate cartilage they are transient and will undergo hypertrophy, eventually transdifferentiating to osteoblasts (Iwamoto et al., 2013). Hyaline chondrocytes regenerated from P3 fibroblasts have been showed to retain a potential for hypertrophic chondrocyte differentiation in vivo and by additional BMP2 treatment in vitro (Yu et al., 2022), we thus tested whether P3_D8 clone differentiated hyaline chondrocytes remain this plasticity in vitro and in vivo. The P3_D8 clone was cultured in BMP2/SA/BMP9 protocol for 18 days followed by another 14 days treatment of either BMP2 to induce cell hypertrophy or BMP9, as a control, to maintain a hyaline chondrocyte phenotype. The histological analysis revealed that BMP2 treated D8 chondrocytes maintain hyaline cartilage phenotype with an abundance of matrix proteins production (Figure 3.9D and E) similar to BMP9 treated control group (Figure 3.9A and B). In addition, ColX immunopositive cells were not found in both BMP2 and BMP9 treated P3_D8 chondrocytes suggesting that P3_D8 clone differentiated hyaline chondrocytes cannot be induced to undergo hypertrophy in vitro by BMP2 treatment (Figure 3.9C and F).

To test whether P3_D8 clone differentiated cartilage remains hyaline chondrocyte phenotype in vivo, we transplanted P3_D8 cartilages into an acute metatarsal-phalangeal (MtP) joint defect model (Yu et al., 2022). The MtP joint includes two multilayer articular cartilages at the ends of the metatarsus (Mt) and the first phalangeal element (P1), and the P1 articulation was used for the joint defect model by surgical removing all layers of articular cartilage and subchondral bone until the bone marrow is exposed. The lacZ-labeled P3_D8 clone was

differentiated by BMP2/SA/BMP9 protocol for 44 days and then implanted into the MtP joint defect. After 90 days, the joint and the engrafted P3_D8 cartilage were collected and evaluated. The histological staining showed that the P3_D8 chondrocytes were alive in the damaged joint, partially integrated with host tissues, and maintained collagens and proteoglycans expression (Figure 3.9G and K). The immunostaining of lacZ and Acan indicated that implanted P3_D8 chondrocytes survived in the injured site and retained chondrocyte function (Figure 3.9H-J). The immunostaining of Sox9, ColX and ColI demonstrated that after 90 days of implantation, P3_D8 chondrocytes maintain hyaline chondrocyte phenotype and did not transdifferentiate to hypertrophic or fibrous cartilages (Figure 3.9L-N). These results suggested that P3_D8 clone differentiated cartilage can survive in the surgical created joint defects, maintain hyaline cartilage phenotype and matrix protein expression, and partially integrate with host tissues. Coupled with in vitro hypertrophy induction study, these results support the conclusion that P3_D8 clone, compared to P3 fibroblasts, is more likely to differentiate toward articular cartilage by BMP2/SA/BMP9 protocol.

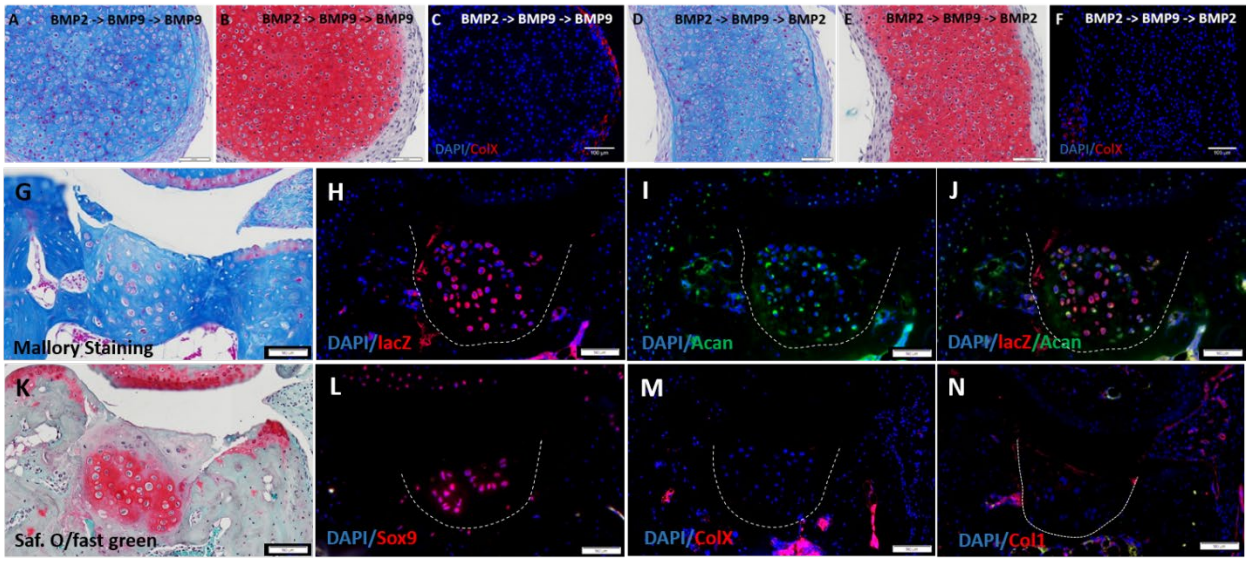

Figure 3.9 D8 clone differentiated chondrocytes remain articular chondrocyte phenotype after BMP2 treatment in vitro or transplanted into acute joint defect in vivo.
D8 clone was additionally treated with BMP9 or BMP2 for 14 days after 18 days of differentiation by BMP2/SA/BMP9 protocol (A-F). D8 aggregates with continually BMP9 treatment were stained by Mallory's trichrome staining (A), Safranin O/fast green staining (B), and ColX immunostaining (C). D8 aggregates with additionally BMP2 treatment were stained by Mallory's trichrome staining (D), Safranin O/fast green staining (E), and ColX immunostaining (F). D8 clone was differentiated by BMP2/SA/BMP9 protocol for 44 days and implanted to surgical created MtP joint defect for 90 days (G-N). Samples were stained by Mallory's trichrome staining (G), lacZ and Acan co-staining (H-J), Safranin O/Fast green staining (K), Sox9 (L), ColX (M), and Col1 (N). The white line indicate the interfaces of grafted cells and host tissues. Scale bar: 100 μM. N=3 for *in vitro* studies and N=12 for *in vivo* studies.

3.4 Discussion

The cell-based therapies of OA disease that aim to restore or repair damaged articular cartilage have been investigated for almost 30 years but their clinical effectiveness remains limited. The significant challenges include 1) the identification of expandable cell sources; 2) a satisfactory methodology for articular cartilage differentiation; and 3) the in vivo stability of transplanted cartilage since there is a tendency to differentiate into nonfunctional fibrous cartilage or hypertrophic cartilage (Brittberg et al., 1994; Correa and Lietman, 2017; Demoor et al., 2014; Medvedeva et al., 2018). To address these problems, our previous studies have

demonstrated that hyaline chondrocyte progenitor cells are present among adult fibroblasts isolated from P3 skeletal elements (P3 fibroblasts). In addition, P3 fibroblasts can be expanded as a cell line (Wu et al., 2013) and can be induced to differentiate into hyaline cartilage by a SA differentiation protocol coupled with BMP9 treatment (Yu et al., 2022). In this chapter, we show that the clonal cell line of P3 fibroblasts display varying chondrogenic potential and identified a hyaline cartilage forming clone (P3_D8 clone) that is distinct from hypertrophic cartilage forming clone (P3_E3 clone). We provided evidence that P3_D8 clone share characteristics with SSCs- and can be induced to differentiate into articular cartilage by a modified SA protocol (BMP2/SA/BMP9). The evidence also indicates that the P3_D8 clonal cells with SSC characteristics become sequestered into a fibrous layer that differentiates around the engineered articular cartilage. Moreover, when implanted into joint defects, P3_D8 clone differentiated cartilage survives and maintains an articular cartilage phenotype without differentiating to fibrous cartilage or hypertrophic cartilage. Therefore, the significance of this study includes: 1) identification of a cell source involved in AC regeneration, 2) development of an effective AC differentiation protocol and 3) the demonstration that in vitro differentiated AC is maintained following in vivo transplantation.

SSCs have been defined with the ability to self-renew during expansion in monolayer culture or transplantation onto kidney capsules (Chan et al., 2015; Murphy et al., 2020). However, our data revealed that expanding the P3_D8 clone can be expanded for at least 6 passages while maintaining an SSC-like phenotype. These results suggest that there are differences between SSCs and the P3_D8 clone and/or differences between culture conditions. P3_D8 clone was isolated from a heterogeneous P3 fibroblast that was originally from the connective tissues associated with the P3 skeletal elements, therefore it could represent cells

derived from endothelial, vascular smooth muscle, periosteum or articular cartilage (Wu et al., 2013). Thus, the sources of the P3_D8 clone remain elusive and difficult to compare with SSCs isolated from different locations that have been published. On the other hand, SSCs are expanded in aMEM with 10% FBS (Chan et al., 2015; Murphy et al., 2020) compared to 2% FBS/MSC medium supplemented with EGF, PDGF and LIF used for P3 and P3_D8 clonal cells. The culture conditions used for expanding digit fibroblasts were initially established to maintain pluripotency of adult marrow MSCs (Jiang et al., 2002) and was found to be well suitable for expanding P3 fibroblasts while maintaining regenerative competency (Wu et al., 2013; Yu et al., 2022). In addition, LIF is essential for culturing and maintaining the developmental potential of murine ES cells (Niwa et al., 1998). Taken together, our results suggest that optimizing the culture conditions for SSCs may extend expansion potential while maintaining differentiation potency.

Chondrogenic condensation is critical to in vivo cartilage development and the in vitro centrifugation to create high-density cell pellets mimic this biological process. However, our results and those of other studies show that differentiation is also associated with cells in the center of the pellet becoming necrotic (Estes and Guilak, 2011; Markway et al., 2010; Yu et al., 2022). Using a self-aggregation differentiation protocol, cell clusters progressively increase in size while undergoing chondrogenesis and attain a size comparable to cell pellets (~1.3 mm), but lack necrotic cells in the central region. Considering that articular cartilage is avascular and that articular chondrocytes prefer to differentiate and survive under low oxygen conditions (Bae et al., 2018; Lafont, 2010; Lee et al., 2013), there is a possible explanation for this phenomenon. In SA culture cells initially form small aggregates so that central P3_D8 clonal cells are in an oxygen/nutrient-rich environment during BMP9-induced differentiation into chondrocytes. Once

the central cells differentiate to chondrocytes, they become adapted to a reduced oxygen/nutrient environment and survive as the aggregate increases in size. On the other hand, cells forced to aggregate by centrifugation place P3_D8 clonal cells in the center of the pellet under conditions of reduced oxygen/nutrient prior to BMP9-induced chondrogenesis where they undergo necrosis, and chondrogenic differentiation is restricted to peripheral cells. Overall, these results indicated that the SA culture protocol displayed a significant advantage for in vitro chondrocyte differentiation.

The ideal treatment for in vitro articular cartilage differentiation should include appropriate treatments at different stages of AC formation (Correa and Lietman, 2017). We have previously established a SA/BMP9 protocol for P3 fibroblast chondrogenesis (Yu et al., 2022). In this study, we showed that sequentially treating with BMP2 during SA followed by BMP9 treatment to stimulate chondrogenesis was an effective strategy for articular cartilage differentiation by P3_D8 clonal cells. BMP2 has been reported to guide the initiation of cell condensation (Giffin et al., 2019) and to induce chondrogenesis of SSCs with the combined treatment of a VEGF signaling inhibitor, sVEGFR1 (Chan et al., 2015; Murphy et al., 2020). In this study, pre-treatment of BMP2, BMP9, or TGF-β3 enhanced P3_D8 clone condensation during the self-aggregation period, however after another 14 days of BMP9 induced chondrogenesis, only BMP2 pre-treated cells differentiated cartilage rich in mucopolysaccharides.. Although the biological effects of pre-treatment with BMP2, BMP9 and TGF remain unclear, the results suggest that differential modification of the cellular status in the early stages of condensation modifies the success of AC differentiation during later stages.

The inability of AC differentiated P3_D8 clonal cells to undergo hypertrophic chondrocyte differentiation in vivo and in vitro following additional BMP2 treatment represents a significant

advance for the field. During skeletal development, hyaline chondrocytes form an anlagen where central cells of the diaphysis participate in endochondral ossification to form bone while terminal cells of the epiphysis participate in articular cartilage formation. Thus, these results support the conclusion that the P3_D8 clone differentiates toward articular cartilage by BMP2/SA/BMP9 protocol. BMP9 induced chondrogenesis of clonal P3 cell lines identified clones that differentiated hypertrophic chondrocytes (i.e. P3_E3 clone) and clones that differentiated articular chondrocytes (i.e. P3_D8). These results suggest that articular cartilage progenitor cells are distinct from hypertrophic cartilage progenitor cells. Interestingly, BMP9 treatment of the parental P3 fibroblasts stimulates differentiation of only hyaline chondrocytes in vitro and hypertrophic chondrocytes differentiation is only observed when BMP9 treatment is withdrawn and replaced with BMP2 (Yu et al., 2022). The evidence suggests that hypertrophic chondrocyte progenitor cells are repressed in BMP9 treated P3 fibroblast cultures which imply the presence of an inhibitory activity within the parental P3 cell population that suppressed hypertrophic chondrocyte differentiation. This conclusion is supported by the differentiation of hypertrophic chondrocytes following transplantation in vivo which curtails BMP9 treatment. Clinically, during OA progression healthy articular chondrocytes undergo hypertrophy-like changes and lose their lubricate function to protect bones, which contributes to the exacerbation of OA symptoms (Dreier, 2010; van der Kraan and van den Berg, 2012). Parallels between hypertrophy during OA progression and the repression of hypertrophy in AC differentiation by BMP9 in culture suggest that BMP9 could function to repress hypertrophic chondrocyte differentiation during OA progression. This possibility represents an important avenue for future studies that could lead to therapeutics to minimize the exacerbation of OA disease.

BMP9 stimulated differentiation of AC using the SA-BMP2→BMP9 protocol stimulates the differentiation of an AC encapsulating fibrous layer that contains cells immunopositive for Col1 and Prg4. Cells within this fibrous layer were found to possess self-renewal properties: they could be isolated, expanded and re-induced by BMP9 to differentiate into AC over two cycles. These studies indicate that under conditions that stimulate chondrogenesis, chondroprogenitor cells become sequestered during the differentiation of associated connective tissues and remain dormant as a stem cell population. Stem cells with chondroprogenitor characteristics are found in a variety of different tissues and must be sequestered during development presumably for a later function, e.g. injury response. The sequestration of stem cells during tissue development is poorly understood and the AC differentiation model we have established provides an experimental setting to explore this important process. Interestingly, a recent study focused on the formation of the secondary ossification center in neonate skeletal development identified mesenchymal progenitor cells expressing Col1 present in a periarticular fibrous tissue layer surrounding the epiphysis that later participates in cartilage canal formation during maturation (Tong et al., 2019). In this case, progenitor cells emerge from a fibrous connective tissue layer to participate in the formation of the secondary ossification center during development. Both this study and our findings point to the importance of progenitor cell sequestration into fibrous connective tissues during tissue formation that can later function for both skeletal development and tissue regeneration.

In summary, this study identified an SSCs-like P3_D8 clonal cell line originally from fibroblasts derived from the mouse digit tip that can differentiate into articular cartilage, self-renew during in vitro chondrogenesis, and lacks the potential to differentiate to hypertrophic chondrocytes or fibrocartilage when implanted into joint defects. Unlike SSCs, this SSC-like cell

type is present in fibroblast cultures, displays stable cell line characteristics under appropriate conditions, and may be clinically beneficial for cell-based osteoarthritis treatment. In addition, cell clones that display hypertrophic chondrocyte progenitor characteristics provide an opportunity to investigate OA and identify molecular targets that can minimize pathological progression. Overall, in this study, we provide a promising cell source and an effective differentiation protocol that has the potential to be utilized in both basic research and clinical application of articular cartilage-related studies.

3.5 References

203. Bae, H.C., Park, H.J., Wang, S.Y., Yang, H.R., Lee, M.C., Han, H.S., 2018. Hypoxic condition enhances chondrogenesis in synovium-derived mesenchymal stem cells. Biomater Res 22, 28.
204. Bekki, H., Duffy, T., Okubo, N., Olmer, M., Alvarez-Garcia, O., Lamia, K., Kay, S., Lotz, M., 2020. Suppression of circadian clock protein cryptochrome 2 promotes osteoarthritis. Osteoarthritis and Cartilage 28, 966-976.
205. Borgens, R.B., 1982. What Is the Role of Naturally Produced Electric Current in Vertebrate Regeneration and Healing?, in: Bourne, G.H., Danielli, J.F. (Eds.), International Review of Cytology. Academic Press, pp. 245-298.
206. Brittberg, M., Lindahl, A., Nilsson, A., Ohlsson, C., Isaksson, O., Peterson, L., 1994. Treatment of deep cartilage defects in the knee with autologous chondrocyte transplantation. N Engl J Med 331, 889-895.
207. Cai, J.J., 2019. scGEAToolbox: a Matlab toolbox for single-cell RNA sequencing data analysis. Bioinformatics (Oxford, England).
208. Chan, C.K., Seo, E.Y., Chen, J.Y., Lo, D., McArdle, A., Sinha, R., Tevlin, R., Seita, J., Vincent-Tompkins, J., Wearda, T., Lu, W.J., Senarath-Yapa, K., Chung, M.T., Marecic, O., Tran, M., Yan, K.S., Upton, R., Walmsley, G.G., Lee, A.S., Sahoo, D., Kuo, C.J., Weissman, I.L., Longaker, M.T., 2015. Identification and specification of the mouse skeletal stem cell. Cell 160, 285-298.
209. Correa, D., Lietman, S.A., 2017. Articular cartilage repair: Current needs, methods and research directions. Semin Cell Dev Biol 62, 67-77.

210. Dawson, L.A., Brunauer, R., Zimmel, K.N., Qureshi, O., Falck, A.R., Kim, P., Dolan, C.P., Yu, L., Lin, Y.L., Daniel, B., Yan, M., Muneoka, K., 2019. Adult Mouse Digit Amputation and Regeneration: A Simple Model to Investigate Mammalian Blastema Formation and Intramembranous Ossification. J Vis Exp.

211. Dawson, L.A., Yu, L., Yan, M., Marrero, L., Schanes, P.P., Dolan, C., Pela, M., Peterson, B., Han, M., Muneoka, K., 2017. The periosteal requirement and temporal dynamics of BMP2-induced middle phalanx regeneration in the adult mouse. Regeneration 4.

212. Demoor, M., Ollitrault, D., Gomez-Leduc, T., Bouyoucef, M., Hervieu, M., Fabre, H., Lafont, J., Denoix, J.M., Audigie, F., Mallein-Gerin, F., Legendre, F., Galera, P., 2014. Cartilage tissue engineering: molecular control of chondrocyte differentiation for proper cartilage matrix reconstruction. Biochim Biophys Acta 1840, 2414-2440.

213. Di Bella, C., Fosang, A., Donati, D.M., Wallace, G.G., Choong, P.F., 2015. 3D Bioprinting of Cartilage for Orthopedic Surgeons: Reading between the Lines. Front Surg 2, 39.

214. Dominici, M., Le Blanc, K., Mueller, I., Slaper-Cortenbach, I., Marini, F., Krause, D., Deans, R., Keating, A., Prockop, D., Horwitz, E., 2006. Minimal criteria for defining multipotent mesenchymal stromal cells. The International Society for Cellular Therapy position statement. Cytotherapy 8, 315-317.

215. Douglas, B.S., 1972. Conservative management of guillotine amputation of the finger in children. Australian paediatric journal 8, 86-89.

216. Dreier, R., 2010. Hypertrophic differentiation of chondrocytes in osteoarthritis: the developmental aspect of degenerative joint disorders. Arthritis research & therapy 12, 216.

217. Estes, B.T., Guilak, F., 2011. Three-dimensional culture systems to induce chondrogenesis of adipose-derived stem cells. Methods Mol Biol 702, 201-217.

218. Finak, G., McDavid, A., Yajima, M., Deng, J., Gersuk, V., Shalek, A.K., Slichter, C.K., Miller, H.W., McElrath, M.J., Prlic, M., Linsley, P.S., Gottardo, R., 2015a. MAST: a flexible statistical framework for assessing transcriptional changes and characterizing heterogeneity in single-cell RNA sequencing data. Genome Biol 16, 278.

219. Finak, G., McDavid, A., Yajima, M., Deng, J., Gersuk, V., Shalek, A.K., Slichter, C.K., Miller, H.W., McElrath, M.J., Prlic, M., Linsley, P.S., Gottardo, R., 2015b. MAST: a flexible statistical framework for assessing transcriptional changes and characterizing heterogeneity in single-cell RNA sequencing data. Genome Biology 16, 278.

220. Giffin, J.L., Gaitor, D., Franz-Odendaal, T.A., 2019. The Forgotten Skeletogenic Condensations: A Comparison of Early Skeletal Development Amongst Vertebrates. J Dev Biol 7.

221. Han, M., Yang, X., Lee, J., Allan, C.H., Muneoka, K., 2008. Development and regeneration of the neonatal digit tip in mice. Dev Biol 315, 125-135.

222. Huang da, W., Sherman, B.T., Lempicki, R.A., 2009a. Bioinformatics enrichment tools: paths toward the comprehensive functional analysis of large gene lists. Nucleic Acids Res 37, 1-13.

223. Huang da, W., Sherman, B.T., Lempicki, R.A., 2009b. Systematic and integrative analysis of large gene lists using DAVID bioinformatics resources. Nat Protoc 4, 44-57.

224. Humason, G.L., 1962. Animal tissue techniques. W.H. Freeman, San Francisco,.

225. Illingworth, C.M., 1974. Trapped fingers and amputated finger tips in children. Journal of pediatric surgery 9, 853-858.

226. Iwamoto, M., Ohta, Y., Larmour, C., Enomoto-Iwamoto, M., 2013. Toward regeneration of articular cartilage. Birth Defects Research Part C: Embryo Today: Reviews 99, 192-202.

227. Jiang, Y., Vaessen, B., Lenvik, T., Blackstad, M., Reyes, M., Verfaillie, C.M., 2002. Multipotent progenitor cells can be isolated from postnatal murine bone marrow, muscle, and brain. Experimental Hematology 30, 896-904.

228. Kragl, M., Knapp, D., Nacu, E., Khattak, S., Maden, M., Epperlein, H.H., Tanaka, E.M., 2009. Cells keep a memory of their tissue origin during axolotl limb regeneration. Nature 460, 60-65.

229. Lafont, J.E., 2010. Lack of oxygen in articular cartilage: consequences for chondrocyte biology. Int J Exp Pathol 91, 99-106.

230. Lee, H.H., Chang, C.C., Shieh, M.J., Wang, J.P., Chen, Y.T., Young, T.H., Hung, S.C., 2013. Hypoxia enhances chondrogenesis and prevents terminal differentiation through PI3K/Akt/FoxO dependent anti-apoptotic effect. Sci Rep 3, 2683.

231. Lorenzo, P., Bayliss, M.T., Heinegård, D., 1998. A novel cartilage protein (CILP) present in the mid-zone of human articular cartilage increases with age. J Biol Chem 273, 23463-23468.

232. Markway, B.D., Tan, G.K., Brooke, G., Hudson, J.E., Cooper-White, J.J., Doran, M.R., 2010. Enhanced chondrogenic differentiation of human bone marrow-derived mesenchymal stem cells in low oxygen environment micropellet cultures. Cell Transplant 19, 29-42.

233. Medvedeva, E.V., Grebenik, E.A., Gornostaeva, S.N., Telpuhov, V.I., Lychagin, A.V., Timashev, P.S., Chagin, A.S., 2018. Repair of Damaged Articular Cartilage: Current Approaches and Future Directions. Int J Mol Sci 19.

234. Muller, T.L., Ngo-Muller, V., Reginelli, A., Taylor, G., Anderson, R., Muneoka, K., 1999. Regeneration in higher vertebrates: Limb buds and digit tips. Seminars in Cell & Developmental Biology 10, 405-413.

235. Muneoka, K., Allan, C.H., Yang, X., Lee, J., Han, M., 2008. Mammalian regeneration and regenerative medicine. Birth Defects Res C Embryo Today 84, 265-280.

236. Murphy, M.P., Koepke, L.S., Lopez, M.T., Tong, X., Ambrosi, T.H., Gulati, G.S., Marecic, O., Wang, Y., Ransom, R.C., Hoover, M.Y., Steininger, H., Zhao, L., Walkiewicz, M.P., Quarto, N., Levi, B., Wan, D.C., Weissman, I.L., Goodman, S.B., Yang, F., Longaker, M.T., Chan, C.K.F., 2020. Articular cartilage regeneration by activated skeletal stem cells. Nat Med 26, 1583-1592.

237. Niwa, H., Burdon, T., Chambers, I., Smith, A., 1998. Self-renewal of pluripotent embryonic stem cells is mediated via activation of STAT3. Genes & development 12, 2048-2060.

238. Osorio, D., Zhong, Y., Li, G., Huang, J.Z., Cai, J.J., 2020. scTenifoldNet: A Machine Learning Workflow for Constructing and Comparing Transcriptome-wide Gene Regulatory Networks from Single-Cell Data. Patterns 1, 100139.

239. Sabik, O.L., Medrano, J.F., Farber, C.R., 2017. Genetic Dissection of a QTL Affecting Bone Geometry. G3 Genes|Genomes|Genetics 7, 865-870.

240. Schmitz, N., Laverty, S., Kraus, V.B., Aigner, T., 2010. Basic methods in histopathology of joint tissues. Osteoarthritis Cartilage 18 Suppl 3, S113-116.

241. Tong, W., Tower, R.J., Chen, C., Wang, L., Zhong, L., Wei, Y., Sun, H., Cao, G., Jia, H., Pacifici, M., Koyama, E., Enomoto-Iwamoto, M., Qin, L., 2019. Periarticular Mesenchymal Progenitors Initiate and Contribute to Secondary Ossification Center Formation During Mouse Long Bone Development. Stem Cells 37, 677-689.

242. van der Kraan, P.M., van den Berg, W.B., 2012. Chondrocyte hypertrophy and osteoarthritis: role in initiation and progression of cartilage degeneration? Osteoarthritis and Cartilage 20, 223-232.

243. Wu, Y., Wang, K., Karapetyan, A., Fernando, W.A., Simkin, J., Han, M., Rugg, E.L., Muneoka, K., 2013. Connective tissue fibroblast properties are position-dependent during mouse digit tip regeneration. PLoS One 8, e54764.

244. Yu, L., Dawson, L.A., Yan, M., Zimmel, K., Lin, Y.-L., Dolan, C.P., Han, M., Muneoka, K., 2019a. BMP9 stimulates joint regeneration at digit amputation wounds in mice. Nature Communications 10, 424.

245. Yu, L., Dawson, L.A., Yan, M., Zimmel, K., Lin, Y.L., Dolan, C.P., Han, M., Muneoka, K., 2019b. BMP9 stimulates joint regeneration at digit amputation wounds in mice. Nat Commun 10, 424.

246. Yu, L., Han, M., Yan, M., Lee, E.C., Lee, J., Muneoka, K., 2010. BMP signaling induces digit regeneration in neonatal mice. Development 137, 551-559.

247. Yu, L., Han, M., Yan, M., Lee, J., Muneoka, K., 2012. BMP2 induces segment-specific skeletal regeneration from digit and limb amputations by establishing a new endochondral ossification center. Dev Biol 372, 263-273.

248. Yu, L., Lin, Y.-L., Yan, M., Li, T., Wu, E.Y., Zimmel, K., Qureshi, O., Falck, A., Sherman, K.M., Huggins, S.S., Hurtado, D.O., Suva, L.J., Gaddy, D., Cai, J., Brunauer,

R., Dawson, L.A., Muneoka, K., 2022. Hyaline cartilage differentiation of fibroblasts in regeneration and regenerative medicine. Development 149.

4 DETERMINE SIGNATURES BETWEEN P3_D8 CLONE AND P3_E3 CLONE

4.1 Introduction

Hypertrophic chondrocytes can be found at several places inside the body including the developing growth plate cartilage (Tsang et al., 2015), the calcified zone of adult articular cartilage (Oegema et al., 1997) and in osteoarthritis (OA) joints (Ferrao Blanco et al., 2021; Rim et al., 2020). Hypertrophic chondrocytes in the growth plate are differentiated from proliferation zone chondrocytes and will eventually become osteoblasts or undergo apoptosis as invading osteoblasts form new bone. Thus growth plate hypertrophic chondrocytes serve as a transient template for endochondral bone formation. Most of what is known about hypertrophic chondrocyte differentiation are based on growth plate studies. On the other hand, hypertrophic chondrocytes are also present in articular cartilage and reside within the calcified zone separating the deep zone articular chondrocytes from the underlying subchondral bone. Unlike growth plate hypertrophic chondrocytes, AC hypertrophic chondrocytes are stable and remain quiescent after maturation but may be reactivated in OA and contribute to enhanced articular cartilage matrix mineralization (Oegema et al., 1997). In this chapter, chondrogenic differentiation of a P3 clonal cell line (P3_E3) screened based on hypertrophic cartilage differentiation induced by BMP9 is investigated to test the hypothesis that P3_E3 cells represent a hypertrophic chondrocyte progenitor cell.

Growth plate cartilage is characterized by a zonal structure corresponding to the progressive proliferation and maturation of hypertrophic cartilage. Pre-chondrocytes in the resting zone are non-proliferative and mature to become proliferating chondrocytes in the

proliferative zone. Proliferating chondrocytes form characteristics columns of chondrocytes that terminally differentiate into hypertrophic chondrocytes in the hypertrophic zone. These hypertrophic chondrocytes then contribute to osteoblasts formation directly (Yang et al., 2014) or by apoptosis where their matrix provides a template for osteogenesis by invading osteoblasts (Demoor et al., 2014). On the other hand, hypertrophic chondrocytes in adult articular cartilage largely resemble the phenotype of growth plate chondrocytes before they become highly proliferative and hypertrophy (Correa and Lietman, 2017). AC hypertrophic chondrocytes are thought to represent an immature state of growth plate hypertrophic cartilage because they express SOX9, Col2A1 and ACAN, and a reduced level of maturing growth plate hypertrophic chondrocytes markers such as IHH, COL10A1 or MMP13 (Correa and Lietman, 2017).

Articular cartilage is a permanent structure that persists throughout life under normal healthy conditions, while growth plate cartilage is a transient structure that eventually forms bone. It remains unclear what factors trigger the development of permanent and transient chondrocytes and how chondrocytes associated with AC, including hypertrophic chondrocytes, are stably maintained throughout maturation and beyond. These questions are significant because, during OA, articular chondrocytes acquire growth plate-like characteristics, differentiating a hypertrophic chondrocyte phenotype that includes expression of degrading matrix proteins such as Mmp13 and culminating in the differentiation of osteocytes that compromise joint function (Decker et al., 2015). Studies focused on minimizing growth plate cartilage-associated changes by articular chondrocytes have identified potential treatments that protect against OA progression by inhibiting hypertrophic chondrocyte differentiation. For example, parathyroid hormone-related protein (PTHrP) has been reported to elicit protection against experimentally induced OA (Macica et al., 2011; Sampson et al., 2011), and epidermal

growth factor signaling has been linked to the maintenance of articular chondrocyte progenitor cells of the superficial layer, thus preventing cartilage degeneration during OA progression (Wei et al., 2021). These studies identify a clear need to better understand the differentiation of hypertrophic chondrocytes outside the context of the growth plate.

Our studies in chapter III have identified two types of clonally derived fibroblasts from P3 cells: P3_D8 clonal cells which we show represent an articular chondrocyte progenitor cell and P3_E3 clonal cells that differentiate hypertrophic cartilage when cell pellets are treated with BMP9. If P3_E3 cells represent a hypertrophic chondrocyte progenitor cell line, then studies using these two cloned cell lines provide an opportunity to identify regulatory pathways that specify chondrocyte differentiation within articular cartilage that can impact the progression of OA. In this chapter, our results show that P3_E3 clonal cells display SSC-like characteristics and are induced to differentiate into hypertrophic cartilage by BMP9 using our modified self-aggregation protocol. RNAseq transcriptomic analyses support the conclusion that P3_E3 clonal cells are hypertrophic chondrocyte progenitors that are distinct from the P3_D8 articular chondrocyte progenitor cell. Comparative transcriptomic analysis identified a number of chondrogenic genes induced by BMP9 that distinguish hypertrophic chondrocyte progenitors from articular cartilage progenitor cells.

4.2 Materials and Methods

Cell Culture: P3_E3 cloned cells were cultured and expanded on fibronectin coated dishes in 2% FBS MSC medium supplemented with EGF, PDGF, LIF (growth medium) as described in

chapter II (Wu et al., 2013). After achieving 70-80% confluence, cells were detached and stored in liquid Nitrogen for future studies.

Differentiation Assay: Chondrogenesis studies using pellet culture protocol were carried out by centrifugation. 2.5×10^5 cells in 0.5 ml of 2% FBS MSC medium supplemented with or without BMP9 (50 ng/mL, R&D) were centrifuged at 150 x g for 5 minutes at room temperature to form a cell pellet. Cell pellets were incubated in a 15 mL polypropylene tube for 21 days. Medium was changed twice a week until the end of the culture period. Chondrogenesis studies using SA culture protocol were carried out by suspension culture. 2.5×10^5 cells in 2.5 ml of 2% FBS MSC medium were plated onto a petri dish for 4 days to allow cells self-aggregate (P3 paper). During the SA period (day 0 - day 4), BMP9 (50 ng/mL), BMP2 (50 ng/mL) or TGFβ3 (50 ng/mL) were supplemented to promote cell aggregation. The cell aggregates were then differentiated by BMP9 (50 ng/mL) until the end of culture period. The sectioned pellets were visualized by Mallory's trichrome staining to identify collagens or Safranin O/fast green staining to detect mucopolysaccharides including proteoglycans. Osteogenic differentiation was induced by StemXVivo mouse/rat osteogenic supplement (#CCM009, R&D systems) in StemXVivo adipogenic/osteogenic base media (#CCM007, R&D Systems) following the manufacturer's instructions. After 14 days, mineralized matrix was detected by Alizarin Red S for osteogenic differentiation. Adipogenic differentiation was induced by incubation in StemXVivo adipogenic supplement (#CCM011, R&D systems) in base media following the manufacturer's instructions. After 21 days, lipid vacuoles were visualized with Oil Red O for adipogenic differentiation.

Flow Cytometry: Cells for flow cytometry studies were detached by trypsin, filtered by 100 μm cell strainer, and incubated in flow buffer (0.5% FBS/PBS) at 4°C, 15 min for blocking. Cells were incubated in the dark with antibodies at the concentration of 1 μL antibody/$2x10^5$ cells/100

μL at 4°C, 30 min. Cells were then washed twice and re-suspended with flow buffer and kept at 4°C in the dark prior to running flow cytometry. In multi-colors studies, fluorescent compensation was performed by UltraComp eBeads (#01-2222, invitrogen). Flow cytometry were conducted using Gallios flow cytometer (Beckmen Coulter) and flow data was analyzed by Kaluza software (Beckmen Coulter). Antibodies used in this study include, CD45 (#11-0454-82, eBioscience), CD90 (#47-0902-82, eBioscience), CD105 (#48-1051-80, eBioscience), CD51 (#12-0512-81, eBioscience), Tie2 (#566716, BD), 6C3 (#46-5891-82, eBioscience), TER-119 (#11-5921-82, eBioscience) and 7-AAD viability staining solution (00-6993, eBioscience).

Histology and Immunochemistry: In vitro differentiated cultures were fixed with Z-fix (Anatech 6269) and in vivo implanted tissues were fixed with Z-fix followed by Decalcifier I (Surgipath, Leica 3800400). Samples then processed for paraffin histology and immunohistochemistry. For histological analysis, the samples were stained with Mallory trichrome (Humason, 1962) or Safranin O/fast green (Schmitz et al., 2010). Immunohistochemical staining for LacZ, Sox9, ColI, Acan, Prg4 and Cilp was carried out using heat retrieval (citrate buffer (pH 6), 65°C, 20 hours) and antigen retrieval for ColX immunostaining used 1% hyaluronidase in PBS (Sigma-Aldrich H3506, room temperature, 30Min). Slides were treated in Protein Block Solution (Dako X0909; room temperature, 1 h). Primary antibodies included anti-ColX (Rabbit polyclonal, Abcam 58632; 1:500), anti-Acan (Rabbit polyclonal, Millipore AB1030; 1:300), anti-Prg4 (Rabbit polyconol, LSbio LS-B8236; 1:200) and anti-Cilp (Rabbit polyclonal, Novus NBP1-81667; 1:100). Secondary antibody included Alexa Fluor 568 goat anti-rabbit IgG (Invitrogen; A11011, 1:500) or Alexa Fluor goat anti-rabbit 488 IgG (Invitrogen, A11008, 1:500). Slides were counterstained with DAPI to label nuclei. Slides were imaged with an Olympus BX61 fluorescence deconvolution microscope

utilizing Slidebook software (Intelligent Imaging Innovations Inc., Denver, CO). Details of immunostaining procedures have been described previously (Dawson et al., 2019; Han et al., 2008; Yu et al., 2012).

RNA Extraction, RT-qPCR and RNA-seq: Total RNA was extracted from cultures using the RNeasy Plus Micro Kit (Qiagen) following the manufacturer's recommended protocol. The aggregation cultured samples were homogenized before RNA extraction. The quantity and quality of total RNAs were checked by Nanodrop ratios of 260/280 and 260/310. Quantitative reverse transcriptase polymerase chain reaction (qRT-PCR) was carried out in triplicate with the SuperScript™ III Platinum™ One-Step qRT-PCR Kit w/ROX on an Eppendorf Realplex machine according to the manufacturer's instruction. The expression levels of target genes were normalized to the housekeeping gene ribosomal protein L12 (RPL12) levels. Statistical significance was determined using a parametric unpaired T-test in "Graphpad". Primers used in this study include mouse Prg4 (Mm01284582_m1), mouse Cilp (Mm00557687_m1), mouse Sox9 (Mm00448840_m1), mouse Enpp2 (Mm00516572_m1), mouse Scrg1 (Mm00485984_m1), mouse Col2a1 (Mm01309565_m1), and mouse Rpl12 (Mm02601627_g1).

For RNA-seq samples, the quantity and quality of total RNAs were checked with concentration, RIN, and 28S/18S ration by Agilent 2100 at BGI Genomics. The 100-bp length paired-end reads from cultures were generated using BGISEQ-500 at BGI Genomics, while the SRA shared datasets are downloaded from NCBI website (Primary ACs: SRR9317861-SRR9317863, (Bekki et al., 2020) and Primary GP: SRR5036053-SRR5036056, (Sabik et al., 2017). All reads are aligned and referenced against the Mus musculus genome (UCSC version mm10) using "HTSAT2" and counted using "htseq-count". The normalization and DE analysis were processed by "DESeq2" running under a Galaxy instance. The significant differentially

expressed genes were defined by a cutoff of log2(FC) ≥ │1.5│ and FDR P-value < 0.05. The volcano plot and correlation analysis were performed and visualized by R/R studio with packages of "gplots", "ggplot2", "corrplot", "heatmap.plus", and "RColorBrewer". The functional annotation was conducted by "DAVID" software (Huang da et al., 2009a, b).

4.3 Results

P3_E3 clone displays SSCs characteristics and differentiates hypertrophic cartilage by BMP2/SA/BMP9 protocol

The clonal study of P3 fibroblasts in chapter III indicated that the P3 fibroblast line is a heterogeneous cell population containing progenitor cells that display distinct chondrogenic responses when cultured under identical culture condition with BMP9 treatment. The hyaline cartilage line (P3_D8) displays SSCs characteristics including the ability to differentiate chondrocytes and osteocytes, but not adipocytes, and the expression of the SSC surface marker profile (CD45-/TER119-/TIE2-/CD51+/CD90-/6C3-/CD105-). To determine whether the hypertrophic cartilage line (P3_E3) displays different characteristics from the P3_D8 clone in surface markers and differentiation ability, the P3_E3 clone was tested with the same assays. The multi-lineage differentiation studies indicated that the P3_E3 clone differentiate to chondrocytes and osteoblasts, but not adipocytes (Figure 4.1A), demonstrating that P3_E3 and P3_D8 clones share the same differentiation potential. Analysis of P3_E3 clonal cells by flow cytometry revealed a flow signature in which 83.97% of P3_E3 cells express an SSC marker profile (Figure 4.1B). These studies indicate that both P3_D8 and P3_E3 clonal cell lines display SSC-like characteristics.

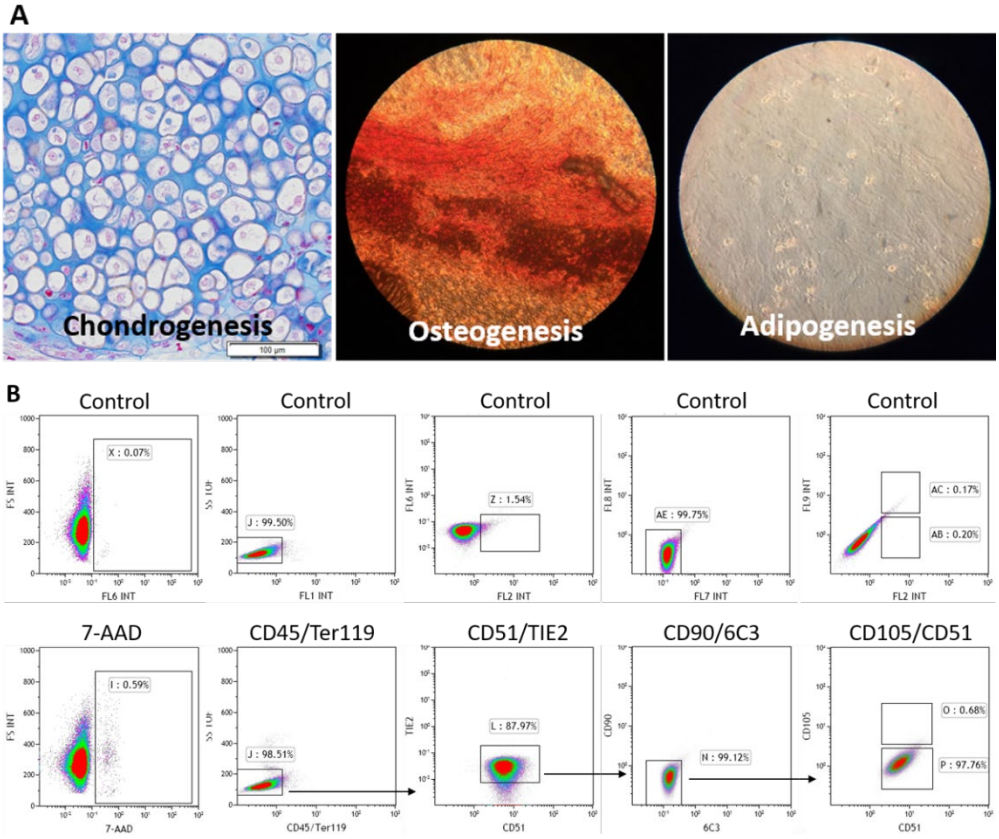

Figure 4.1 P3_E3 clone displays SSCs characteristics.
(A) P3_E3 clone has ability to differentiate to chondrocytes (Left), osteocytes (Middle), but not adipocytes (Right). (B) P3_E3 clone expresses SSCs surface marker prolife: un-stained control of P3_E3 clone (Top panels); P3_E3 clone stained with SSCs markers (Bottom panels). N=3 for both studies.

In chapter III we found the P3_E3 clonal cells differentiate into hypertrophic chondrocytes when treated with BMP9 as cell pellets generated by centrifugation. Creating high-density cell culture conditions by self-aggregation is effective for BMP9 induced chondrogenesis of P3_D8 clonal cells (SA/BMP9 protocol), and articular cartilage differentiation is induced by BMP9 when self-aggregation is enhanced with BMP2 (BMP2/SA/BMP9 protocol) (Chapter III). Parallel studies with P3_E3 cells indicated a much reduced self-aggregation response resulting in very small cell clusters after BMP9 treatment, however chondrocytes were still identified in

these small clusters (Figure 4.2A, E and I). This indicated that P3_E3 cells display a limited self-aggregation response but remained responsive to BMP9. To determine whether treatment with BMP2, BMP9 or TGFβ3 could enhance self-aggregation, P3_E3 cells were treated with BMP2, BMP9 or TGFb3 during the 4-day self-aggregation phase as previously described (Chapter III), then cultured with BMP9 for an additional 14 days. Similar to P3_D8 cells, all three growth factor treatments enhanced self-aggregation (Figure 4.2B-D). At the end of the culture period, all treatments resulted in the formation of large irregularly shaped cell clusters (Figure 4.2F-H), and histological analysis of Safrannin O/fast green stained sections indicated that all three protocols resulted in cartilage containing chondrocytes with large lacunae embedded in a matrix rich in mucopolysaccharides (Figure 4.2J-L). Since all treatments were equivocal, we adopted the BMP2/SA/BMP9 protocol for P3_E3 chondrogenic differentiation studies so the results could be compared to P3_D8 studies (Chapter III).

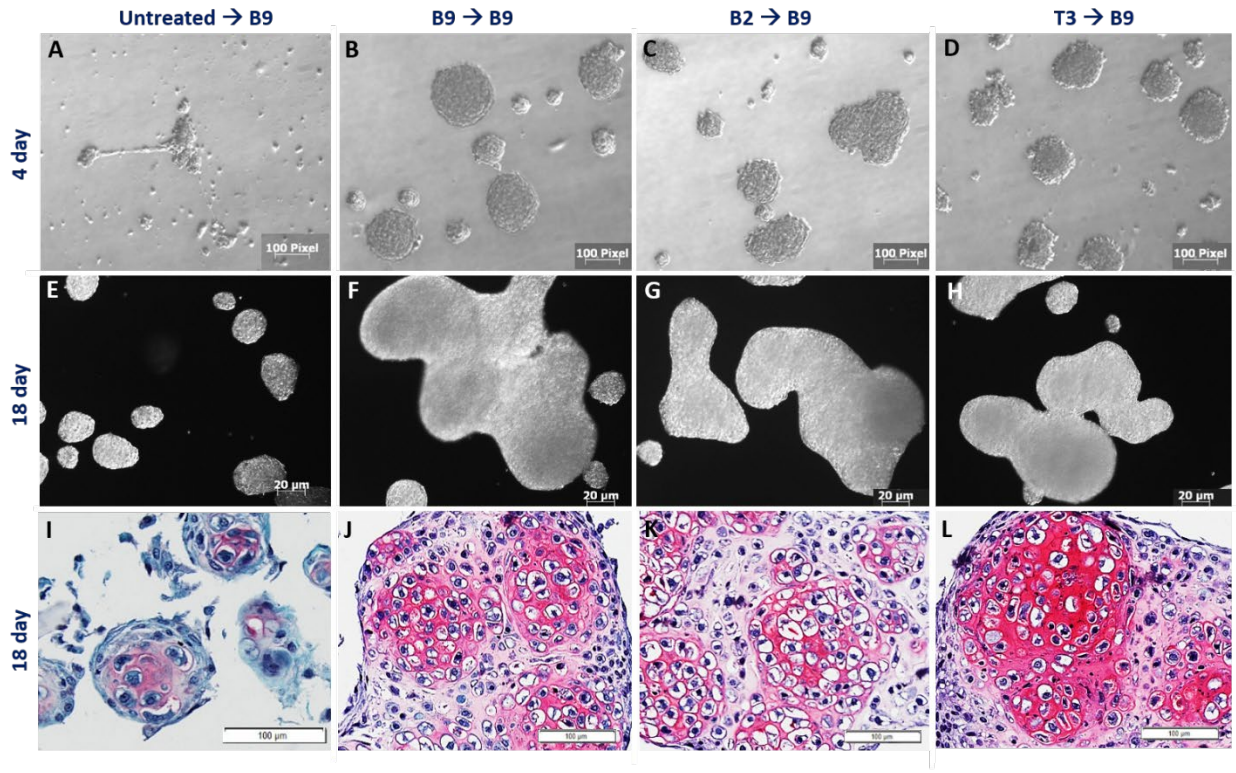

Figure 4.2 Treating growth factors during self-aggregation period enhances the size of P3_E3 aggregate and maintains P3_E3 chondrocyte differentiation with mucopolysaccharides rich matrix. At day 4, the size of P3_E3 aggregate in untreated control (A), BMP9 treated (B), BMP2 treated (C) and TGFβ3 treated (D). After 14 days of BMP9 treatment, the size of P3_E3 chondrospheres in no pre-treatment control (E), BMP9 pre-treatment (F), BMP2 pre-treatment (G) and TGFβ3 pre-treatment (H). Safranin O/fast green staining of P3_E3 chondrospheres in no pre-treatment control (I), BMP9 pre-treatment (J), BMP2 pre-treatment (K) and TGFβ3 pre-treatment (L). Scale bars: 200 µM for E-H; 100 µM for A-D and I-L.

Using the BMP2-SA(4d)→BMP9(14d) differentiation protocol, P3_D8 cells differentiate chondrocytes that are small but produce a matrix that is rich in mucopolysaccharides including proteoglycans such as aggrecan (Chapter III, Figure 3.4K). Using an identical differentiation protocol, P3_E3 cells differentiate chondrocytes that produce a matrix that is rich in mucopolysaccharides but are enlarged and histologically distinct. P3_E3 differentiated

chondrocytes contain large lacunae which make hypertrophic chondrocytes distinct from other chondrocytes. To better characterize chondrogenesis of P3_E3 cells, cell aggregates were collected after 5 days of BMP9 treatment (BMP2-SA(4d)-BMP9(5d)) for histological analysis based on Mallory's trichrome staining. At this early stage, clusters of small chondrocytes are differentiated and many have distinct lacunae suggestive of hypertrophic chondrocyte differentiation (Figure 4.3A). These samples display reduced collagen production based on Mallory's staining. After 18 days of culture (BMP2-SA(4d)□BMP9(14d)), larger chondrocytes with prominent lacunae are found embedded in a matrix rich in both collagen (Mallory's trichrome) (Fig 4.3B) and mucopolysaccharides (Safrannin O/Fast green) (Fig 4.3C). At day 44 (BMP2-SA(4d)-BMP9(40d)), P3_E3 cells form large chondrospheres with distinct external chondrogenic characteristics that include a glossy blue-white appearance and resilient to pressure (Fig 4.3D). Histologically, Mallory's trichrome staining identifies cells that appear hypertrophic with a collagen-rich matrix and a distinct fibrous layer surrounding the cartilage similar to P3_D8 differentiated articular cartilage (Fig 3.3E). Safranin O/fast green staining of 44 days P3_E3 differentiated cartilage similar to 18 days cultures with a matrix rich in mucopolysaccharides (Figure 4.3 F). Immunohistochemical staining of 44 days P3_E3 differentiated cartilage identified high expression of Acan and ColX throughout the tissue indicative of hypertrophic cartilage (Fig 4.3G, H). Low-level immunostaining for Prg4 and Cilp was also observed (Fig 4.3I, J). Prg4 expression was noted both within the cartilage tissue and in the fibrous layer similar to P3_D8 differentiated articular cartilage. Taken together, these results demonstrate that P3_E3 clonal cells differentiate hypertrophic cartilage by the BMP2-SA□BMP9 protocol, thus identifying a hypertrophic chondrocyte progenitor cell that is distinct from the articular chondrocyte progenitor cell.

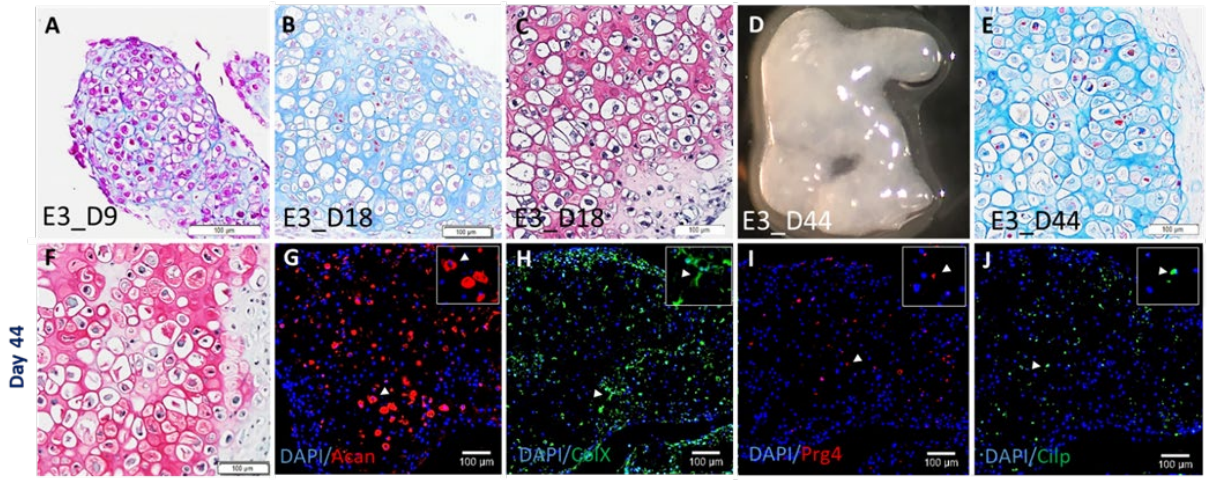

Figure 4.3 P3_E3 clone differentiated to hypertrophic chondrocytes following the process of cartilage maturation during development.
BMP2/SA/BMP9 protocol differentiated P3_E3 cartilages were stained by Mallory's trichrome staining for samples collected at day 9 (A); day 18 (B) and day44 (E). 44-day differentiated P3_E3 clone form a cartilage-like tissue (D). P3_E3 differentiated cartilage was stained by Safranin O/fast green at day 18 (C) and day 44 (F). 44-day differentiated P3_E3 cartilage was immunostained by Acan (G), ColX (H), Prg4 (I) and Cilp (J). Slides were counterstained with DAPI to label nuclei. Scale bars: 100 µM.

The gene expression patterns between 18 days cultured P3_E3 derived cartilage and P3_D8 derived cartilage are highly correlated

To investigate the chondrogenic response of the P3_E3 clone to BMP2/SA/BMP9 protocol, a genome-wide transcriptome study was performed using RNA-seq. The P3_E3 clone was differentiated for 18 days, and total RNA was extracted from cartilage aggregates for RNA-seq (P3_E3_B2B9). Monolayer culture of the P3_E3 clone was used for comparison (P3_E3_control). Using a cutoff of $\log2(FC) \geq |1.5|$ and FDR P-value < 0.05, the differential expressed gene analysis identified 2359 up-regulated and 1376 down-regulated genes (Figure 4.4A). Functional annotation analysis identified the top 6 associated biological activities of up-regulated genes (cell adhesion, biological adhesion, cartilage development, extracellular structure

organization, extracellular matrix organization and protein maturation) and all have obvious links with induced chondrogenesis (Figure 4.4B). To study the differentiation of cartilage from P3_E3 clone, we compared our datasets to RNA-seq datasets of mature murine (5 month old) articular cartilage (Bekki et al., 2020) and developing (PN21) mouse growth plate cartilage (Sabik et al., 2017) from NCBI shared resource. The top 30 differentially expressed genes between articular cartilage and growth plate cartilage that were established for comparing P3_D8 derived cartilage with primary cartilages in chapter III were used as a model for comparing P3_E3 derived cartilage with chondrogenic tissues. Analysis of the relationship between articular cartilage and growth plate cartilage indicated a negative correlation ($r = -0.33$), suggesting that these 60 genes can separate these two types of cartilage (Figure 4.4C). When the P3_E3_B2B9 RNAseq dataset is compared, the correlation analysis indicates a positive relationship with mature articular cartilage ($r = 0.51$) and a neutral correlation with growth plate cartilage ($r = -0.01$; Figure 4.4C), suggesting that the chondrogenic response of the P3_E3 clone is more similar to articular cartilage than it is to growth plate cartilage. When the P3_E3_B2B9 RNAseq dataset is compared with P3_D8_B2B9, the correlation analysis indicates a positive relationship ($r = 0.87$; Figure 4.4C), suggesting that at the time point of day 18, P3_E3 derived cartilage and P3_D8 derived cartilage are highly similar. The expression of 6 established BMP9 target genes (Col2a1, Sox9, Prg4, Cilp, Enpp2, Scrg1) between P3_E3_B2B9 cartilage RNAs and P3_E3 control RNAs were tested by quantitative RT-PCR (qRT-PCR). This analysis revealed that P3_E3_B2B9 cartilage was induced to express all these chondrogenic genes (Figure 4.4D). Compared to a similar genome-wide transcriptome study of P3_D8 cells (Chapter III), this level of analysis was unable to identify gene expression patterns that distinguish induced differentiation of articular cartilage from hypertrophic cartilage in P3 clonal progenitor cell lines.

Thus, a transcriptional link that complements the histological distinction between different types of engineered cartilage was not elucidated using this approach.

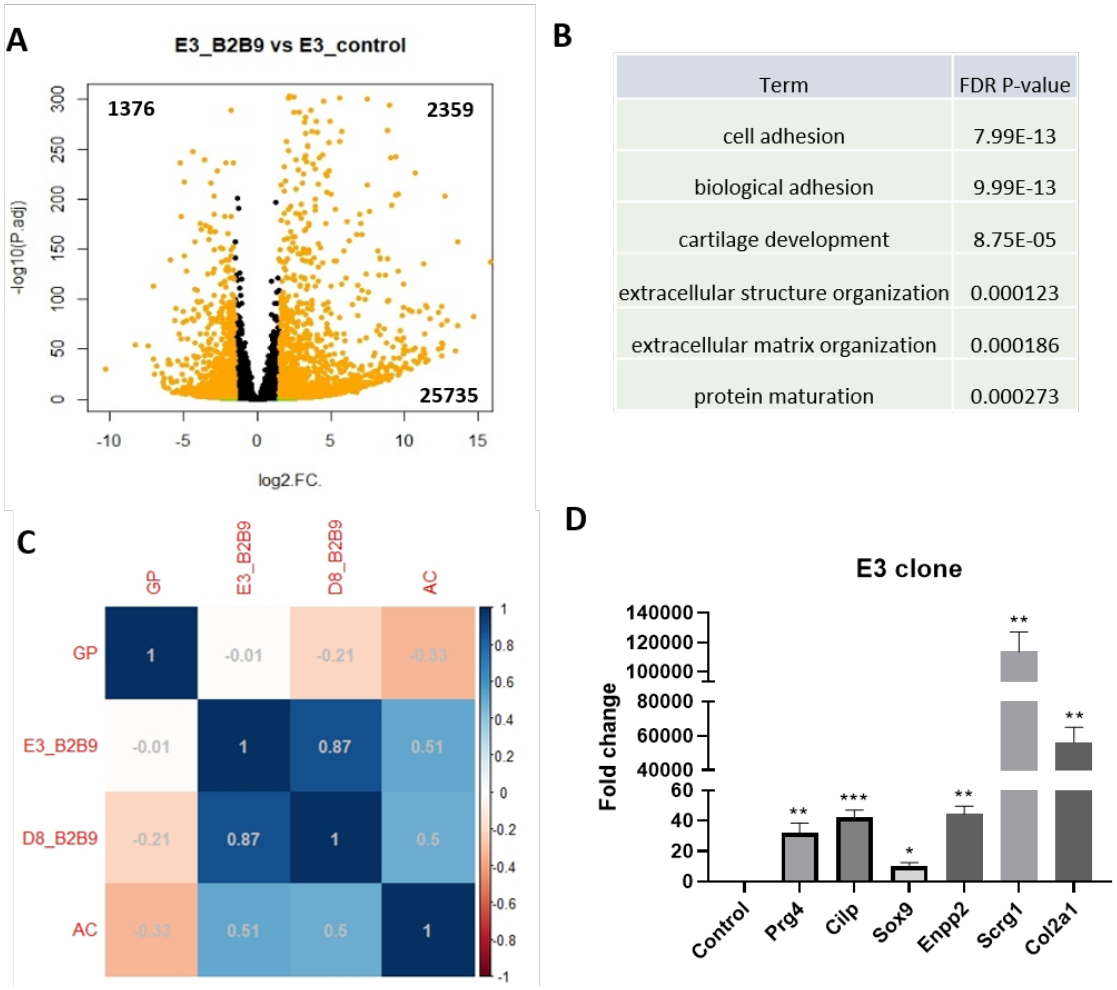

Figure 4.4 Genome-wide RNA-seq analysis of P3_E3 clone differentiated cartilage.
P3_E3 clone was cultured by BMP2/SA/BMP9 protocol for 18 days (E3_B2B9) and RNAs was extracted for RNA sequencing. P3_E3 clone cultured by monolayer serve as control (E3_control). The datasets were analyzed by volcano plot (A) and functional annotation (B). The E3_B2B9 dataset was also compared with D8_B2B9, growth plate cartilage and articular cartilage by correlation studies (C). The gene expression of targeted chondrocyte-related genes (Prg4, Cilp, Sox9, Enpp2, Scrg1 and Col2a1) were determined by qRT-PCR and normalized by individual E3_controls (D). Statistical analysis: default adjusted analysis for RNA-seq analysis and unpaired t test for qPT-PCR study, N=3 for all analysis.

The genome-wide transcriptome comparisons identified potential factors related to hypertrophic chondrocyte maturation.

To explore transcriptomic differences between the P3_E3 and P3_D8 progenitor cell lines, we compared P3_E3 and P3_D8 RNAseq datasets ($\log2(FC) \geq \left| 1.5 \right|$; FDR P-value < 0.05) and this comparative analysis identified a total of 775 differentially expressed genes of which 592 genes were up-regulated in P3_D8 cells and 183 genes were up-regulated in P3_E3 cells) (Figure 4.5A). These differentially expressed genes were further filtered by a list of 269 cartilage-related genes (Yu et al., 2022) and identified 5 genes up-regulated in P3_E3 cells (Gdf5, Nog, Hoxd11, Thra, Maf) and 9 genes up-regulated in P3_D8 cells (Mgp, Pthlh, Mmp13, Bmp2, Msx2, Dcn, Slc29a1, Loxl3, Ors1) (Figure 4.5B). P3_E3 specific genes include 2 genes critical for joint development during embryogenesis (Gdf5, Nog) (Bian et al., 2020; Brunet et al., 1998; Chen et al., 2016; Shwartz et al., 2016) however, it is important to note that Noggin is a well-known antagonist of multiple BMP family members including BMP2 and Gdf5 but not BMP9 (Seemann et al., 2009). P3_D8 specific genes include genes that induce (BMP2) and inhibit (Msx2) chondrogenesis (Gibson et al., 2017; Giffin et al., 2019; Takahashi et al., 2001; Wei et al., 2006), and genes that are expressed during hypertrophic differentiation (Mmp13) as well as genes that prevent hypertrophic chondrocyte differentiation (i.e. Pthlh; (D'Angelo et al., 2000; Macica et al., 2011; Sampson et al., 2011)). These studies identify a relatively small number of chondrogenic genes that distinguish P3_E3 cells from P3_D8 cells. In addition, the ambiguous function of some of the differentially expressed genes in each of these two progenitor cell lines suggests that the cells are uncommitted with respect to chondrogenic gene expression.

Using the same approach, we determined differential gene expression of P3_E3 and P3_D8 cells treated with BMP9 for 24 hours since qRT-PCR analyses indicated that

chondrogenic genes were induced within this time frame (Figure 2.4A; Figure 3.5F). This analysis identified a total of 591 differentially expressed genes of which 143 genes were up-regulated in P3_E3 cells and 448 genes were up-regulated in P3_D8 cells (Figure 4.5C). Differentially expressed chondrogenic genes identified included only 3 genes up-regulated in P3_E3 cells compared to P3_D8 cells (Nog, Itgb8, Hoxd3), and 15 genes up-regulated in P3_D8 cells compared to P3_E3 (Atp6v0d2, Bmp2, Cfh, Cilp, Col10a1, Ctsk, Dcn, Edn1, Frzb, Mgp, Mmp13, Msx2, Nov, Ptger1, Sdc3) (Figure 4.5D). Of the P3_E3 specific genes, Noggin expression, which is enhanced in untreated cells, continues to be differentially expressed following BMP9 treatment, and the enhanced expression of Gdf5 in untreated cells is not found following BMP9 treatment. These observations suggest that one immediate action of BMP9 is to inhibit the expression of other BMP family members, such as Gdf5, and by enhancing Noggin production, effectively inhibiting activation of other BMP signaling pathways. Of the 9 chondrogenic genes differentially expressed in untreated P3_D8 cells, 4 (Bmp2, Dcn, Mmp13, Msx2) are found to be differentially expressed following BMP9 treatment. These observations suggest that both P3_E3 and P3_D8 progenitor cell lines are undifferentiated and primed for specific chondrogenic responses to BMP9 treatment.

A similar comparative analysis was carried out on the transcriptomes of cartilage differentiated for 18-days from P3_E3 and P3_D8 cells (BMP2-SA(4d)-BMP9(14d)). A total of 717 differentially expressed genes were identified that included 462 genes up-regulated in P3_D8 cells and 255 genes up-regulated in P3_E3 cells (Figure 4.5E). By selectively focusing on cartilage-related genes, we identified 13 genes differentially expressed in P3_E3 derived cartilage compared to P3_D8 derived cartilage (Mmp13, Ror2, Bmp6, Frzb, Nog, Col11a1, Sost, Gdf5, Epyc, Clec3a, Ihh, Mia, Col9a2), and 16 genes differentially expressed in P3_D8 derived

cartilage compared to P3_E3 derived cartilage (Msx2, Cilp, Scx, Bmp1, Prrx1, Egfr, Ereg, Bmp2, Adamts12, Dcn, Ors1, Smad3, Enpp2, Trps1, Itgb8, Sfrp2) (Figure 4.5F). This comparison provided new insight into hypertrophic and articular chondrocyte differentiation and maturation. First, differential Noggin expression is common to all stages of hypertrophic chondrocyte differentiation of P3_E3 cells; from untreated progenitor cells to early treatment with BMP9 and finally in BMP9 differentiated hypertrophic cartilage. This suggests that continuous BMP9 treatment in culture is associated with a reduced level of signaling by other BMP family members and this may play a critical role in postnatal hypertrophic chondrocyte differentiation. Second, the up-regulation of cartilage ECM genes (Col11a1 and Col9a2) and hypertrophic chondrocyte-specific genes (Ihh, Mmp13, Ror2) in response to BMP9 confirms hypertrophic chondrocyte induction (Ferrao Blanco et al., 2021; Rim et al., 2020; St-Jacques et al., 1999; Thorup et al., 2020) and supports the conclusion that P3_E3 cells are undifferentiated hypertrophic chondrocyte progenitor cells. Third, the 3 genes that are differentially expressed in P3_D8 derived cartilage relative to P3_E3 derived cartilage in untreated and 24 hours BMP9 treatment (Dcn, BMP2 and Msx2) are also differentially expressed in 18 days differentiated articular cartilage, thus identifying a consistent transcriptome signature for induced articular chondrocyte progenitor cells that is distinct from hypertrophic chondrocyte progenitor cells.

A

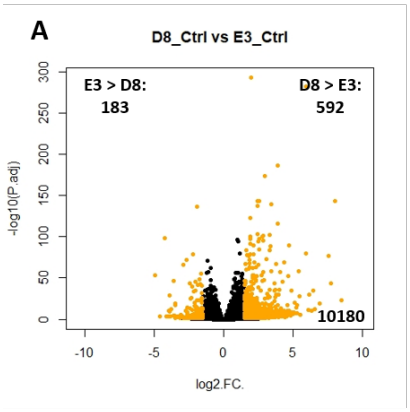

B

D8_Ctrl > E3_Ctrl			E3_Ctrl > D8_Ctrl		
Gene Name	log2(FC)	FDR P value	Gene Name	log2(FC)	FDR P value
Mgp	7.993092	3.53E-144	Gdf5	-3.90134	2.78E-10
Pthlh	3.033537	1.92E-19	Nog	-1.90084	0.000261867
Mmp13	3.021187	8.26E-14	Hoxd11	-1.68602	0.005575365
Bmp2	2.734451	1.01E-08	Thra	-1.64343	1.02E-08
Msx2	2.527144	0.04582724	Maf	-1.64046	1.08E-55
Dcn	5.943305	2.39E-80			
Slc29a1	2.035471	0.00337671			
Loxl3	1.848741	9.57E-73			
Osr1	1.57751	2.32E-34			

C

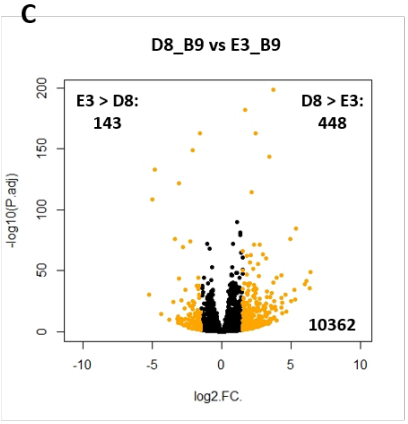

D

D8_B9 > E3_B9			E3_B9 > D8_B9		
Gene Nam	log2(FC)	FDR P valu	Gene Nam	log2(FC)	FDR P valu
Dcn	5.306317	3.33E-27	Nog	-2.60853	4.43E-11
Mmp13	4.963884	2.39E-76	Itgb8	-2.39382	1.42E-23
Atp6v0d2	3.510706	3.83E-08	Hoxd3	-1.57425	0.002398
Cilp	3.49264	5.66E-09			
Msx2	3.274466	4.11E-07			
Bmp2	2.885691	2.75E-12			
Cfh	2.789758	1.97E-05			
Mgp	2.471104	2.78E-06			
Edn1	1.952559	1.53E-07			
Ptger1	1.941087	1.1E-06			
Frzb	1.935185	1.44E-05			
Ctsk	1.909587	0.004447			
Col10a1	1.759063	0.000319			
Sdc3	1.754786	5.02E-13			
Nov	1.562661	5.9E-13			

E

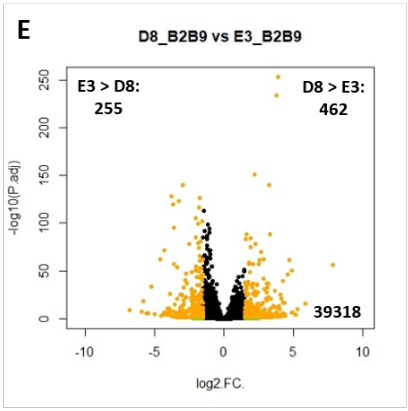

F

D8_B2B9 > E3_B2B9			E3_B2B9 > D8_B2B9		
Gene Name	log2(FC)	FDR P value	Gene Name	log2(FC)	FDR P value
Msx2	6.157674	3.10E-12	Mmp13	-1.57111647	2.56E-06
Cilp	3.8687425	7.83E-92	Ror2	-1.66136171	1.80E-23
Scx	3.0772613	2.67E-29	Bmp6	-1.7854545	0.021412296
Bmp1	2.8614049	0.007603891	Frzb	-1.87213978	1.48E-08
Prrx1	2.7013823	5.53E-17	Nog	-2.03533948	1.07E-51
Egfr	2.6345682	0.037074481	Col11a1	-2.21182465	1.15E-05
Ereg	2.4376024	2.48E-15	Sost	-2.21507721	3.23E-06
Bmp2	2.4262663	1.99E-10	Gdf5	-2.36627137	0.005058315
Adamts12	2.3737611	2.94E-16	Epyc	-2.39979486	2.66E-35
Dcn	2.1831913	2.61E-09	Clec3a	-3.14348549	8.38E-10
Osr1	1.9376347	6.75E-09	Ihh	-3.96316926	3.80E-06
Smad3	1.7943364	1.85E-06	Mia	-4.04226939	1.43E-11
Enpp2	1.7104272	3.52E-17	Col9a2	-4.60808842	4.57E-45
Trps1	1.6174079	0.028938216			
Itgb8	1.5806194	0.006681599			
Sfrp2	1.5394199	0.001837332			

Figure 4.5 Differential expressed gene analysis of P3_D8_control vs P3_E3_control, P3_D8_B9 vs P3_E3_B9 and P3_D8_B2B9 vs P3_E3_B2B9.
Volcano plot analysis of P3_D8_control vs P3_E3_control (A), P3_D8_B9 vs P3_E3_B9 (C) and P3_D8_B2B9 vs P3_E3_B2B9 (E). Differential expressed gene analysis filtered by 269 cartilage-related genes were listed as: P3_D8_control vs P3_E3_control (B), P3_D8_B9 vs P3_E3_B9 (D) and P3_D8_B2B9 vs P3_E3_B2B9 (F). P3_D8_control and P3_E3_control are cells cultured under monolayer with untreated condition. P3_D8_B9 and P3_E3_B9 are cells cultured under monolayer with 24 hours of BMP9 treatment. P3_D8_B2B9 and P3_E3_B2B9 are cells cultured by BMP2/SA/BMP9 protocol for 18 days. Statistical analysis: default adjusted analysis. N=3 for all analysis.

4.4 Discussion

During the OA progression, normal articular chondrocytes become hypertrophy and express their specific markers (ColX and Mmp13) and early osteogenic marker (Alp). These growth plate-like changes result in osteocyte generation in OA joints (Rim et al., 2020). The treatment strategies of OA therapy therefore focuses on identifying factors that can prevent hypertrophic chondrocyte differentiation. The studies in this thesis identified a clone that responds to BMP9 treatment by differentiating articular chondrocytes (P3_D8) and another clone (P3_E3) that differentiates hypertrophic chondrocytes under identical culture conditions. Studies utilizing these two clonal cell lines provide an opportunity to discover potential regulatory factors involved in the stimulation and inhibition of hypertrophic chondrocyte differentiation. For example, the parental P3 fibroblast cell line contains hypertrophic chondrocyte progenitor cells that are repressed during BMP9 treatment and de-repressed when BMP9 treatment is withdrawn (Yu et al., 2022; Chapter II). The possibility that BMP9 actively represses hypertrophic chondrocyte differentiation can be ruled out based on BMP9 induced hypertrophic chondrocyte differentiation of P3_E3 cells. This suggests that BMP9 induced hypertrophic chondrocyte inhibition is mediated indirectly by other cell types present in the P3 parental cell line. It is interesting to note that RNAseq analyses identified two genes that are differentially expressed by P3_D8 clonal cells that have been linked to the inhibition of hypertrophic chondrocyte differentiation, Pthlh and Egfr (Macica et al., 2011; Sampson et al., 2011; Wei et al., 2021). We propose that extending this type of analysis to P3 clonal cell lines can be used to

identify other genes linked to the inhibition of hypertrophic chondrocyte differentiation that represent potential therapeutic targets of the treatment of OA.

The RNA-seq based differential expression analysis identified a number of highly expressed genes specific to the P3_D8 clone when compared to the P3_E3 clone, and three genes (Msx2, Bmp2, Dcn) display continuous higher expression in P3_D8 clone from untreated progenitor cells, 24 hours BMP9 treated, to 18 days differentiated cartilages. Msx2 and BMP2 are known to regulate chondrocyte differentiation and maturation, and DCN is a cartilage matrix protein that links to aggrecan providing biomechanical functions of the joint (Han et al., 2019). On the other hand, the only gene that identified continuous higher expression in the P3_E3 clone at all stages is Noggin, a BMP signaling antagonist including BMP2 but excluding BMP9. These results suggest that BMP signaling plays a potential role in early BMP9 induced chondrogenesis but plays an inhibitory role in hypertrophic chondrocyte differentiation. BMP2 induced chondrogenesis has been reported by several studies (Gibson et al., 2017; Sekiya et al., 2005; Shintani and Hunziker, 2007; Valcourt et al., 1999; Wei et al., 2006) however, an inhibitory role of BMP2 with respect to hypertrophic chondrocyte differentiation is less discussed (Gamer et al., 2018). In contrast, BMP2 has been showed to stimulate chondrocyte maturation and hypertrophy in in vitro chondrogenic studies and during endochondral ossification of ectopic bone in vivo (Zhou et al., 2016). However, in vivo overexpression of BMP2 in mice results in the normal joint formation, and an increase in hypertrophic chondrocyte differentiation was not observed in experimentally induced OA studies suggesting that articular chondrocytes might not respond to BMP2 by hypertrophy chondrocyte differentiation (Thielen et al., 2019). Our studies suggest that differential BMP2 production by articular chondrocyte progenitor cells is offset by the production of Noggin by hypertrophic chondrocyte progenitor cells creating a tissue

microenvironment in which overall BMP signaling is highly regulated, and heavily influenced by BMP9 since it is not antagonized by Noggin. Clearly, future studies are needed to clarify the role of BMP2/Noggin signaling during chondrocyte maturation and hypertrophy.

Msx2 is a known chondrogenic repressor that acts by interfering with Sox9 regulated chondrogenesis and contributes to early patterning of the craniofacial skeleton (Semba et al., 2000; Takahashi et al., 2001). In osteogenic studies, knockout or mutation of Msx2 in mice and human results in defective skull ossification, suggesting that Msx2 promotes osteogenesis (Satokata et al., 2000; Wilkie et al., 2000). These studies used craniofacial morphogenesis and calvarial osteogenesis as models where the bones are formed by intramembranous ossification and not by endochondral ossification. This conclusion is supported by in vitro studies using C2C12 and C3H10T1/2 cell lines that report overexpression of Msx2 stimulates mesenchymal cell differentiation to osteoblasts (Cheng et al., 2003; Ichida et al., 2004; Nishimura et al., 2012). In contrast, other studies using the same cell lines found that BMP2-induced osteogenic gene (Alp and Runx2) expression (Kim et al., 2004; Shirakabe et al., 2001) is repressed by Msx2. These studies found that BMP2 regulates Alp and Runx2 expression by controlling the ratio of the stimulating activity of Dlx5 to the repressive activity of Msx2. While these findings appear contradictory, the conclusion that osteogenic gene expression is fine-tuned by interactions between both activating and repressing transcriptional regulators indicates that gene function cannot be determined in isolation. The role of Msx2 in BMP9 induced articular cartilage differentiation remains unclear and needs to be considered in the context of other transcriptional regulators that may interact with Msx2 in controlling chondrogenic gene expression.

Prrx1 is a limb-specific fibroblast marker that identifies multipotent early limb bud cells that give rise to much of the limb connective tissue including skeletal structures (Leavitt et al.,

2020). Prrx1 is also differentially expressed in 18 days differentiated P3_D8 cartilage compared to P3_E3 cartilage, suggesting the presence of skeletal progenitor cells. In chapter III we revealed that P3_D8 clonal cells express Prrx1 based on scRNA-seq analysis (Figure 3.3D) and that cells with self-renew ability are sequestered to the fibrous layer during articular cartilage differentiation (Figure 3.8). Thus, a high level of expression of Prrx1 in 18 days differentiated P3_D8 cartilage could be linked to the self-renewal properties of sequestered P3_D8 progenitor cells during cartilage differentiation that niched in the surrounding fibrous layer. This raises the possibility that Prrx1 may represent a gene marker to identify sequestered progenitor cells during BMP9 induced articular cartilage differentiation in vitro. Future studies are needed to identify a transcriptomic profile of these sequestered progenitor cells that can be used to identify them to gain a mechanistic understanding of how they become sequestered during cartilage differentiation.

4.5 References

249. Bekki, H., Duffy, T., Okubo, N., Olmer, M., Alvarez-Garcia, O., Lamia, K., Kay, S., Lotz, M., 2020. Suppression of circadian clock protein cryptochrome 2 promotes osteoarthritis. Osteoarthritis and Cartilage 28, 966-976.

250. Bian, Q., Cheng, Y.H., Wilson, J.P., Su, E.Y., Kim, D.W., Wang, H., Yoo, S., Blackshaw, S., Cahan, P., 2020. A single cell transcriptional atlas of early synovial joint development. Development 147.

251. Brunet, L.J., McMahon, J.A., McMahon, A.P., Harland, R.M., 1998. Noggin, cartilage morphogenesis, and joint formation in the mammalian skeleton. Science 280, 1455-1457.

252. Chen, H., Capellini, T.D., Schoor, M., Mortlock, D.P., Reddi, A.H., Kingsley, D.M., 2016. Heads, Shoulders, Elbows, Knees, and Toes: Modular Gdf5 Enhancers Control Different Joints in the Vertebrate Skeleton. PLOS Genetics 12, e1006454.

253. Cheng, S.L., Shao, J.S., Charlton-Kachigian, N., Loewy, A.P., Towler, D.A., 2003. MSX2 promotes osteogenesis and suppresses adipogenic differentiation of multipotent mesenchymal progenitors. J Biol Chem 278, 45969-45977.

254. Correa, D., Lietman, S.A., 2017. Articular cartilage repair: Current needs, methods and research directions. Semin Cell Dev Biol 62, 67-77.

255. D'Angelo, M., Yan, Z., Nooreyazdan, M., Pacifici, M., Sarment, D.S., Billings, P.C., Leboy, P.S., 2000. MMP-13 is induced during chondrocyte hypertrophy. Journal of Cellular Biochemistry 77, 678-693.

256. Dawson, L.A., Brunauer, R., Zimmel, K.N., Qureshi, O., Falck, A.R., Kim, P., Dolan, C.P., Yu, L., Lin, Y.L., Daniel, B., Yan, M., Muneoka, K., 2019. Adult Mouse Digit Amputation and Regeneration: A Simple Model to Investigate Mammalian Blastema Formation and Intramembranous Ossification. J Vis Exp.

257. Decker, R.S., Koyama, E., Pacifici, M., 2015. Articular Cartilage: Structural and Developmental Intricacies and Questions. Curr Osteoporos Rep 13, 407-414.

258. Demoor, M., Ollitrault, D., Gomez-Leduc, T., Bouyoucef, M., Hervieu, M., Fabre, H., Lafont, J., Denoix, J.M., Audigie, F., Mallein-Gerin, F., Legendre, F., Galera, P., 2014. Cartilage tissue engineering: molecular control of chondrocyte differentiation for proper cartilage matrix reconstruction. Biochim Biophys Acta 1840, 2414-2440.

259. Ferrao Blanco, M.N., Domenech Garcia, H., Legeai-Mallet, L., van Osch, G., 2021. Tyrosine kinases regulate chondrocyte hypertrophy: promising drug targets for Osteoarthritis. Osteoarthritis Cartilage 29, 1389-1398.

260. Gamer, L.W., Pregizer, S., Gamer, J., Feigenson, M., Ionescu, A., Li, Q., Han, L., Rosen, V., 2018. The Role of Bmp2 in the Maturation and Maintenance of the Murine Knee Joint. Journal of Bone and Mineral Research 33, 1708-1717.

261. Gibson, J.D., O'Sullivan, M.B., Alaee, F., Paglia, D.N., Yoshida, R., Guzzo, R.M., Drissi, H., 2017. Regeneration of Articular Cartilage by Human ESC-Derived Mesenchymal Progenitors Treated Sequentially with BMP-2 and Wnt5a. Stem Cells Transl Med 6, 40-50.

262. Giffin, J.L., Gaitor, D., Franz-Odendaal, T.A., 2019. The Forgotten Skeletogenic Condensations: A Comparison of Early Skeletal Development Amongst Vertebrates. J Dev Biol 7.

263. Han, B., Li, Q., Wang, C., Patel, P., Adams, S.M., Doyran, B., Nia, H.T., Oftadeh, R., Zhou, S., Li, C.Y., Liu, X.S., Lu, X.L., Enomoto-Iwamoto, M., Qin, L., Mauck, R.L., Iozzo, R.V., Birk, D.E., Han, L., 2019. Decorin Regulates the Aggrecan Network Integrity and Biomechanical Functions of Cartilage Extracellular Matrix. ACS Nano 13, 11320-11333.

264. Han, M., Yang, X., Lee, J., Allan, C.H., Muneoka, K., 2008. Development and regeneration of the neonatal digit tip in mice. Dev Biol 315, 125-135.

265. Huang da, W., Sherman, B.T., Lempicki, R.A., 2009a. Bioinformatics enrichment tools: paths toward the comprehensive functional analysis of large gene lists. Nucleic Acids Res 37, 1-13.

266. Huang da, W., Sherman, B.T., Lempicki, R.A., 2009b. Systematic and integrative analysis of large gene lists using DAVID bioinformatics resources. Nat Protoc 4, 44-57.

267. Humason, G.L., 1962. Animal tissue techniques. W.H. Freeman, San Francisco,.

268. Ichida, F., Nishimura, R., Hata, K., Matsubara, T., Ikeda, F., Hisada, K., Yatani, H., Cao, X., Komori, T., Yamaguchi, A., Yoneda, T., 2004. Reciprocal Roles of Msx2 in Regulation of Osteoblast and Adipocyte Differentiation*. Journal of Biological Chemistry 279, 34015-34022.

269. Kim, Y.J., Lee, M.H., Wozney, J.M., Cho, J.Y., Ryoo, H.M., 2004. Bone morphogenetic protein-2-induced alkaline phosphatase expression is stimulated by Dlx5 and repressed by Msx2. J Biol Chem 279, 50773-50780.

270. Leavitt, T., Hu, M.S., Borrelli, M.R., Januszyk, M., Garcia, J.T., Ransom, R.C., Mascharak, S., desJardins-Park, H.E., Litzenburger, U.M., Walmsley, G.G., Marshall, C.D., Moore, A.L., Duoto, B., Adem, S., Foster, D.S., Salhotra, A., Shen, A.H., Griffin, M., Shen, E.Z., Barnes, L.A., Zielins, E.R., Maan, Z.N., Wei, Y., Chan, C.K.F., Wan, D.C., Lorenz, H.P., Chang, H.Y., Gurtner, G.C., Longaker, M.T., 2020. Prrx1 Fibroblasts Represent a Pro-fibrotic Lineage in the Mouse Ventral Dermis. Cell reports 33, 108356-108356.

271. Macica, C., Liang, G., Nasiri, A., Broadus, A.E., 2011. Genetic evidence of the regulatory role of parathyroid hormone-related protein in articular chondrocyte maintenance in an experimental mouse model. Arthritis Rheum 63, 3333-3343.

272. Nishimura, R., Hata, K., Matsubara, T., Wakabayashi, M., Yoneda, T., 2012. Regulation of bone and cartilage development by network between BMP signalling and transcription factors. The Journal of Biochemistry 151, 247-254.

273. Oegema, T.R., Carpenter, R.J., Hofmeister, F., Thompson, R.C., 1997. The interaction of the zone of calcified cartilage and subchondral bone in osteoarthritis. Microscopy Research and Technique 37, 324-332.

274. Rim, Y.A., Nam, Y., Ju, J.H., 2020. The Role of Chondrocyte Hypertrophy and Senescence in Osteoarthritis Initiation and Progression. Int J Mol Sci 21.

275. Sabik, O.L., Medrano, J.F., Farber, C.R., 2017. Genetic Dissection of a QTL Affecting Bone Geometry. G3 Genes|Genomes|Genetics 7, 865-870.

276. Sampson, E.R., Hilton, M.J., Tian, Y., Chen, D., Schwarz, E.M., Mooney, R.A., Bukata, S.V., O'Keefe, R.J., Awad, H., Puzas, J.E., Rosier, R.N., Zuscik, M.J., 2011. Teriparatide as a chondroregenerative therapy for injury-induced osteoarthritis. Sci Transl Med 3, 101ra193.

277. Satokata, I., Ma, L., Ohshima, H., Bei, M., Woo, I., Nishizawa, K., Maeda, T., Takano, Y., Uchiyama, M., Heaney, S., Peters, H., Tang, Z., Maxson, R., Maas, R., 2000. Msx2 deficiency in mice causes pleiotropic defects in bone growth and ectodermal organ formation. Nature genetics 24, 391-395.

278. Schmitz, N., Laverty, S., Kraus, V.B., Aigner, T., 2010. Basic methods in histopathology of joint tissues. Osteoarthritis Cartilage 18 Suppl 3, S113-116.

279. Seemann, P., Brehm, A., Konig, J., Reissner, C., Stricker, S., Kuss, P., Haupt, J., Renninger, S., Nickel, J., Sebald, W., Groppe, J.C., Ploger, F., Pohl, J., Schmidt-von Kegler, M., Walther, M., Gassner, I., Rusu, C., Janecke, A.R., Dathe, K., Mundlos, S., 2009. Mutations in GDF5 reveal a key residue mediating BMP inhibition by NOGGIN. PLoS Genet 5, e1000747.

280. Sekiya, I., Larson, B.L., Vuoristo, J.T., Reger, R.L., Prockop, D.J., 2005. Comparison of effect of BMP-2, -4, and -6 on in vitro cartilage formation of human adult stem cells from bone marrow stroma. Cell Tissue Res 320, 269-276.

281. Semba, I., Nonaka, K., Takahashi, I., Takahashi, K., Dashner, R., Shum, L., Nuckolls, G.H., Slavkin, H.C., 2000. Positionally-dependent chondrogenesis induced by BMP4 is co-regulated by Sox9 and Msx2. Dev Dyn 217, 401-414.

282. Shintani, N., Hunziker, E.B., 2007. Chondrogenic differentiation of bovine synovium: bone morphogenetic proteins 2 and 7 and transforming growth factor beta1 induce the formation of different types of cartilaginous tissue. Arthritis Rheum 56, 1869-1879.

283. Shirakabe, K., Terasawa, K., Miyama, K., Shibuya, H., Nishida, E., 2001. Regulation of the activity of the transcription factor Runx2 by two homeobox proteins, Msx2 and Dlx5. Genes to Cells 6, 851-856.

284. Shwartz, Y., Viukov, S., Krief, S., Zelzer, E., 2016. Joint Development Involves a Continuous Influx of Gdf5-Positive Cells. Cell Rep 15, 2577-2587.

285. St-Jacques, B., Hammerschmidt, M., McMahon, A.P., 1999. Indian hedgehog signaling regulates proliferation and differentiation of chondrocytes and is essential for bone formation. Genes & development 13, 2072-2086.

286. Takahashi, K., Nuckolls, G.H., Takahashi, I., Nonaka, K., Nagata, M., Ikura, T., Slavkin, H.C., Shum, L., 2001. Msx2 is a repressor of chondrogenic differentiation in migratory cranial neural crest cells†. Developmental Dynamics 222, 252-262.

287. Thielen, N.G.M., van der Kraan, P.M., van Caam, A.P.M., 2019. TGFβ/BMP Signaling Pathway in Cartilage Homeostasis. Cells 8, 969.

288. Thorup, A.S., Strachan, D., Caxaria, S., Poulet, B., Thomas, B.L., Eldridge, S.E., Nalesso, G., Whiteford, J.R., Pitzalis, C., Aigner, T., Corder, R., Bertrand, J., Dell'Accio, F., 2020. ROR2 blockade as a therapy for osteoarthritis. Sci Transl Med 12.

289. Tsang, K.Y., Chan, D., Cheah, K.S., 2015. Fate of growth plate hypertrophic chondrocytes: death or lineage extension? Dev Growth Differ 57, 179-192.

290. Valcourt, U., Ronzière, M.C., Winkler, P., Rosen, V., Herbage, D., Mallein-Gerin, F., 1999. Different effects of bone morphogenetic proteins 2, 4, 12, and 13 on the expression of cartilage and bone markers in the MC615 chondrocyte cell line. Experimental cell research 251, 264-274.

291. Wei, Y., Hu, Y., Lv, R., Li, D., 2006. Regulation of adipose-derived adult stem cells differentiating into chondrocytes with the use of rhBMP-2. Cytotherapy 8, 570-579.

292. Wei, Y., Luo, L., Gui, T., Yu, F., Yan, L., Yao, L., Zhong, L., Yu, W., Han, B., Patel, J.M., Liu, J.F., Beier, F., Levin, L.S., Nelson, C., Shao, Z., Han, L., Mauck, R.L., Tsourkas, A., Ahn, J., Cheng, Z., Qin, L., 2021. Targeting cartilage EGFR pathway for osteoarthritis treatment. Sci Transl Med 13.

293. Wilkie, A.O., Tang, Z., Elanko, N., Walsh, S., Twigg, S.R., Hurst, J.A., Wall, S.A., Chrzanowska, K.H., Maxson, R.E., Jr., 2000. Functional haploinsufficiency of the human homeobox gene MSX2 causes defects in skull ossification. Nature genetics 24, 387-390.

294. Wu, Y., Wang, K., Karapetyan, A., Fernando, W.A., Simkin, J., Han, M., Rugg, E.L., Muneoka, K., 2013. Connective tissue fibroblast properties are position-dependent during mouse digit tip regeneration. PLoS One 8, e54764.

295. Yang, L., Tsang, K.Y., Tang, H.C., Chan, D., Cheah, K.S., 2014. Hypertrophic chondrocytes can become osteoblasts and osteocytes in endochondral bone formation. Proceedings of the National Academy of Sciences of the United States of America 111, 12097-12102.

296. Yu, L., Han, M., Yan, M., Lee, J., Muneoka, K., 2012. BMP2 induces segment-specific skeletal regeneration from digit and limb amputations by establishing a new endochondral ossification center. Dev Biol 372, 263-273.

297. Yu, L., Lin, Y.-L., Yan, M., Li, T., Wu, E.Y., Zimmel, K., Qureshi, O., Falck, A., Sherman, K.M., Huggins, S.S., Hurtado, D.O., Suva, L.J., Gaddy, D., Cai, J., Brunauer, R., Dawson, L.A., Muneoka, K., 2022. Hyaline cartilage differentiation of fibroblasts in regeneration and regenerative medicine. Development 149.

298. Zhou, N., Li, Q., Lin, X., Hu, N., Liao, J.-Y., Lin, L.-B., Zhao, C., Hu, Z.-M., Liang, X., Xu, W., Chen, H., Huang, W., 2016. BMP2 induces chondrogenic differentiation, osteogenic differentiation and endochondral ossification in stem cells. Cell and Tissue Research 366, 101-111.